Internet of Things (IoT) enabled smart nitrate sensor for real- time water quality monitoring

By

Md Eshrat E Alahi

A thesis submitted to Macquarie University

for the degree of Doctor of Philosophy

Department of Engineering

November 2018

Except where acknowledged in the customary manner, the material presented in this thesis is, to the best of my knowledge, original and has not been submitted in whole or part for a degree in any university.

Md Eshrat E Alahi

Acknowledgements

I would like to acknowledge many people's effort and contribution to successfully finish my Ph.D. journey which would not be possible without there valuable contribution.

Firstly, I want to express my earnest gratitude towards my principal supervisor, Prof. Subhas Mukhopadhyay who has inspired me to become an independent researcher and helped me realize the power of critical reasoning. His regular guidance helps me to finish this research in due time. I would like to thank my co-supervisor Dr. Lucy Burkitt for providing constant support when I was in Massey University, New Zealand.

I would like to thank Massey University, New Zealand where I did the first year of my research and got the quality laboratory facilities. I would like to thank the administrative staff and laboratory managers of Massey University. I would also like to thank Mr. Keith Imrie, Honorary Associate, Macquarie University to do the proofreading of this thesis.

I would like to express my sincere thanks to Dr. Hemant Ghyavat, Dr. Asif Zia, Mrs. Li Xie, Dr. Nasrin Afsarimanesh, Mr. Anindya Nag, Mr. Shilun Feng, and Dr. Sandeep Pirbhulal fro their active collaborations in the research. I would like to thank the administrative team of the School of Engineering, the Higher Degree Research team, Macquarie Engineering and Technical Services (METS), and laboratory facilities of Macquarie University.

I am especially grateful to my father, Mr. Md. Lutfar Rahman and my mother, Mrs. Romena Begum to support me emotionally. They believed in me and wanted the best for me throughout my life. I am also thankful to my brothers Mr. Md. Eshfaque E Alahi and Mr. Md. Eshrak E Alahi and my sister Mrs. Sharmin Nahar for their unconditional support. I would like to thank also to my in-laws parents for their support and love.

Last but not the least, I am indebted to my wife Dr. Fahmida Wazed Tina who has been my best friend and great companion, loved, supported, encouraged, and helped me get through

this agonizing period in the most positive way.

Abstract

Nitrate-N is a naturally occurring ionic compound that is part of nature's nitrogen cycle. Nitrates-N are readily lost to ground and surface water as a result of intensive agriculture, industrial wastes, disposal of human and animal sewage. The impact of elevated nitrate-N concentrations on water quality has been identified as a critical issue of a healthy environment for the future. Presently, water quality managers follow the traditional measurement systems that involve physically collecting the sampling water from remote sites and testing it in the laboratory. These methods are expensive, require trained people to analyse the data and produce much chemical waste. Therefore, low-cost Ion Imprinted Polymer (IIP) coated impedimetric nitrate-N sensor was developed, and the detection range of nitrate-N was 1-10 (mg/L). The selective IIP material was sensitive to nitrate-N ions in an aqueous medium, and the results are validated through standard UV-spectrometric methods. MEMS (micro-electro-mechanical-system) based interdigital sensor and sensing system was also developed to measure nitrate-N, and the range was 0.01 – 0.5 (mg/L). The graphene-based low-cost sensor was also fabricated, and the sensor was characterized to measure nitrate-N in the range of 1-70 (mg/L). Temperature compensation was added for both the sensors (MEMS and Graphene) and WiFi connectivity was provisioned in the system to transfer the measured data in real time. An improved LoRa based sensing system (solar panel and rechargeable battery powered) was developed and trial in the field successfully which can measure the nitrate-N concentration in real-time and transfer the data to IoT cloud server to overcome the limitations of lab based sensing system.

Contents

List of Figures

List of Tables

List of Symbols

R	Resistance
T	Temperature
KCL	Potassium chloride
V_t	voltage difference at time t
V_0	the amplitude of the signal
ω	the angular frequency (radians/second)
I_t	the response signal
θ	a phase shift
I_o	amplitude
Z	impedance
$Z_o \cos\theta$	a real part of impedance
$Z_o \sin\theta$	an imaginary part of impedance
σ_w	Warburg diffusion coefficient
Z_w	Warburg impedance
R_{ct}	resistance
C	Concentration of Nitrate
Q	Mass of nitrate adsorbed per gram of Ion Imprinted Polymer(mg/g)
C_i	Initial concentration of nitrate-N (mg/L)
C_f	Final concentration of nitrate-N (mg/L)
m	Mass of the polymer(g)
$NaNO_2$	Sodium nitrite
KNO_3	Potassium nitrate
Na_2SO_4	Sodium sulfate

List of Abbreviation

LOD	Limit of detection
GCE	Glassy-carbon electrode
ISE	Ion-selective electrode
PVC	Polyvinyl chloride
$THTDPIC$	Trihexyltetradecylphosphonium chloride
$HPLC$	high-performance liquid chromatography
PPy	Polypyrrole
CV	Cyclic voltammetry
DPV	Differential pulse voltammetry
NR	Nitrate reductase
CNT	Carbon nanotubes
$PESA$	Planar Electromagnetic Sensor Array
PCB	Printed Circuit Board
IoT	Internet of Things
$RFID$	Radio Frequency Identification
$WLAN$	Wireless Local Area Network
WAN	Wide Area Network
WSN	Wireless Sensor Network
IMS	Information Management System
$LoRaWAN$	Long-range, low-powerWireless Area Network
CSS	Chirp Spread Spectrum
FSK	Frequency Shift Keying
QoS	Quality of Service
MUT	Material under test
EIS	Electrochemical impedance spectroscopy
$TMAH$	Tetra-Methyl Ammonium Hydroxide
DDS	Direct Digital Synthesis
PWM	Pulse width modulation

Research Outputs

0.1 List of Journals

1. **Alahi, Md Eshrat E** and Xie, Li and Mukhopadhyay, Subhas and Burkitt, Lucy. *A temperature compensated smart nitrate-sensor for agricultural industry*. IEEE Transactions on Industrial Electronics **64**, 7333–7341 (2017).

2. **Alahi, Md Eshrat E** and Nag, Anindya and Mukhopadhyay, Subhas Chandra and Burkitt, Lucy. *A temperature-compensated graphene sensor for nitrate monitoring in real-time application*. Sensors and Actuators A: Physical **269**, 79–90 (2018).

3. **Alahi, Md Eshrat E** and Mukhopadhyay, Subhas Chandra and Burkitt, Lucy. *Imprinted polymer coated impedimetric nitrate sensor for real-time water quality monitoring*. Sensors and Actuators B: Chemical **259**, 753–761 (2018).

4. **Alahi, Md Eshrat E** and Pereira-Ishak, Najid and Mukhopadhyay, Subhas Chandra and Burkitt, Lucy. *An Internet-of-Things enabled Smart Sensing System for Nitrate Monitoring*. IEEE Internet of Things Journal , (2018).

5. **Alahi, Md Eshrat E** and Mukhopadhyay, Subhas Chandra. *Detection methodologies for pathogen and toxins: A review*. Sensors **17**, 1885 (2017).

6. **Alahi, Md Eshrat E** and Mukhopadhyay, Subhas Chandra. *Detection methods of Nitrate in water: A review*. Sensors and Actuators A: Physical (2018)

7. Afsarimanesh, Nasrin and **Alahi, Md Eshrat E** and Mukhopadhyay, Subhas Chandra and Kruger, Marlena *Development of IoT-Based Impedometric Biosensor for Point-of-Care Monitoring of Bone Loss*. IEEE Journal on Emerging and Selected Topics in

Circuits and Systems **8**, 211–220 (2018).

8. Pirbhulal, Sandeep, Heye Zhang, **Md Eshrat E Alahi**, Hemant Ghayvat, Subhas Chandra Mukhopadhyay, Yuan-Ting Zhang, and Wanqing Wu. *A novel secure IoT-based smart home automation system using a wireless sensor network.*. Sensors **17**, 69 (2016).

9. Afsarimanesh, Nasrin and **Alahi, Md Eshrat E** and Mukhopadhyay, Subhas Chandra and Kruger, Marlena *Smart Sensing System for Early Detection of Bone Loss: Current Status and Future Possibilities*. Journal of Sensor and Actuator Networks **7**, 10 (2018).

10. Ghayvat, Hemant, Subhas Mukhopadhyay, Jie Liu, Arun Babu, **Md Eshrat E. Alahi**, and Xiang Gui. *Internet of things for smart homes and buildings*. Australian Journal of Telecommunications and the Digital Economy **3**, 4 (2015).

0.2 List of Conference Publications

1. **Md. Eshrat E Alahi**, S.C. Mukhopadhyay, H. Ghayvat, R. Wang, L. Jie, “Comparative studies of Embedded Platform for IoT based Implementation”, pp.748-752,ISBN 978-1-4799-6313-3,in 2015 *Ninth International Conference on Sensing technology*,2015.

2. **Alahi, Md Eshrat E.**, Li Xie, Asif I. Zia, Subhas Mukhopadhyay, and Lucy Burkitt. "Practical nitrate sensor based on electrochemical impedance measurement." In 2016 IEEE International Instrumentation and *Measurement Technology Conference Proceedings (I2MTC)*, pp. 1-6. IEEE, 2016.

3. **Alahi, Md Eshrat E.**, Nasrin Afsarimanesh, Subhas Mukhopadhyay, Lucy Burkitt, and Pak-Lam Yu. "Highly selective ion imprinted polymer based interdigital sensor for nitrite detection." In 2016 *10th International Conference on Sensing Technology (ICST)*, pp. 1-5. IEEE, 2016.

4. **Alahi, Md Eshrat E**, Nasrin Afsarimanesh, Subhas Mukhopadhyay and Lucy Burkitt. “Development of the Selectivity of Nitrate Sensors Based on Ion Imprinted Polymerization Technique”. pp. 531-536, ISBN 978-1-5090-6526-4, in *2017 11th International Conference on Sensing Technology* (ICST).

5. Afsarimanesh, Nasrin, **Md Eshrat E. Alahi**, Subhas Mukhopadhyay, Marlena Kruger, and Pak-Lam Yu. "Development of molecular imprinted polymer interdigital sensor for C-terminal telopeptide of type I collagen." In 2016 *10th International Conference on Sensing Technology (ICST)*, pp. 1-5. IEEE, 2016.

6. Nasrin Afsarimanesh, **Md Eshrat E Alahi**, Subhas Mukhopadhyay and Marlena Kruger. "A Novel Electrochemical Biosensor for Bone Turnover Detection Based on Molecular Imprinting Technology". pp. 6-11, ISBN 978-1-5090-6526-4, in 2017, *11th International Conference on Sensing Technology* (ICST).

7. Noushin Poursafar, **Md Eshrat E Alahi** and Subhas Mukhopadhyay. "Long-range Wireless Technologies for IoT Applications: A Review", pp. 310-315, ISBN 978-1-5090-6526-4, in 2017 *11th International Conference on Sensing Technology* (ICST).

8. H. Ghayvat, Liu. Jie, A. Babu, **Md. Eshrat E Alahi**, U.A.B.U.A. Bakar, S.C. Mukhopadhyay, X. Gui,"Simulation and Evaluation of Zigbee based Smart Home using Qualnet Simulator", pp. 579-585, ISBN 978-1-4799-6313-3,in 2015 *Ninth International Conference on Sensing technology*,2015 .

0.3 List of Book Chapters

1. **Alahi, Md Eshrat E.**, Xie Li, Subhas Mukhopadhyay, and L. Burkitt. "Application of Practical Nitrate Sensor Based on Electrochemical Impedance Spectroscopy." In Sensors for Everyday Life, pp. 109-136. Springer International Publishing, 2017.

2. **Alahi, Md Eshrat E.**, A. Nag, N. Afsari Manesh, S. C. Mukhopadhyay, and J. K. Roy. "A Simple Embedded Sensor: Excitation and Interfacing." In Advanced Interfacing Techniques for Sensors, pp. 111-138. Springer International Publishing, 2017.

0.4 Seminars/Presentations

1. Presented in IEEE Postgraduate Presentation Day 2015, "Development of Data and control protocol of smart sensor node for Internet of Things (IoT)"20th Oct, Massey University, New Zealand.

2. Presented in 2015 Ninth International conference of Sensing technology, “Comparative studies of Embedded Platform for IoT based Implementation”, Auckland, New Zealand.

3. Presented in International Instrumentation and Measurement Technology Conference, 2016, IEEE, “Practical Nitrate Sensor Based on Electrochemical Impedance Measurement”, Taipei, Taiwan.

4. Presented in IEEE Instrumentation and Measurement Society, NSW Chapter,2017, “ Imprinted polymer coated impedimetric nitrate sensor for water quality monitoring” in Macquarie University, Australia.

5. Presented in 2017 11th International Conference on Sensing Technology, “Development of the Selectivity of Nitrate Sensors based on Ion Imprinted Polymerization Technique”.

6. Presented in Outlook Conference in July 2018 at Macquarie University, "Future of Internet of Things".

Chapter 1

Introduction

Nitrogen is the most available natural element in the atmosphere, being nearly 80% of the air we breathe [2]. Nitrogen can be found in gaseous form in the air, such as Nitrogen (N_2), Nitrous oxide (N_2O), Nitric oxide (NO), Nitrogen dioxide (NO_2), and Ammonia (NH_3) [3]. Some of these gases react with rainwater and produce nitrate and ammonium ions, which can become part of the soil layer, or mix with groundwater in solution. Intake of the nitrate ion has several positive aspects of the human body, such as improved blood flow, reducing the pressure of blood, cardio and vasoprotective effects. However, adverse effects can occur to the human body due with an excessive intake of nitrate ions, especially through drinking water, such as gastric, cancer and Parkinson's diseases. Infants can suffer "blue baby syndrome" or methemoglobinemia [4] which reduces the oxygen content of the blood [5, 6]. It affects those infants who are less than six months old.

The nitrate ion has been successfully utilized in some of our various activities, but there is no doubt that our fondness for them has diminished in recent years due to their excessive use. The extreme and continuous use of nitrate has caused enormous problems and raised numerous concerns [7, 8]. These problems have been identified widely all over the world, and as a result, different international and government organizations have created frameworks to control the level within the environment and in food products, with appropriate regulations in most industrialized countries.

The need and desire to monitor nitrates is undisputable, yet observing their presence can present a substantial challenge to the research community. Other similar ions are available, such as nitrite, ammonium, phosphate, and sulfate. Therefore, improved detection methods are essential to avoid any interference that can be encountered in the environment, industries, food, and industrial activities. A large number of analytical methods and sensing methods have been developed to overcome the peculiarities of the various media. In recent years,

a number of reviews have been undertaken to investigate the different detection methods [9–13].

In our daily life, nitrate is a vital ion, and various nitrogen species commonly occur in the environment. The excessive use of fertilizers in agriculture and general mismanagement of the use of natural resources is responsible for the perturbation of the global and local nitrogen cycle [14]. Waste materials can be one anthropogenic source of nitrates in groundwater. Disposal of animal sewage, industrial waste, and excessive use of organic fertilizers in agriculture are significant sources of nitrate pollution for water [15–17]. Nitrate in an aquatic medium stimulates excessive production of algae and phytoplankton, which leads to eutrophication. The process consumes more oxygen during the decomposition process, that affects fish or other marine life. Therefore, monitoring the environmental fate of nitrates has gained increasing importance.

Recently, pollutant removal from water using membrane technology has received considerable attention. It has a high adsorption capacity with low cost and has been integrated into sensor technology to enhance the selectivity towards the targeted ions. [18]. Appropriate characteristics and selection of the membrane material are essential in order to produce highly selective materials and systems. Many research studies have reported different types of membrane for the detection of nitrate in water. Modified silica polymer, trihexyltetradecylphosphonium chloride polymeric membrane [19], and doped polypyrrole, zinc (II) complex polymeric membrane [20], have been used for membrane development. Much research is going on to improve the sensitivity of membrane materials and to improve the selectivity.

In natural water, there are other environmental impacts such as temperature, vibration; the presence of other polluting ions, which will affect the precision of the measurements. All these ecological impacts might come naturally or via industrial and experimental waste. Therefore, obtaining reliable data is essential and can be achieved by controlling the measurement conditions. Precision instrumentation and measurement methods are essential to get highly reliable data. Different ways are available to detect nitrates in water, such as chromatography, flow injection analysis, electrochemical sensors, biosensors, optical fiber sensors, electromagnetic sensors. All of them have different characteristics and sensitivities. Some of the laboratory-based methods require expensive equipment and trained staff to conduct measurements in addition to the limitation on water sample collection, which can only be collected periodically. This approach risks missing critical changes in nitrate-N concentration

when river-flow rapidly rises or falls. Typically nutrient and sediment concentrations change with increasing and decreasing stream or river flow rates, therefore a monthly or fortnightly sampling regime may not adequately represent the nutrient concentration profile. The lack of information could influence our understanding of the seasonal effects on the nutrient loss and the total loads of nutrients (i.e., kg of nitrate/ha) estimated to be leaving a catchment. This information is critical for regional councils to implement policy and management around water quality in their catchments. Although high-frequency nitrate sample equipment is available, these cost in the order of AUD $\$10 - 50,000$. All the detection methods and the overall current technologies of nitrate ion detection will be discussed in Chapter 2.

1.1 Research Contributions

The major contribution of this research work lies in the design and development of selective material to detect nitrate-N in water and smart sensing system to do the real-time measurement in the sampling field. MEMS-based sensor and printed graphene sensor were also designed and developed to develop low-cost sensing system. All the results are validated through standard laboratory technique. The contributions are summarised as follows:

1. A temperature compensated MEMS-based nitrate sensor has developed to detect low nitrate concentration and measured data can be transferred to IoT based cloud server.
2. A temperature compensated graphene-based printed sensor has developed to identify nitrate and sensing system was also proposed.
3. A selective polymer material has developed to detect nitrate which was used as a coating material on the sensing surface.
4. An Internet of Things enabled smart sensing system has developed and trialed in the sampling field to collect the data from the sampling field.

1.2 Organization of the Thesis

Chapter 1

The background and the introduction of the research are explained in this chapter. The importance of nitrate sensor and in-situ based sensing system with real-time monitoring have

explained. The original research contributions have also explained in this chapter.

Chapter 2

There are varieties of detection methods are available for nitrate detection. Some of them are laboratory-based, and some of them can be used in the sampling locations. The advantages and shortcomings of those methods are discussed in this chapter. Internet of Things enabled sensing system for nitrate detection are also discussed in this chapter.

Chapter 3

In this research, capacitive interdigital sensors are designed and developed. Electrochemical Impedance Spectroscopy (EIS) method is used to detect nitrate in water. The relationships of those electrodes with impedance measurement and the technique of data acquisition are also discussed in this chapter.

Chapter 4

This is the first experiment in this research. A temperature compensated nitrate sensor has developed and experimental setup, results, and discussions are included in this chapter. The sensor was used to measure low concentration nitrate, and temperature compensation was added to improve the results. The smart IoT enabled sensing system was also explained in this chapter. The real-time data collection was shown in laboratory-based setup, and the system has the potential to use in the real sampling location.

Chapter 5

This chapter explains the fabrication process of carbon printed sensors and the advantage of using a graphene sensor to measure the concentration of nitrate in water. The range of the nitrate measurement was larger compared to the earlier chapter. A smart sensing system has also developed which can transfer the real-time data from the sampling location to a IoT based cloud server for remote monitoring.

Chapter 6

A selective material was developed to detect nitrate in water. The Ion imprinting polymerization technique has been used to develop the selective material. The material is characterized to find out the linear range, limit of detection, pH sensitivity and so on. The material was used as a coating on the developed sensor to measure the concentration of nitrate in water. The performance of the sensor is compared with the commercial sensor and all those results are explained in this chapter.

Chapter 7

A low-cost IoT enabled smart sensing system has developed and trialed in the sampling location for nitrate measurement. A LoRa based system is developed which is solar powered and consumes three times less energy compared to the earlier smart sensing system. The LoRa and WIFI based system is also compared to understand the performances in this chapter.

Chapter 8

The chapter gives an overview of the full research work in conclusions and some recommendations are made for the future work.

Chapter 2

Literature Review

2.1 Introduction

This chapter has taken from some papers([1], [2])and give a detailed overview of the different methods of detection methods of nitrate in water. Nitrate can be measured in the laboratory or outside of the laboratory for in situ measurement. Various detection methods have distinct advantages and limitations. The overview of different detection methods is explained. It is required the internet connectivity to develop a smart sensing system. The smart sensing system is useful when it is essential to implement the vast distributed network. The definition of IoT, necessary things need to develop a wireless sensor network, different IoT devices are explained in this chapter.

2.2 Detection Methodologies

There are two methods for nitrate detection: direct and indirect methods. Indirect methods are expensive as costly instrumentation is required for accurate measurement. They are also complicated, requires chemical reagents, produce a lot of chemical waste and need the expertise to make the measurements. On the other hand, direct methods are accurate and provide economical methods for detection. One of the significant disadvantages of using a direct method is measurement errors due to interference from other contaminants. Both methods are discussed in the subsequent sections.

[1] **Alahi, Md Eshrat E.**, and Subhas Chandra Mukhopadhyay. "Detection methods of Nitrate in water: A Review." Sensors and Actuators A: Physical (2018).

[2] **Alahi, Md Eshrat E**, S. C. Mukhopadhyay, H. Ghayvat, R. Wang, L. Jie, and Helen Zhou. "Comparative Studies of Embedded Platform For IoT Based Implementation."in IEEE International Conference on Sensing Technology, 2015.

2.3 Electrochemical Detection

The electrochemical detection of nitrate can be divided into some different categories depending on their different sensing methods. The system can convert the nitrate ions into an impedance, potential difference or current, and they can be grouped into impedimetric, potentiometric and voltammetric, respectively. In an electrochemical cell, various electrodes can be used for nitrate detection, such as copper, silver, platinum, gold, glassy-carbon electrode (GCE), graphite-epoxy, chitosan/bentonite, graphene, etc. The LOD, the sensitivity of the sensor, and its reusability depend on the material of the electrodes and the sensing method.

This method is used widely due to its simple operation, good sensitivity to nitrate ions in water, easy miniaturization, and low power consumption. However, the conventional electrochemical cells are large and not suitable as a portable device. A few types of research [21–23] are reported where nitrate detection was done through a miniature electrochemical cell. One of the significant reasons to develop a low-cost portable device is to monitor the nitrate concentration continuously in aqueous media. Hence, the advanced analytical system needs to be highly miniaturized and sensitive enough for nitrate detection over a long period. Therefore, the reusability of any proposed analytical system is extremely important. Different electrochemical detection methods are discussed in the following sub-sections.

2.3.1 Potentiometric Detection

The conventional potentiometric system consists of two half-cells which contain an electrode immersed in a solution of ions where the activities of the electrode's potential are determined. An inert electrolyte in the salt bridge, such as potassium chloride (KCl), connects the two half-cells. Porous frits are fixed to the ends of the salt bridge. The arrangement allows moving the electrolyte's ions to move between the half-cells and the salt bridge. Figure 2.1 represents the architecture of a potentiometry system.

This detection method was first introduced in late 1976 for detection of nitrate ions in water. It does not require any additional chemical reagent and is considered a direct detection method. In the last few years, this method has been utilized to improve the selectivity and detection limit of nitrate detection. Many improvements have been made to enhance the performance of the system, such as the integration of ion-selective electrodes (ISE). The ISE

method is useful to determine the free ion concentration directly in water. The advantage of using ISE are low cost, non-destruction of the sample, portable device, and no requirement of pre-treatment of the samples.

In 1976, Hassan et al. [24] reported organic nitrate and nitramine determination based on the reaction of a mercury sulphuric-acid mixture. The developed potentiometric method was simple, selective and accurate for rapid detection at the micro and sub-micron level. The detection limit was 1 to 50 (μ mol) with the precision of ± 0.2%. Mendezo et al.[25] developed a nano biocomposite as ISE to determine nitrate ions in water. The nanocomposite is based on intercalation of chitosan in bentonite, and the detection limit was 20 milliMole to 800 milliMole. Mahajan et al. [20] developed a polymeric membrane by means of two $Zn(II)$ complexes coordinated by neutral tetradentate ligands, N,N'-ethylene-bis (N-methyl-(S)-alanine methylamide) and N,N'-ethylene-bis (N-methyl-(S)-alanine dimethylamide), utilized as-as anion-selective carriers. The blending of these new Zn (II) complexes with dioctyl sebacate offered a high sensing selectivity for nitrate ions in water. The detection range was near-Nernstian slopes in the wide linear concentration range of 50 μM to 100 mM. Li [26] and Nunez [27] developed the potentiometric sensor and used an Artificial Neural Network (ANN) to determine the nitrate contamination level in water. Bendikov and Harmon [28] have reported doped polypyrrole, which is a selective membrane in an ISE electrode for nitrate detection in water. The doped polypyrrole is a highly conductive polymer material, which is widely used due to its high conductivity and stability. Zhang et al. [29] used this doped polypyrrole as a sensitive polymer membrane for a potentiometric system for nitrate detection in water. The polypyrrole improves the selectivity with a simple recipe procedure and has low toxicity compared to polyvinyl chloride (PVC) which is a conventional membrane [29]. Moreover, this reported study also demonstrated that carbon-nanostructure based materials between the membrane and the substrate layers are useful to prevent water formation during the potentiometric measurement. Wardak et al. [19] developed trihexyltetradecylphosphonium chloride (THTDPIC) which is an active polymeric membrane and enhances the PVC membrane sensitivity by reducing electrical resistance.

Most of the potentiometric sensors are bulky due to the internal reference electrode and the reference electrolyte solution with a true-liquid or liquid polymeric membrane. Thus, a micro-fabricated polymeric sensor [30, 31] was introduced to reduce the problem of these potentiometric sensors. The advantages of using micro-fabrication are small size, simple

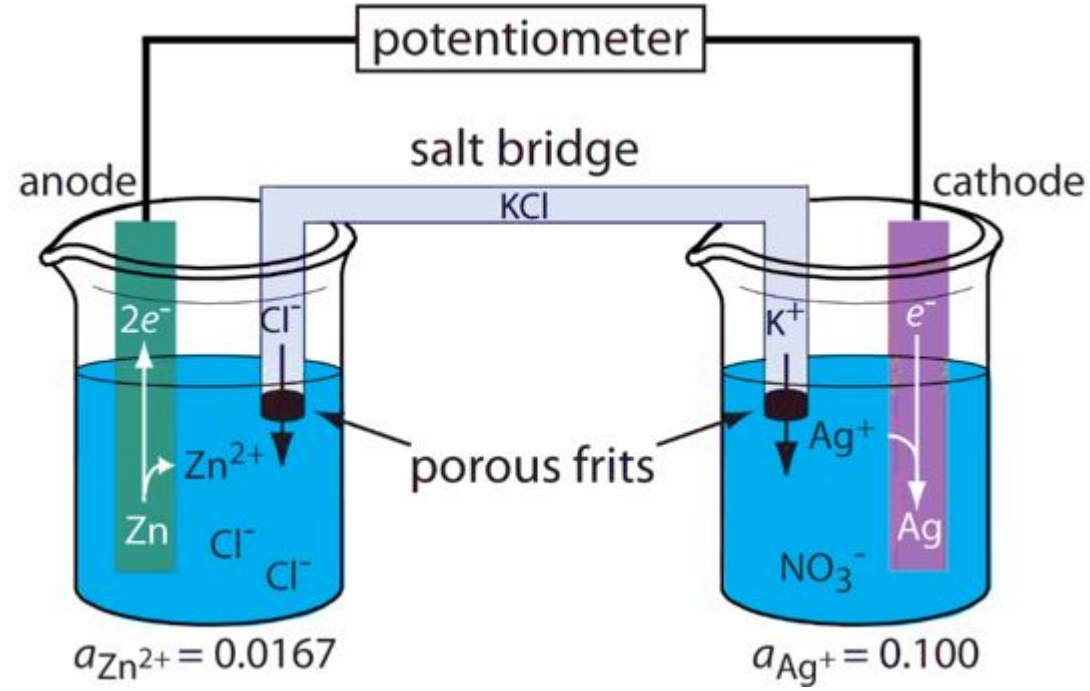

FIGURE 2.1: Architecture of potentiometry system

design, reduced cost, and mass production. A lot of different materials have been introduced, such as screen-printed thick film, silicon-based transducer, metal-printed flexible film to produce micro-scale potentiometric sensors. They have shown a good response to detecting nitrate ions in water. Figure 2.2 is an example of the response from a potentiometric sensor and figure 2.3 is the layout and design of a potentiometric sensor. Table 2.1 is summarized the characteristics of different potentiometric sensors.

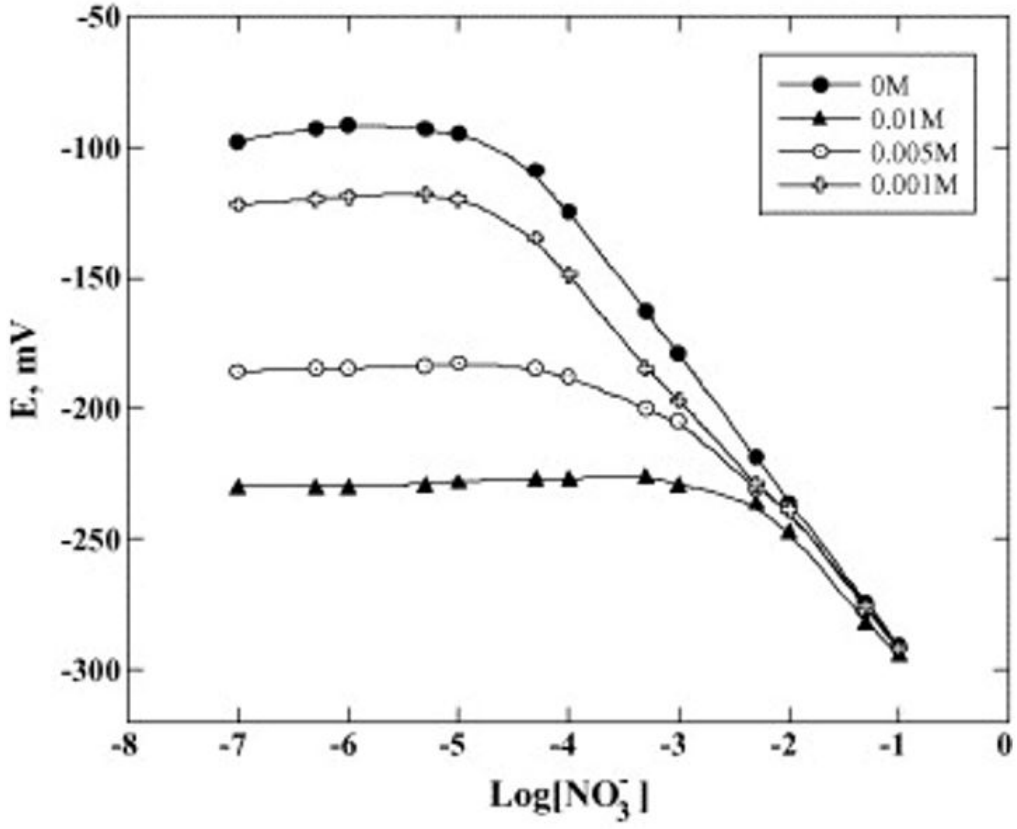

FIGURE 2.2: Potentiometric response of an electrode at varying concentrations [20]

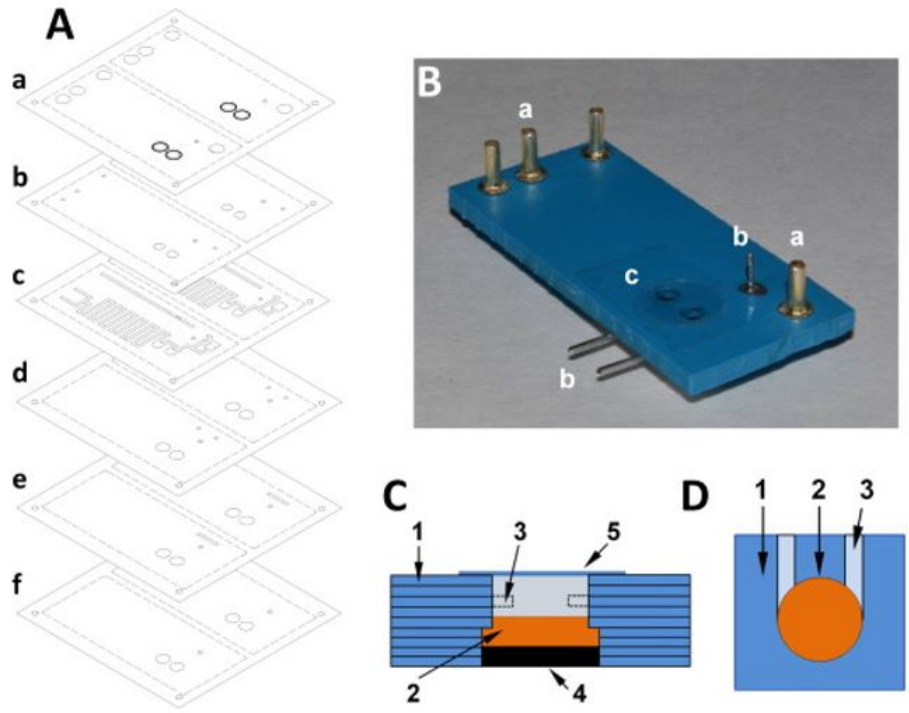

FIGURE 2.3: (A) Layout of the biparametric prototype; (B) picture of the final constructed device; (C): front view of the detection chamber scheme; (D) Top view of the detection chamber scheme [30]

TABLE 2.1: Characteristics of different potentiometric sensors

Electrode and Membrane	Reference Electrode	Limit of Detection	Nernstian Slope (mV/decade)	Response Time (s)	Application	Characteristics	Ref.
Silver bis (bathophenanthroline) nitratein plasticized PVC	Ag/AgCl	0.05 µg/L	-55.1 ± 0.1	<15	Determination of nitrate in industrial wastewater,fertilizers and pharmaceuticals.	Fast response, high sensitivity,long- term stability and good selectivity.	[31]
Graphite-epoxy and PVC	Ag/AgCl	4.6 µm/L	-68.2	Not reported	Photoelectrocatalytic treatment of nitrate monitoring	Simple operation, does not require any preparative or pre-treatment stage.	[27]
Nitrate polymeric	Ag/AgCl	9.56 mg/L	-59.5	Not reported	In the water treatment process plant	Small in size, simultaneous and on-line detection	[30]
Glassy carbon electrode and polypyrrole with nitrate doped	Ag/AgCl	10-4.8 mol/L	-55.1 ± 0.1	85	Monitoring of soil micronutrient	Rapid response, inexpensive cost, simple operation	[29]
Chitosan/bentonite and graphite-epoxy	Ag/AgCl	2 ×10 -4 M	-54.6	Not reported	Determination of nitrate in water	Low cost, easy to use	[25]

2.3.2 Amperometric Detection

Amperometry is one of the electrochemical, methods where the potential of the sensing electrode is controlled through instrumentation, and the current is recorded as the analytical signal, appearing because of oxidation/reduction. The applied potential is constant, and the resulting current is measured as a function of time. This technique first introduced in 1976 as high-performance liquid chromatography (HPLC) [32], and a conventional benchtop was introduced in 1987 [33]. During the amperometry process, the magnitude of the generated current in any given sample is determined by the number of molecules and can be calculated using Faraday's law (equation 2.1):

$$i_t = \frac{dQ}{dT} = \eta F \frac{dN}{dt} \tag{2.1}$$

where it is the current generated at the sensing surface electrode during time t, Q is the charge at the sensing surface, η is the number of moles, N is the number of moles of the analyte during oxidation/reduction, and F is the Faraday constant (96487 C mol^{-1}). The detection limit can be at attomole or femtomole levels [34, 35]. Therefore, this method is useful to determine nitrates in the water.

N.G. Carpenter et al. [36] reported an amperometric method to determine the nitrate in water. The nitrate concentration range was 0.1-1 mM, and interferences from other similar ions in water can be avoided. X Zhang [37] has reported Polypyrrole (PPy)-nanowire modified electrodes based on graphite electrodes for nitrate detection. The detection limit was 1.52 µM, and the sensitivity reaches 336.28 mA/M cm2. The results showed that it has significant effects on the morphology of PPy nanowires and the current density of nitrates during the electrochemical preparation of the modified electrodes. Other amperometric detectors [38–47] are reported to determine nitrate in water. The design of the sensing electrode is important to increase the sensitivity of the detection method.

2.3.3 Voltammetric Detection

Cyclic voltammetry (CV) is a powerful and popular electrochemical detection method which measures the reduction and oxidation process of any molecular species. It usually performs with three electrodes named reference electrode, working electrode and counter electrode. The working electrode carries out the electrochemical event of interest by changing the potential applied these to give the desired potential at the reference electrode. The

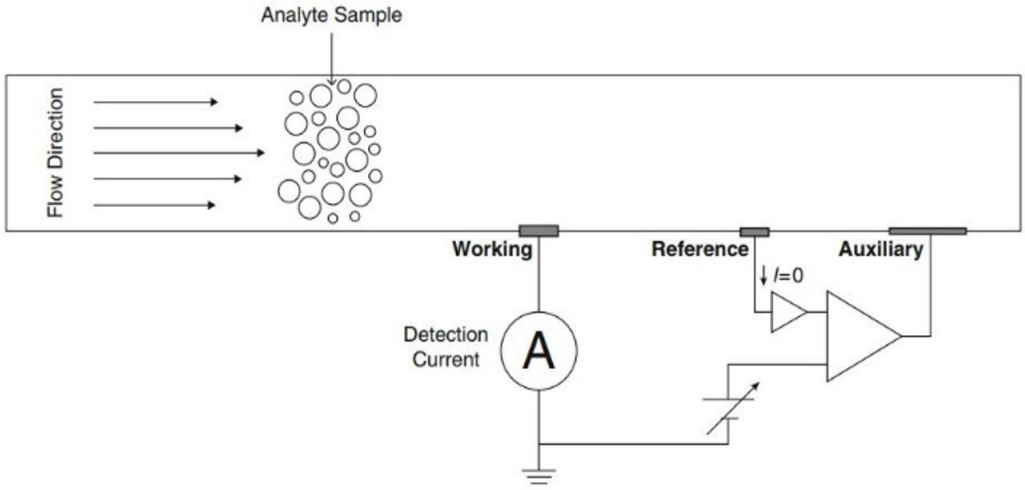

FIGURE 2.4: Schematic diagram of amperometric detection cell for lab-on-a-chip application [1]

reference electrode is used as a reference point to measure the potential of the other electrodes. During proving the potential to the working electrode, current begins to flow, and the counter electrode completes the circuit to continue the flow of electrons due to the reduction or oxidation process.

In 1977, M.E. Bidini et al. [48] reported a voltammetric method to determine the nitrate in irrigation water samples. Copper and cadmium were electrochemically deposited on the pyrolytic graphite electrode which was the working electrodes. The linear detection range was from 1µM to 1 mM. R. J. Davenport et al. [49] reported a voltammetric determination of nitrate and nitrite using a rotating cadmium disk. J. Krista et al. [50] reported a system where the electrodes were prepared from a mixture of silver, graphite powder and methacrylate resin. The detection range of nitrate ion was up to 31 mg/L, and LOD was 7 mg/L. The arrangement showed good reproducibility, but a computer-controlled system was necessary to get those results. S. M. Shahriar et al. [51] reported in-situ copper- based electrode with a low detection limit. Differential pulse voltammetry (DPV) was applied for simultaneous nitrate determination in river water. Neuhold et al. and Mareček, V et al. [52, 53] reported the voltammetric determination of nitrate in drinking water. The detection limit was 0.5-60 µg/mL, and a carbon-paste electrode was used as the working electrode. A differential pulse voltammetric method [54] has been reported to determine the nitrate in natural water. The detection limit was 2.8 µM, and the linear detection range was 2.8 µM – 80 µM. Copper-plated glassy carbon was used, with the sensitivity of 0.9683 A. L/mol. A square-wave voltammetric method [55] has been reported with similar copper- plated glassy carbon electrodes. The

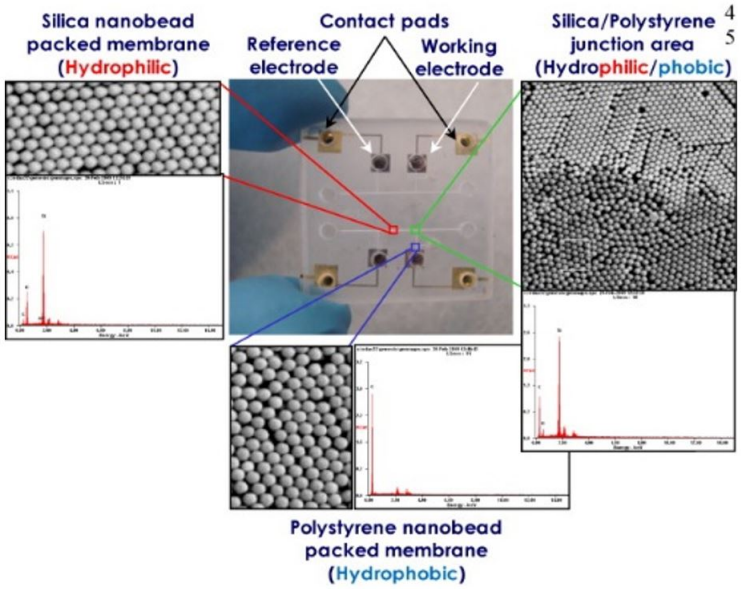

FIGURE 2.5: Photograph of the dual ion-selective lab chip with self-assembly nBP columns [56]

linear working range of determination of nitrate was 0.61 µM- 50 µM and LOD was 0.18 µM. Jang et al. [56] reported a new electrochemical sensing platform with self-assembly nanobeads-packed (nBP) hetero columns. Figure 2.5 is the sensing platform which was reported in the article.

2.3.4 Chromatography Detection

Chromatography detection is a laboratory-based technique used for different kinds of chemical mixture separation. An anion or cation of the analyte sample can be extracted when performing a chemical reaction with an eluent. It is an important technique for various chemical and biological analyses. There are available several chromatography techniques, such as ion chromatography [57], high-performance liquid chromatography [58] , ultra-performance liquid chromatography [59]. Ion chromatography is widely used for nitrate detection in water [60–66]. An ion chromatography system consists of solvents, solvent degasser, pump, injector, pre-column heat exchanger, guard column, post-column heat exchanger, electrolytic suppressor, and detector. The system is expensive, bulky, and not suitable for in-situ nitrate measurement.

This detection method also includes UV spectrometry, fluorimetric, electron capture, and mass spectroscopy [67–69] . UV detection is a popular method due to its simplicity. The low absorbance of water maintains a low background, which reduces the complications for direct

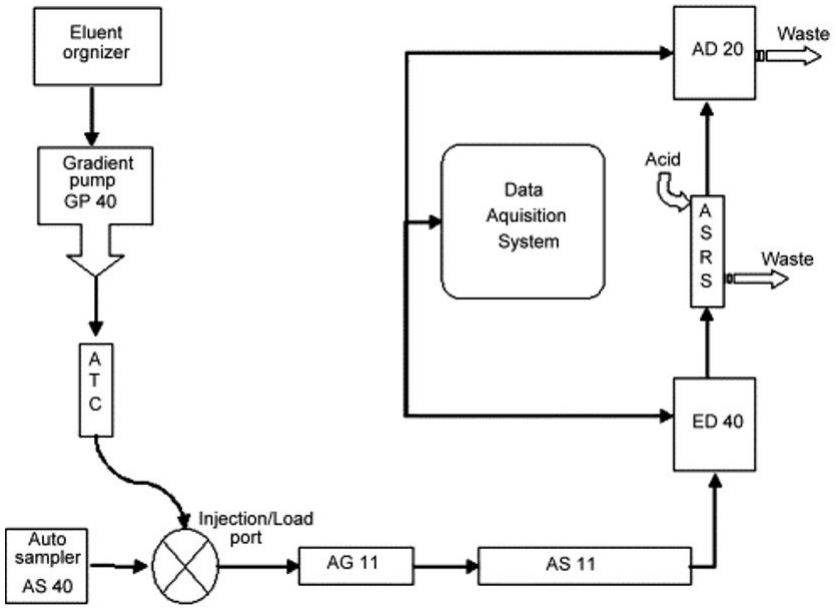

FIGURE 2.6: Schematic representation of the ion chromatography setup used for simultaneous determination [61]

detection of nitrate ions in water. However, rising of the high background UV absorbance is always avoidable which might come using the aromatic eluent during the detection of nitrate.

A novel HPLC method is also available to detect nitrate with improved sensitivity [58]. It is simple, easy to handle and selective towards nitrate ions in water, and it is based on a photochemical reaction and ion-exchange separation. Niedzielski et al. [60] reported a technique which can be useful to determine nitrate, nitrite and ammonium ions in water. Zuo et al. [69] developed a simple, fast, accurate HPLC method to detect nitrate and nitrite ions in lake water. The method produced good sensitivity, a high detection range, and good LOD. Table 2.2 summarizes the type of Chromatography methods with their characteristics.

TABLE 2.2: The types of Chromatography with eluent and LOD

Chromatography Type	Detector	Eluent	LOD	Application	Ref.
Ion Chromatography	Ion exchange and diode-array detection	NaCl	0.05 mg/L	Detection of nitrate in rain	[60]
Ion Chromatography	low-capacity anion exchange column with amperometric and adsorbance	NaOH	6 µg/L	Detection of nitrate in water	[61]
HPLC	Ion-exchange separation and photochemical reaction	Borate buffer (pH 10)	$2x10^{-8}$ M	Detection of nitrate in natural water	[58]
HPLC	UV light adsorption	Tetrabutylammonium hydroxide, Na_2HPO_4 and Acetonitrile	5 miro g/L M	Detection of nitrate in water	[69]
Liquid Chromatography Chromatography	Fluorescence detection	Toluene and NaOH Na_2HPO_4	0.3 pg/L	biological, food and environmental samples	[67]

2.3.5 Bio Sensors

The biosensing method is a direct method to detect nitrates in the water. In biosensing systems, the biological materials are employed with a detection system and a signal-conditioning circuit to measure the concentration of the targeted ions in a sampling solution. The sampling or analyte solution is exposed directly to the biosensor and the sensing material to measure the concentration of the sample. The target ions interact with the biological material to provide the necessary information. The interaction process needs to convert to an electrical signal such as voltage, current or impedance to measure from the sensing system. The conversion of the sensing signal depends on the biosensing method. Useful articles have reported [70–73] on biosensors and differentiated them based on the nature of the transducer. The biological components such as DNA, enzymes, immunological systems, receptor proteins, and whole cells can be used as recognition units. A transduction component that may be acoustic, chemical, electrochemical, microbalance, optical, or piezoelectric is required. They should have high sensitivity, specificity, and the ability to work in a wide range of matrices. They are also useful if they operate remotely to make in situ measurements.

For the last two decades, nitrate biosensors have been developed due to the easy availability of appropriate enzymes and their use in a substrate as a selective material. Zeng et al. [74] reported a fluorescence-based fiber-optic bio-sensor to trace various contaminants in seawater. The protein molecule was used as a recognition unit. Xuejiang et al. [75] reported a fast, sensitive and stable conductometric enzyme biosensor for the determination of nitrate in water. A methyl viologen mediator modified the electrodes of the biosensor and was mixed with nitrate reductase (NR). The developed biosensor had a quick response and reached 95% of the constant conductance value in 15 s. The calibration range is 0.02-0.25 mM with a detection limit of 0.005 mM. The lifetime of the sensor was 2 weeks. Cosnier et al. [76] used NR by entrapping in a laponite clay gel which was cross-linked by glutaraldehyde. The developed sensor was useful to detect nitrate in low concentration. The use of biosensors for the measurement of nitrate in water would enhance the sensitivity for in situ remote monitoring. Can et al. [23] reported an amperometric nitrate biosensor where the film was produced from Polypyrrole (PPy)/ Carbon nanotubes (CNTs). The sensitivity of the developed sensor was 300 nA/mM, and the detection range was 0.44-1.45 mM. The biosensor gave a higher response than the standard methods of nitrate measurement. Z. Zhang et al. [77] have reported a conductometric biosensor. Table 2.3 tabulates the type of biological materials,

detection systems, and limit of detection.

TABLE 2.3: Types of biological materials, detection systems, limit of detect

Detection method	Biological material	LOD	Application	Characteristics	Ref.
Conductometric	methyl viologen mediator with NR	0.005 mM	Detection of nitrate in waste water and river water	Response time was 15 s, low detection limit,good operational and thermal stability.	[75]
Amperometric	CNT/PPy film electrode with NR	0.17 mM	Measurement of nitrate in water	Better performance than standard methods. response time is 20s	[23]
Cyclic Voltammetry	NaR–SOD1–CNT–PPy–Pt	200 nM	Nitrate detection in saliva and blood	very sensitive. required large sample	[78]
Amperometric	Escherichia coli with NR	0.1 M	Detection of nitrate in drinking water	Longer stability and cheap method to prepare biosensor	[79]
Cyclic Voltammetry	Laponite clay gel, glutaraldehyde with NR	7 µM	Determination of nitrate	Low detection limit	[76]

2.3.6 Flow-Injection Analysis

Flow-based methods have been used for nitrate measurement for various applications. This detection method is desirable in the laboratory and is a good alternative to other traditional methods. It has high-throughput analysis, requires low volumes of reagent and sample, is low-cost and easy to operate. Hence, the reported work [80–89] used the flow-injection analysis method and developed a procedure to determine the nitrate concentration in water.

Generally, flow-injection methods consist of four different processes: distribution, reduction, pre-detection, and detection. The sample is carried on to the next process with a constant flow rate with the distribution process. The pump of the flow-injection methods allows the supplied sample endlessly within a specific period. Second is a reduction process which works by converting the nitrate ions into active nitrite ions by elevating the nitrate ions inside the sample. In the pre-detection process, a compound is formed due to the reaction of the reduction agent with the nitrate ions produced in the earlier process. Then, the responsibility of the detection system is to detect nitrate ions. The most common detection agents are Griess-illosvay, acidic hydrogen peroxide, sulfanilamide and N-(1-naphthyl) ethylenediamine dihydrochloride (NED). In the flow injection process, several reduction reagents have been used for nitrate detection. A zinc column, a cadmium column, vanadium (III), titanium (III) chloride and hydrazine sulphate are the most common reduction reagents. Selecting the correct reduction reagent is imperative. Otherwise, it will take an excessive amount of time to complete the injection process.

Different types of detectors are involved with the numerous flow-injection methods, and they have been reported earlier for nitrate detection. Among the different types of detection systems, spectrophotometric and chemiluminescence are preferred methods for nitrate detection. Absorbance is the output of the detector which is proportional to the sample concentrations. Lambert's law explains this behavior where absorbance is considered the proportional factor to the concentration of sample nitrate. The chemical reagent, pH of the solution, the flow rate of the sample carrier, sample volume and coil length of the reaction are related to getting the maximum output of detection. All these parameters must be controlled to achieve accurate results, sample throughput, peak shape of the output. Therefore, all those parameters optimized during the analysis. Figure 2.7 shows the schematic diagram of essential components of the flow-injection analyser.

Yaqoob et al. [82] reported on luminal chemiluminescence where the efficiency depends

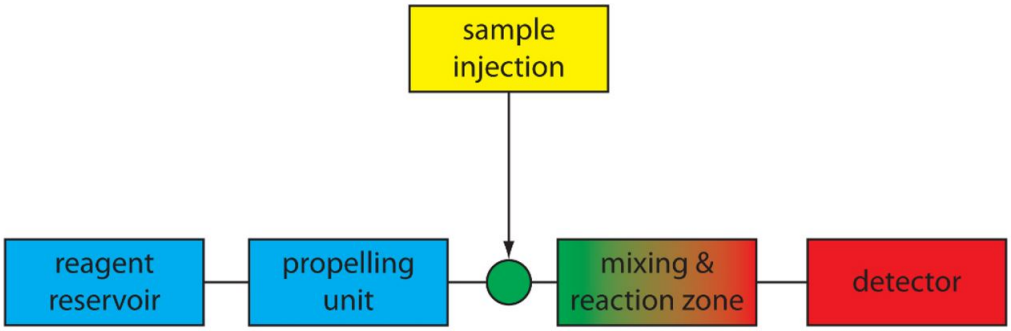

FIGURE 2.7: Schematic diagram of basic components of a simple flow-injection analyzer

on the pH, and pH helps in reduction of nitrate; increasing the pH changes the absorbance or the detector's response significantly to develop the azo dye formation which increases the efficiency of spectrophotometric detection. The flow rate is the vital parameter, and it is controlled for sample, carrier and reagent solutions. The significance of the flow rate is reported [83] and it is essential for time-consuming reactions. Furthermore, it can enhance the sensitivity and sample throughput for nitrate ions [86]. It is essential to find the optimum flow rate which helps to stabilize the baseline on the detection area and improve the output such as intensity and absorbance.

2.3.7 Electromagnetic Sensors

Nowadays, much research on the impedance-based sensor has been introduced. The impedance-based sensor is excellent to measure physical properties and suitable for direct measurement. A Planar Electromagnetic Sensor Array (PESA) is one those sensors which measure physical properties regarding impedance. A sample has different properties, such as conductivity, dielectric properties, permeability which can be estimated to measure the nitrate in water samples [90–96]. Enhancing the sensor's sensitivity is essential and can be done by optimizing the sensor design and configuration. PESA is convenient to use as an in-situ measurement which is highly durable, with fast response, and low cost.

Yunus et al. [90] had reported a planar electromagnetic sensor for nitrate detection in an aqueous medium. The performance of the sensor was measured through two arrangements: series and parallel connections. The study showed that the series connection provided the better performance regarding the sensor's sensitivity to detect the nitrate. Therefore, it was recommended to use the series connection for electromagnetic sensors. The sensitivity of

the sensors also depends on the material of the electrodes. The reported work used gold electrodes due to the attraction of nitrate towards the gold material. It is also essential to use a high-dielectric substrate to increase the penetration depth of the electric field, to develop a high-sensitivity sensor. Three configurations are available to design the electrodes: parallel, star, and delta.

Nor et al. [94] reported a sensor array with a thin substrate on a Printed Circuit Board (PCB) by using a conventional PCB fabrication technique. The designed sensor consisted of several coils or loops of electrodes, spiral or square in shape. The distance of the coils is vital to improving the sensitivity of the sensor. Wang et al. [97] reported the design of a sensor where the impedance of the sensor increased due to increasing the distance of the two electrodes and decreasing their area.

2.3.8 Fibre-Optic sensor

In the last three decades, an optical sensor has been developed to determine various parameters in water. It consists of three important parts: a source, an optical fiber and a photodetector to detect the optical signal. The optical sensor can be chosen from two categories: intrinsic and extrinsic sensors. The intrinsic sensors require continuous, consistent light sources to permit a phase-modulation technique. The modulation occurs inside the optical fiber, and only a single-mode fiber is used for the design of the sensor. Fiber is used as a transmitting channel for an extrinsic optic sensor. It is widely used in remote sensing due to its low power requirement and small size. It is also used to detect nitrate and nitrite [98] in water. Lauth's violet-triacetyl cellulose membrane was used to detect nitrate concentration using absorption spectrophotometry, and the detection range is 10.12 to 1012 ng/mL. B. Mahieuxe et al. [99] reported a modified fiber-optic sensor using fluorescence emission to detect nitrate in water. It presents a bathochromic shift and hypochromic effect with different nitrate concentrations. An external sensor was reported [100] with Lophine used as a sensitive layer on the fiber. The detection range was from 1 to 70 mg/L and the response time was 20 ms. The detection wavelength was 300 -1100 nm. 350 nm to 2500 nm [101] wavelengths have been reported to detect the nitrate, and the range was 0 – 2.50 mg/L. An ASD FieldSpec 3 Hi-Res Portable Spectroradiometer and halogen lamp were used as light source. Recently, Moo et al. reported [102] a technique to detect nitrate and nitrite in water. The spectroscopic measurement was implemented through different techniques which included transmittance,

absorbance, and reflectance. All measurements were presented by using Channel 0 of the Jaz Spectrometer. Tungsten halogen light was used as the light source. The wavelength was 302 nm to 356 nm with the detection range from 0 mg/L to 50 mg/L. The obtained results showed a good linear relationship with the minimum effect of interference from other ions. Johnson et al. [103] reported an in-situ ultraviolet spectrophotometry method to do long-term nitrate measurements in ocean water. The nitrate concentration is measured by the absorption of the UV light produced by a deuterium light source and guided through fibers to a reflection probe. The in-situ ultraviolet spectrometer is controlled by a microcontroller, which also contained a global positioning system and satellite antenna. The linear range of detection of nitrate is 0-10 ppm. This sensor has been used in various applications [104–109] due to the improved sensitivity. Table 6 represents various characteristics of optical-fiber sensors.Table 2.4 represents the various characteristics of optical fibre sensors.

TABLE 2.4: Different optical fibre sensors and their characteristics

Type of Sensor	Analytical wavelength	LOD	Linear range	Application	Ref.
UV fibre optic sensor	302 nm	0.0017 mg/L	(0-50) mg/L	Detection of nitrate and nitrite in water	[102]
UV spectrometry	-667.97 240 nm	0.4 µmol/L	(1-45) µmol/L	Ocean water measurement	[103]
Caoting-based optical sensor	300-1100 nm	-	(1-70) mg/L	Nitrate measurement in drinking water	[100]
Chemical-based optical fibre sensor	515 nm	-	(0-0.2) µ mol/L	Nitrate detection in water	[99]

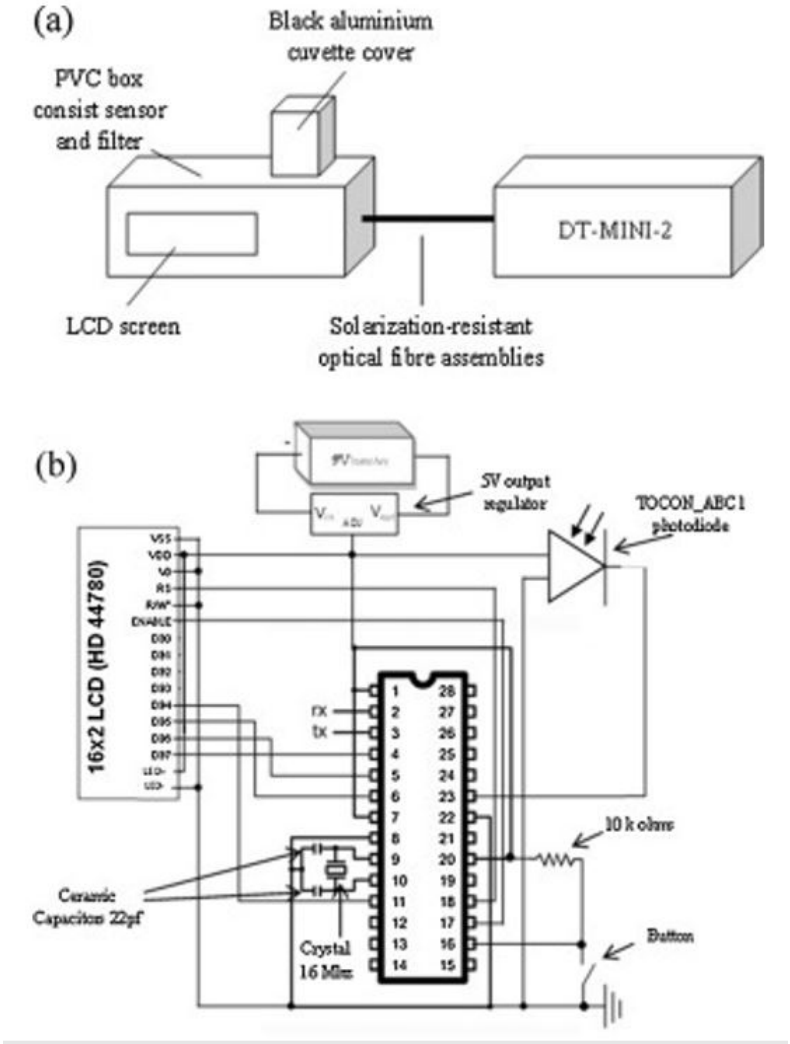

FIGURE 2.8: (a) Setup of the Fiber-optic sensor and (b) Schematic of the sensor with microcontroller system [102]

2.3.9 Commercial Sensors

Hach is well-known as suppliers of analytical instruments and chemical reagents for the laboratory-based purpose, especially for water quality and other liquid solutions. Take IntelliCal ISENO3181 Nitrate Ion Selective Electrode (ISE) for nitrate detection as an example, it is designed by the solid-state PVC membrane with epoxy, and solid gel ion exchange eliminates the frequency of replacing membrane. The ISE can only be used periodically in the laboratory or field and is not suited to continual measurement. It can detect the nitrate-N concentration from 0.1 to 14000 mg/L. It has an integrated temperature sensor which can measure the temperature range from 0-50^oC. The price is at $2100. Hach Nitratax sc tank sensor is being used extensively internationally and in New Zealand. It uses the UV absorption measurement with a reagent-free technique. There are three different models with the

different detection range: 0.1 - 100 mg/L by Nitratax plus sc; 1.0 - 20 mg/L by Nitratax exo sc; and 0.5 - 20 mg/L by Nitratax clear sc. These models cost around $\$40K$ to $60K$.

"S :: can" is Austria-based Company which provides varied product range for water and environmental monitoring. All "s::can" instruments are operated followed by the "plug and measure" principle, so all of them are ready to use with pre-calibrated works. The "spectro::lyser" UV monitors can be used to $NO_3 - N$ detection. It is measured based on the UV-Vis spectrometry with the nitrate detection range from 0 - 20 mg/L. This instrument is also being used extensively internationally and in New Zealand. However, the whole set of the system is costly (around $\$60 - 70K$).

Hanna Instruments is focused on developing electro-analytical instrumentation. They provide the products like nitrate portable/benchtop photometer and nitrate ion selective electrode. For example, Hanna HI96728 is a portable checker to detect nitrate in freshwater based on the colorimetric method. A particular Tungsten lamp is used as the light source, and silicon photocell with narrow band interference filter at the wavelength of 525 nm used to detect the light. It uses the cadmium reduction method to determine the nitrate-nitrogen concentration range from 0.0 to 30.0 mg/L. The price is at around $\$350NZD$.

Xylem is a world leader in providing compact instruments for water technology. It has a broad range of products under different brands. YSI is one of Xylem brand, which provides the environmental monitoring products. IQ SensorNet 182 is a modular water quality terminal which allowed connecting additional sensors such as 6884 Nitrate ISE sensor and it provides a continuously measurement of water quality parameters like pH, Dissolved oxygen, temperature, conductivity, ammonium, nitrate, potassium, TOC (total organic carbon), COD (chemical oxygen demand), DOC (dissolved organic carbon share of TOC), BOD (biochemical oxygen demand) and SAC (spectral absorption coefficient). It has an easy-to-read digital display and wireless connection via radio transmission with a range of 100 meters. However, when it uses the nitrate sensor such as NitraLyt, the function of real-time monitoring is disabled. Another Xylem brand - WTW, it provides online measurement system - TresCon Analyzer which can monitor Ammonium, Nitrate, and Nitrite continuously. A continuous water sample supply with low solids contents is required for operating this system. For nitrate detection, the UV light is absorbed by the nitrate ions and determines the nitrate concentration at a wavelength of 254 nm.

ABB is a multinational corporation which mainly designs and manufactures power and

automation products, including flow measurement, gas, and liquid analyzer and environmental monitoring systems. For example, UV Nitrate Monitor AV455 provides a continuous analysis without chemical reagents. It can detect the nitrate concentration at the range of 0 to 100 mg/L at a wavelength of 220 nm. It requires low-maintenance and straightforward calibration with auto cleaning for the optical component. It uses de-nitrification as a process to reduce the nitrate concentrations for nitrate monitoring.

ASA Analytics Inc. specializes in the manufacture of the automatic chemical analysis system. ChemScan 6101 Process Analyzer can monitor Ammonia, Phosphate, Nitrate-Nitrite, and Phosphate in surface water based on the UV-spectrometric method. The light is absorbed by nitrate ions and into 256 wavelengths of 200 to 450 nm. The detection range of nitrate is from 0.5 - 20 mg/L.

TABLE 2.5: Summary of commercially available sensors

Model	Method of Detection	Detection range (mg/L)
IntelliCal ISENO3181	Ion Selective Electrode	(0.1-14000)
Nitratax plus sc	UV-photometric	(0.1-100)
S::can	UV-spectrometric	(0 - 20)
Hanna HI96728	Colorimetric	(0 to 30)
YSI 6884 Nitrate Sensor sc	Ion Selective Electrode	(0-200.0)
TresCon Analyzer	UV-spectrophotometric	(0.1 - 60)
UV Nitrate Monitor AV455	Ion Exchange	(0 - 100)
ChemScan 6101 Process Analyzer	UV-spectrometric	(0.5 - 20)

2.3.10 Internet of Things

Internet of Things (IoT) is the general concept of things that are readable, recognizable, locatable, addressable, and controllable via the Internet. Things communicate through the internet via Radio Frequency Identification (RFID), Wireless Local Area Network (WLAN), Wide Area Network (WAN) and other means. In the last few years, it has been a gaining appreciation for the revolution of advanced wireless technology. The IoT can be defined as a global network structure, linking physical and virtual objects, things, and devices through intelligent objects, sensors, and communication and actuation capabilities [110].

Different types of sensors are becoming available for sensing physical events and transmitting sensor data via wireless communications. Sensor networks are becoming the major component of network architecture and applications. However, more current sensor networks are designed and deployed to provide only a particular application. The sensor-nodes/platforms where the sensors are capable of connecting with embedded electronics, real-time sensing capability, and access to any other nodes are the most crucial part of the future IoT [111]. Figure 2.9 shows the architecture of IoT of three-tier communication, i.e., the local, regional and global tiers. The first tier consists of wireless sensing nodes/platforms. The next tier is the regional base station tier where the first tier acquires raw sensor data or intelligence and sends them to this tier through light-weight protocol stack [i.e., Zigbee, 6LoWPAN, RFID]. The base station works as the medium between the sensor-node tier and the clouds which are also a global tier and routes the raw sensing data to another node or a remote server [111]. Appropriate tools and approaches are needed for testing and managing an application on real hardware on a large scale to design a robust application. In early IoT research, the availability of smart devices is limited. Only recent advances in technology have increased their availability at lower cost. Although the experiments were mainly on a small scale and conducted in a research laboratory, they allowed for an opportunity to enhance understanding of the impact and limitations of protocols and design choices on performances of real hardware [112].

Another important term of IoT application is cloud computing. It is a model for enabling convenient, on-demand network access to a shared pool of configurable computing resources that can be rapidly provisioned and released with minimal management effort or service provider interaction [113]. In an IoT based cloud computing platform, instead of having local servers for collecting and managing information coming from WSN networks, remotely located servers (implemented using virtual and physical machines) are dynamically provisioned and changed, according to the actual application. So IoT based application should have the ability to access remotely through internet [114].

2.4 Wireless Sensor Networks (WSNs)

A wireless sensor network (WSN) consists of some dedicated sensor nodes with physical sensing and computing abilities, which can sense and monitor the surrounding physical

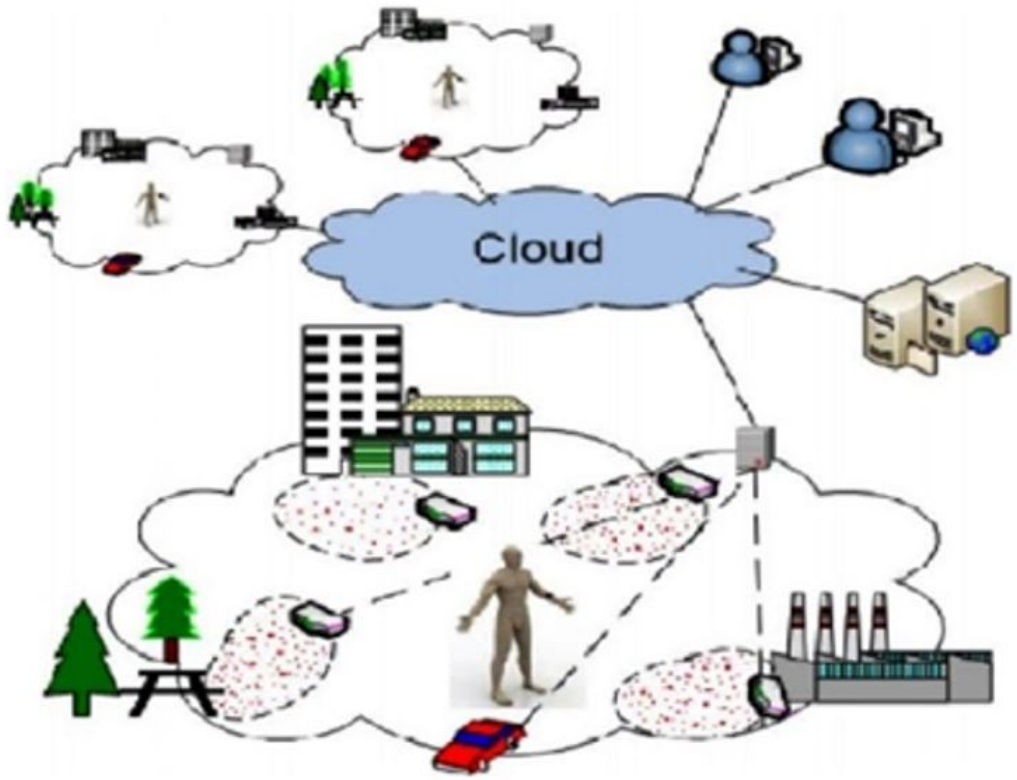

FIGURE 2.9: The architecture of three-tier IoT

parameters. The sensing systems transmit the collected information to a "gateway" through wireless communication. The gateway can handle the collected data and send to the cloud server where an "Information Management System (IMS)" analyzes the data in real time or for statistical analysis. A WSN has a lot of essential characteristics and a few constraints, such as limited energy and computational power. During the last decades, WSNs have been widely used in different applications related to water monitoring [115–117] , forests [118, 119], industrial [120], and agricultural [121, 122]. Some researches were reported [123–125] to monitor the nitrate concentration through the WSN network.

2.4.1 Structure of WSN

A WSN consists of three different subsystems. They are the nodes, the gateway, and the Information Management System.

2.4.2 Sensor Node

The sensor node is also called a sensing system with a low-cost, small low-power sensor, which can get appropriate measurements from the environment, process the measured data, and send them directly to the cloud server through the gateway. It consists of the following elements:

1. Microcontroller-based system: This is the core of the sensing node, which will be a low-cost, small, low-power chip. Unfortunately, it is difficult to get all these characteristics due to certain limitations, especially regarding the computer power and memory.

2. Power Supply Unit: Sensor nodes require an autonomous functioning system, which can provide continuous power to run the system all day round. Sensor nodes always depend heavily on the power supply unit.

3. Wireless Communication Network: This network will allow the necessary communication between the sensor nodes and the gateway. They use certain standard protocols which have different coverage regions, power consumptions and suitability for different applications.

4. Sensors: The sensor node also contains sensors, which convert the physical parameter into an electrical signal to allow the microcontroller to process the filtered output data and send the data during transmissions.

2.4.3 The Gateway

The gateway is also called the “base station” of a network. It is the core of the network, and collects data from the sensor node, processes and helps to store the data to a cloud server. It also has a computing system, which is based on a high-power microcontroller or has high computing ability. It had to be static and plugged into the mains power supply, as it requires more energy than the sensor nodes. It also should have a wireless communication system, which is utilized by the sensing nodes. The gateway sends the collected data to the cloud server through Ethernet, WiFi, or 3G/4G, etc.

2.4.4 Cloud Server

The cloud server is the last component of a WSN network. It consists of a database and suitable management software. It might be located in the gateway or any other remote computer. Users can get access to the management software through the internet.

2.4.5 LoRaWAN Protocol

LoRaWAN (Long-range, low-power Wireless Area Network) is a data-link layer with long range, low power, and a low bit rate, which is a promising solution for IoT applications. A LoRa-enabled sensor node consumes low energy and transmits only a few bytes, and so is an excellent candidate for use in many different applications (such as smart healthcare, smart cities, environmental monitoring, industry, etc.). There are two distinct layers: i) a physical layer, based on radio modulation called CSS (Chirp Spread Spectrum); and ii) a MAC-layer protocol which is responsible for getting access in LoRa architecture [126]. LoRa modulation has the same characteristics as FSK (Frequency Shift Keying) regarding the communication range in between gateway and sensor node. Thus, LoRaWAN is considered as a communication protocol and network architecture, while LoRa supports the long-range link. The node's battery life, the network capacity, the QoS (Quality of Service), security and reliability are determined by the network architecture and the defined protocol. It also supports virtualized wireless networking technologies, where all base stations work together and are collectively seen by the sensor nodes [126].

2.4.6 Energy Harvesting

Sensor nodes are rarely connected to a fixed power supply; rather they are an independent, autonomous system with an energy-harvesting capability. Their energy consumption must be limited, which can be achieved by having low-consumption operating modes. Therefore, chargeable batteries are always used in WSN applications with smart modes (sleep, active). For some applications, it is also required to have a provision to collect the required energy from the environment. These are called energy-harvesting techniques [127]. Energy sources should be clean and environmentally friendly. Different energy sources are available, such as fluid flow, vibration, electromagnetic fields, and so on. However, the most-used energy source for WSN applications is photovoltaic panels or solar panels. The solar panels convert light

(sunlight or artificial light) into electricity. Batteries can store the converted electricity and utilize the energy when there is no sunlight, such as on cloudy days or at night. Sensor nodes and systems should run cleverly to extend the battery life, and therefore energy harvesting is an important factor in WSN application.

2.4.7 Challenges of IoT

A range of different sensor-nodes has provided a solid basis for experimentation with solutions to overcome the problems and challenges. However, IoT opens up new challenges that demand new capabilities and features from suitable sensor-nodes. The primary focus of Wireless Sensor Network (WSN) research was to develop advances in a WSN network, providing optimized solutions for the resource-constrained devices of which they are composed. In contrast, IoT research is to integrate these WSN systems and technologies into a globally interconnected infrastructure, moving from the currently existing Intranet to a real IoT. As a result, the challenge is for IoT solutions which can cope with an increasingly large scale. Another challenge is the growing heterogeneity of devices and device technologies. Both require new approaches to support interoperability at different layers of the communication stack for resource-constrained devices. IoT applications have increased greatly, and it is also a challenge to develop new platforms, test bed or sensor-nodes for different applications. Real-world applications and services will rely on IoT infrastructures. The realism of the environment for experimentation is becoming more important during the design of IoT. Finally, the extensiveness of the infrastructure and the potential social impact of IoT technologies call for human users to be included in the research loop-. Thus another challenge is to design a mechanism that supports adequate user involvement during experimentation.

2.4.8 Existing Sensor Nodes for IoT

The solutions to overcome the problems and challenges relevant to the wireless sensor network (WSN) research have developed widely in recent years. A variety of sensor-nodes have provided a solid basis for experimentation and moving the IoT to a globally networked infrastructure. This opens up new challenges that demand new capabilities and features from suitable sensor-nodes. In the following section, we have reviewed the currently available sensor-nodes for IoT experiments in a range of different applications [128–130]. Most of the

old sensor systems have been built using early-stage wireless sensor network platforms such as TelosB [131], Imote2 [132], MICAz and TinyOS software framework. The sensor network hardware platforms are low-power embedded microcontroller systems with some embedded sensors and analog I/O ports to connect. A set of software components also needs to be developed for IoT application, such as a real-time operating system (OS), sensor/hardware drivers, networking protocols, and application-specific sensing and processing algorithms. MoteLab2 was one of the first and longest lasting testbeds which are used by Harvard University to set up an experimental wireless sensor network [133]. INDRIYA3 is a three-dimensional wireless sensor network testbed developed at the National University of Singapore, following the same design as MoteLab [134]. SHIMMER was used for biomedical health care purposes, and it was one of the extremely flexible sensor platforms. It could expand seamlessly to meet the various biomedical research project requirements. The sensor platform had massive research potential, as explained in [135]. Imote2 was used to analyze the health of a civil structure that was capable of localizing the damage at different solutions. It selectively activates nodes in the damaged region to achieve fine-grained localization [135]. CoSMoS is another platform that was used to monitor the health and safety of construction workers. More work has been done on environmental monitoring compared to other applications. In most of the cases, they have used Arduino and Raspberry Pi which are robust, low-cost platforms for sensor-nodes [136]. Sensor4PRI is another platform where they have used a vast network based on Arduino MEGA [137] . It is also a powerful platform to analyze the sensor data. The IEEE 802.15.4 standard has the physical and medium access control layers for low data-rate wireless personal area networks. ZigBee is a low-cost, low-power, wireless mesh networking standard. It is offered as commercial-off-the-shelf (COTS) modules for developing different prototyping of wireless sensing and actuation systems. It is also used in the different applications of IoT.

Chapter 3

Interdigitated Sensing and Electrochemical Impedance Spectroscopy

3.1 Introduction

The objective of this chapter is to explain the operating principle of the sensors regarding their electrical behaviour. It also displays the phenomenon of impedance spectroscopy used to characterise the sensor and the material under test (MUT). Electrochemical impedance spectroscopy (EIS) was used as the measurement tool for the developed prototypes to determine the amount of nitrate in water. This chapter also provides a detailed insight into the EIS method. The response of the system was determined as a function of frequency to calculate the changes occurring in linear and non-linear systems. EIS served as an excellent tool for measurement, as the sensors were operated at dynamic interfaces where specific system parameters were monitored. All the subsequent chapters and the related experiments followed the EIS method to characterise the sensor.

3.2 Planar Interdigital Sensors

Interdigital sensors are made of a comb-like or finger-like periodic pattern of parallel electrodes on a solid-phase substrate. These electrodes are used to build up a capacitance which is related to the electric fields that penetrate into the test material and carry useful information about the properties of the material sample [138]. One of the most significant benefits of the planar interdigital sensors is the single-sided access to the Material Under Test (MUT). This property helps to penetrate the sample with magnetic, electric, or acoustic fields from only one side. The strength of the output signal can be controlled by changing

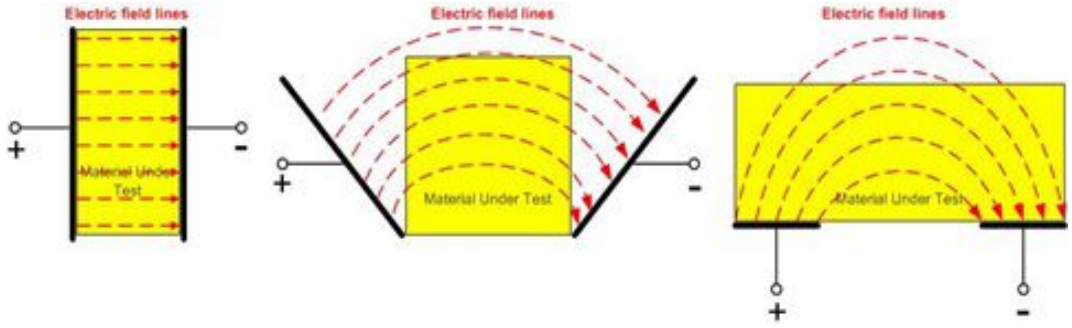

FIGURE 3.1: Gradual transition from the parallel-plate capacitor to a planar capacitor

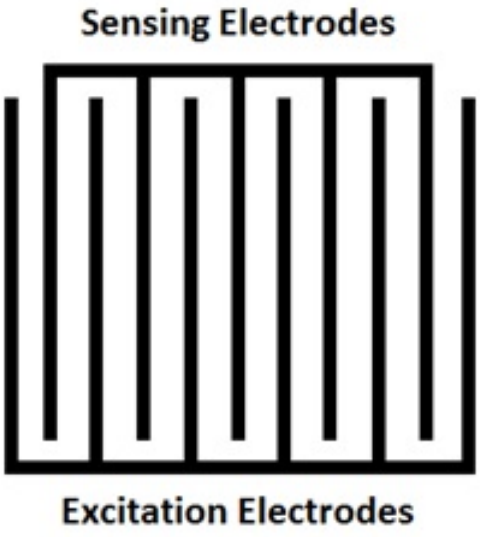

FIGURE 3.2: Geometric structure of conventional planar interdigital sensor

the area of the sensor, the number of fingers, and the spacing between them. The capability of being used for non-destructive testing is another advantage of these sensors, which makes them more useful for inline testing and process-control applications [139].

Planar interdigital sensors follow the operating principle of parallel plate capacitors. Figure 3.1 [41] shows a gradual transition from the parallel-plate capacitor to a planar, fringing-field capacitor, where the electrodes open up to provide single-sided access to the MUT. The electrode pattern of the interdigital sensor can be repeated several times, to get a stronger signal and keep the signal-to-noise ratio in an acceptable range [140]. The configuration of the conventional interdigital sensor is shown in Figure 3.2.

When an AC signal is applied as an excitation voltage to the terminals, an electric field is set up from the positive to the negative terminal. This electric field bulges through the test sample from the excitation electrode and is received by the sensing electrode, which carries

useful information about the properties of the MUT such as impedance, density, chemical composition and so on. A change in the dielectric properties of materials is a function of the chemical and physical properties of the MUT. Figure 3.3 shows the electric field formed between positive and negative electrodes for different pitch lengths- the distance between two consecutive electrodes of the same polarity. As it is illustrated in the Figure 3.3, different pitch length (l_1, l_2 and l_3) shows different penetration depth. The penetration depth improves by increasing the pitch length, at the cost of the electric field strength that will get weaker with greater distance between the electrodes at the same potential (pitch length).

3.3 Novel Planar Interdigital Sensor

Novel interdigital sensors are designed with more sensing electrodes than excitation electrodes, to increase the penetration depth of the fringing electric field. Different geometries have been studied in the research literatures [141–144]. Figure 3.4 shows the excitation pattern for a multi-sensing electrode in interdigital sensor geometry.

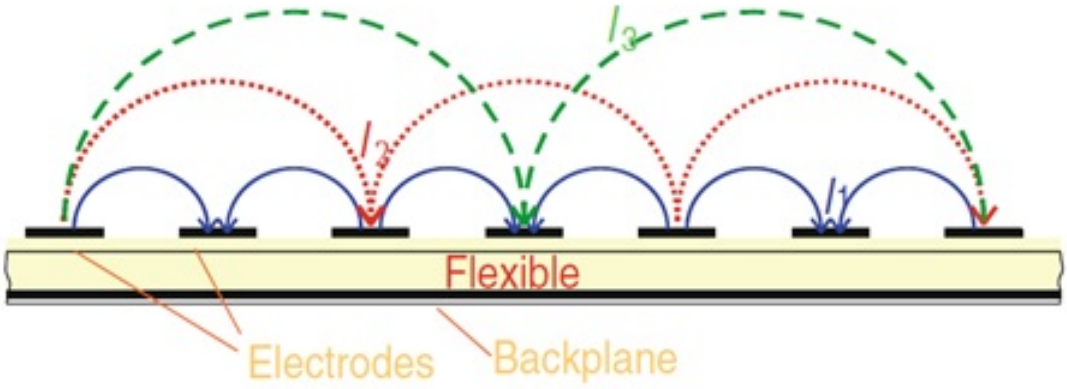

FIGURE 3.3: Electric field formed for various pitch length

The novel interdigital sensors have been fabricated based on various geometric parameters. Table 3.1 shows the geometric parameters of four different interdigital sensors and Figure 3.5 shows the schematic of the 1-5-25 and 1-11-25 configurations of newly designed planar interdigital sensors [142].

A time-dependent sinusoidal electrical perturbation is applied to the excitation electrodes

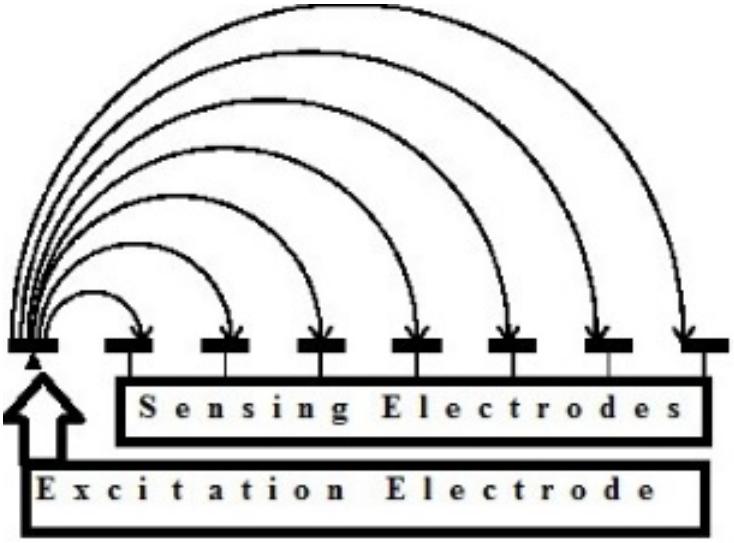

FIGURE 3.4: Schematic excitation patterns for multi-sensing-electrode interdigital sensors

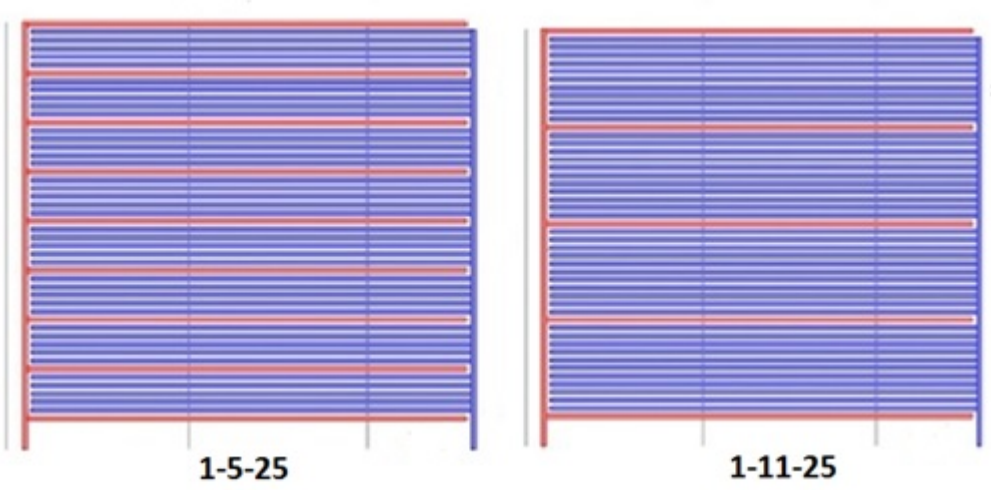

FIGURE 3.5: 1-5-25 and 1-11-25 configurations of novel interdigital sensors

of the interdigital sensor. The switching electric field bulges through the test sample via excitation electrode and is received by the sensing electrode, which carries useful information about the properties of the material under test nearby of the sensing area [138, 139]. These sensors have several applications in manufacturing process [145], environmental monitoring [141, 141, 146–148], humidity and moisture sensing system [149, 150], photosensitive detection [151] and gas sensor [152]. A sensing system was developed based on the interdigital sensor to detect the dangerous contaminated chemical in seafood [141, 143]. Another one was developed based on the electrochemical impedance spectroscopy technique to monitor the presence of phthalates in aqueous solution [146–148].

Sensor Type	Pitch Length (µm)	Number of Sensing Electrodes	Number of Excitation Electrodes	Sensing Area (mm^2)
1-5-25	25	40	9	6.25
1-5-50	50	30	7	6.25
1-11-25	25	44	5	6.25
1-11-50	50	33	4	6.25

TABLE 3.1: Geometric design parameters for four types of Interdigital sensors

3.4 Electrochemical Impedance Spectroscopy (EIS)

Electrochemical Impedance Spectroscopy (EIS) is a popular and powerful technique to measure the resistive and capacitive properties of materials by applying a small AC signal. The EIS method can be applied in non-destructive testing, label-free detection and single-sided access for different chemical analyses. Different applications of EIS have been reported such as the detection of fat contents in meat [153], biotoxins in shellfish [143, 147], bacterial endotoxins in food [154], phthalates in water and juices [147], determination of the corrosive behavior of materials [155, 156])and analysis of electrical properties for soymilk coagulation process ([157]. EIS has several applications in different research areas such as, corrosion mechanisms [158], coating evaluation [159, 160], optimization of batteries [161] and biosensing [162].

Among the methods available for impedance measurements, Frequency Response Analysis (FRA) has become a de-facto standard for EIS measurement and is a rapid approach to evaluating the impedance variation in real-time. This technique measures the impedance of the system over a wide frequency range and compares the results with reference data. In order to ensure the system stability, linearity, and repeatability, this method is viable only for a stable and reversible system in equilibrium [163–165].

3.4.1 Basic Principles of EIS

An electrochemical impedance can be measured by applying a small AC signal and then measuring the phase shift in the current signal concerning the applied potential. Electrochemical impedance is measured using a low excitation signal so that the cell's response is pseudo-linear. In a linear system, this current response to a sinusoidal excitation potential

will result in a sinusoidal current at the same frequency but shifted in phase as shown in Figure 3.6.

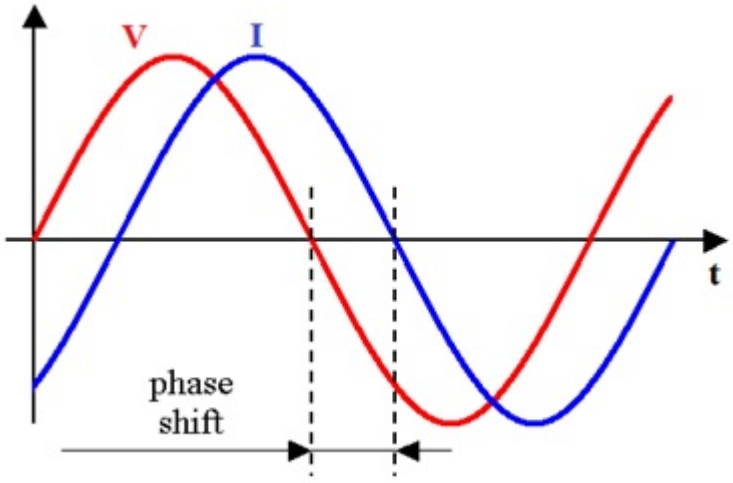

FIGURE 3.6: Phase shift in current signal with reference to the applied voltage

Impedance is defined as the measurement of the ability of a circuit to opposite the flow of electrical current when a voltage is applied. In an AC circuit, impedance is represented as a complex value, which involves real part (resistance) and imaginary part (reactance). According to the basic Ohm's law, the impedance is defined as the ratio of potential, V and current, I; $R = \frac{V}{I}$

The excitation signal can be explained as a function of time;

$$V_t = V_o sin\omega t \tag{3.1}$$

Where V_t is the voltage difference at time t, V_0 is the amplitude of the signal, and the angular frequency is ω . It is given by $\omega = 2\pi f$, with ω expressed in radians/second and frequency, f, in hertz [146]. For a linear system, the response signal, I_t, has a phase shift,θ , with an amplitude of I_o which can be explained by-

$$I_t = I_o sin(\omega t - \theta) \tag{3.2}$$

The impedance of the system can be calculated by;

$$Z = \frac{V_t}{I_t} = \frac{V_o \sin \omega t}{I_o \sin(\omega t - \theta)} = Z_o \frac{sin\omega t}{sin(\omega t - \theta)} \tag{3.3}$$

The impedance, Z, now can be expressed in term of a magnitude of Z_o and a phase shift, θ. From the above equation , it can also be expressed in term of Euler's relationship which can be given by;

$$e^{j\theta} = \cos\theta + j\sin\theta \tag{3.4}$$

The impedance, Z, can be also expressed in terms of potential, V, and current response, I. It can be written in the following manner:

$$V_t = V_o e^{j\omega t} \tag{3.5}$$

$$I_t = I_o e^{j\omega t-\theta} \tag{3.6}$$

Therefore, the impedance, Z is-

$$Z(\omega) = \frac{V_t}{I_t} = \frac{V_o e^{j\omega t}}{I_o e^{j\omega t-\theta}} \tag{3.7}$$

$$Z = Z_o(\cos\theta + j\sin\theta) \tag{3.8}$$

The impedance now is in the form of a real part $Z_o\cos\theta$ and imaginary part $Z_o\sin\theta$. The Calculated impedance characteristics can be analysed using Nyquist plot or a Bode plot.

3.4.2 Data Representation in Nyquist Plot and Bode Plot

The Nyquist plot is a popular format for evaluating electrochemical impedance data such as the electrolytic solution resistance (R_s), electrode polarisation resistance (R_p) and double-layer capacitance (C_{dl}). These parameters will be discussed in the following sections. The Nyquist plot represents the imaginary impedance component against the real impedance component at each excitation frequency and offers several advantages. The effects of the solution resistance can be observed easily using this format. One major drawback of the Nyquist plot is that there is no information about the frequency in the Nyquist plot, which makes it difficult to calculate the double layer capacitance [165].

The Bode plot represents the absolute impedance and the phase shift in the frequency domain. Since frequency appears at one of the axes, the effect of frequency on the impedance and phase shift can be studied. R_s, R_p, C_{dl} and frequency values, with phase shift, can be studied where they are maximum/minimum. The Bode plot is desirable to provide a clearer description of electrochemical cells which shows their frequency-dependent behaviour, unlike the Nyquist plot.

3.4.3 Randle's Electrochemical Cell Equivalent Circuit Model

Randle's equivalent circuit is the most frequently discussed equivalent circuit [166] used to interpret EIS experimental results in electrical form and shown in Figure 3.7. It consists of a solution resistance R_s in series with the parallel combination of the double layer capacitance C_{dl} and the charge transfer resistance R_{ct} in series with the Warburg impedance Z_w [161].

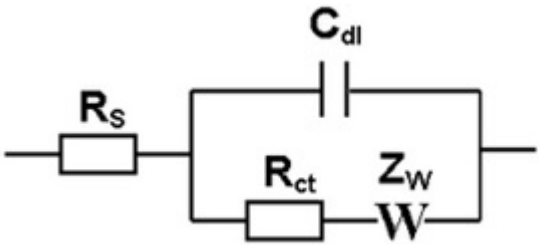

FIGURE 3.7: Randle's equivalent circuit model

This model was introduced by Randle in 1947 [167] and it can be used to describe both kinetics and diffusion processes taking place at the electrode-electrolyte interface. The

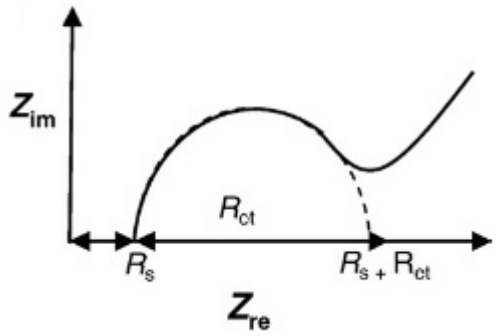

FIGURE 3.8: The Nyquist plot for the Randle's equivalent circuit

Nyquist plot from the equivalent circuit consists of a semi-circular region followed by a 45º straight line, as shown in Figure 3.8. In this model, the impedance of a faradaic reaction consists of an active-charge-transfer resistance R_{ct}, and a specific electrochemical element of diffusion, which is called the Warburg element. The semi-circular region represents a slower charge transfer at higher frequencies, whereas the straight line describes a faster mass transfer at lower frequencies. R_{ct} can be calculated by extrapolating the semicircle to Z_{real} axis. The solution resistance R_s can be calculated by reading the real axis value at the high-frequency intercept, which is the intercept near the origin of the Nyquist plot. R_{ct} can be calculated by

extrapolating the semicircle to the Z_{real} axis as illustrated in Figure 3.8. C_{dl} can be obtained from the frequency at the maximum of the semicircle portion in the Nyquist plot using [166]

$$\omega = \frac{1}{R_{ct}C_{dl}} \tag{3.9}$$

The complex impedance as a function of frequency is given as

$$Z(\omega) = R_s + \frac{R_{ct}}{1 + \omega^2 R_{ct}^2 C_{dl}^2} - \frac{j\omega R_{ct}^2 C_{dl}}{1 + \omega^2 R_{ct}^2 C_{dl}^2} \tag{3.10}$$

Where the real part ($Z^{'}$) is given by

$$Z^{'} = R_s + \frac{R_{ct}}{1 + \omega^2 R_{ct}^2 C_{dl}^2} \tag{3.11}$$

and the imaginary part ($Z^{''}$) is given by

$$Z^{''} = -\frac{\omega^2 R_{ct}^2 C_{dl}}{1 + \omega^2 R_{ct}^2 C_{dl}^2} \tag{3.12}$$

The rate of an electrochemical reaction can be strongly influenced by diffusion of reactants towards, or away from, the electrode-electrolyte interface. This situation can exist when the electrode is covered with adsorbed solution components, or a selective coating. An additional element called the Warburg impedance, Z_w, appears in series with resistance R_{ct}. Mathematically the Warburg impedance is given by

$$Z_w = \frac{\sigma_w}{\sqrt{\omega}} \tag{3.13}$$

where σ_w is the Warburg diffusion coefficient. The diffusion of reactants to the electrode surface is a slow process, which can happen at low frequencies only. However, at higher frequencies, the reactants do not have enough time to diffuse. The slope of this line gives the Warburg diffusion coefficient.

3.5 Chapter Summary

This chapter gives a summary of the working principle of the sensor prototypes. Electrochemical Impedance Spectroscopy was used as the technique to monitor the responses of the sensor for nitrate measurement. The impedance analysers were chosen to do the measurements for the linear and non-linear systems in the succeeding chapters.

Chapter 4

Temperature Compensation for Low Concentration Nitrate Measurement

4.1 Introduction

This chapter has taken from some papers([1], [2], [3]) and describes the design and development of a portable sensing system that could be used in-situ to detect the concentrations of nitrate present in groundwater. Electrochemical Impedance Spectroscopy (EIS) was employed to identify and display nitrate concentrations by using a planar interdigital sensor immersed in the stream's water samples. Calibration samples were prepared by serial dilution of nitrate stock solution in the laboratory, and test samples were collected from different surface-water sources. The test samples were evaluated by commercial equipment and designed system. Although a difference was observed between these two results, the designed system showed a good linear relationship between the measured nitrate-concentrations (range from 0.1 to 0.5 mg/L) of the water solution in the real part of the impedance. The promising comparative results showed the extraordinary potential of the developed system for its in-situ nitrate contamination detection with real-time monitoring. The temperature-compensation capability is added to the system to compensate for any change of measurement due to

[1] **Alahi, Md Eshrat E.**, Li Xie, Subhas Mukhopadhyay, and Lucy Burkitt. "A temperature compensated smart nitrate-sensor for the agricultural industry." IEEE Transactions on Industrial Electronics 64, no. 9 (2017): 7333-7341.

[2] **Alahi, Md Eshrat E**., Li Xie, Asif I. Zia, Subhas Mukhopadhyay, and Lucy Burkitt. "Practical nitrate sensor based on electrochemical impedance measurement." In Instrumentation and Measurement Technology Conference Proceedings (I2MTC), 2016 IEEE International, pp. 1-6. IEEE, 2016.

[3] **Alahi, Md Eshrat E.**, Xie Li, Subhas Mukhopadhyay, and L. Burkitt. "Application of practical nitrate sensor based on electrochemical impedance spectroscopy." In Sensors for Everyday Life, pp. 109-136. Springer, Cham, 2017.

temperature changes in water. The WiFi-based Internet of Things (IoT) has been included, making it a connected sensing system. The system is capable of sending data directly to an IoT-based web server, which will be useful to develop distributed monitoring systems in the future. The developed system has the potential to monitor the impact of the industrial, agricultural or urban activity on water quality, in real time.

4.2 Fabrication of Sensor

The sensors were fabricated with two pitch lengths, and 50 µm, respectively. Two repeated patterns of 1 excitation, five sensing electrodes and one excitation and 11 sensing electrodes. The interdigital sensor was fabricated by DC magnetron sputtering process on a single silicon wafer which was p-doped, 4-inch diameter and 525 µm thick. The dimension of the sensor was 10mm x 10mm; sensing area was 2.5 mm x 2.5 mm, and the electrodes width was 25 µm. One silicon wafer can produce 36 sensors.

All patterns were printed on 5-inch soda lime transparent mask using a laser mask writer. 150°C heat was performed on the wafer substrate to attach the photoresist better on the surface. A spin-coated was used to coat 4 µm of positive photoresist on a 4-inch wafer. 100°C for 1 minute was used for post-baking temperature. The design of the sensor pattern was transferred to the photoresist of the wafer by exposing UV light. The wafer was then developed under a solution of Tetra-Methyl Ammonium Hydroxide (TMAH) for one minute.

"Descum" process was used to remove residual photoresist during the plasma etching at 70°C. Following this, 20nm of Chromium (Cr) and 500 nm of Gold (Au) were sputtered on the wafer substrate by sputtering. Gold electrodes have the advantage of being inert and flexible and act as a barrier layer for proper adhesion.

The next step was "Lift-off" which was performed under a solution of acetone. Figure 4.1 shows the steps involved in the fabrication process of the sensor.After lift-off,1 µm Parylene C was used as a coater. The passivation layer is required to protect the sensing area from corrosion by the sample solution during the experiment. Another purpose of using Parylene C on the sensing surface is to protect the sensor from oxidation due to moisture and Faradic currents. Laser cutting was used for dicing the sensor from each other.

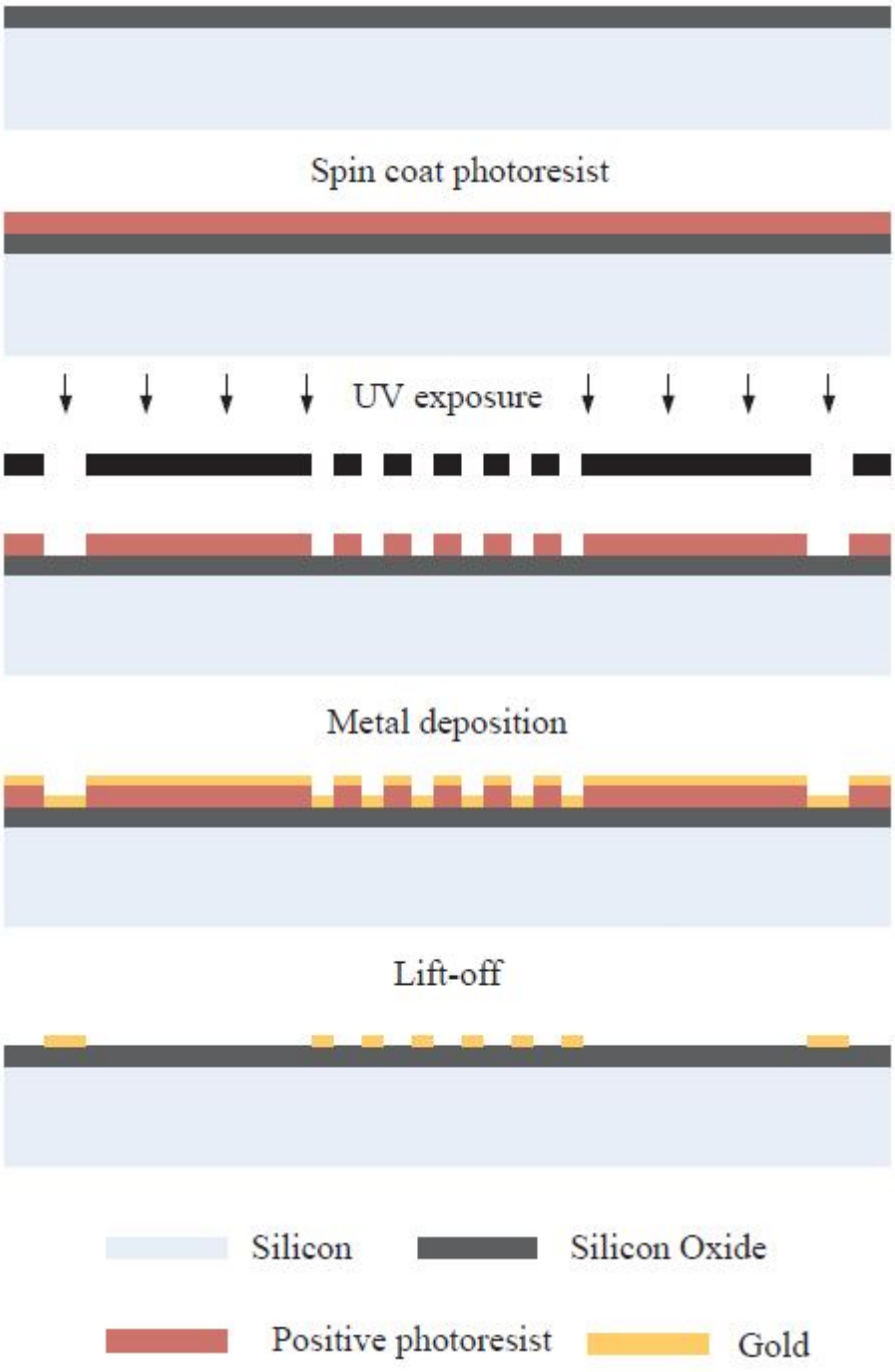

FIGURE 4.1: Fabrication process of the sensor

4.3 Experimental Setup

4.3.1 MEMS based Sensor

The interdigital sensor with thin-film coated layer of Parylene C was used as shown in Figure 4.3 and the schematic diagram is shown in Figure 4.2. The configuration is 1-5-50,

which means a repeated pattern of five sensing electrodes is present on one excitation electrode with a distance of 50 µm between two consecutive electrodes. The working principle and EIS measurement of the sensor was explained in Chapter 3.

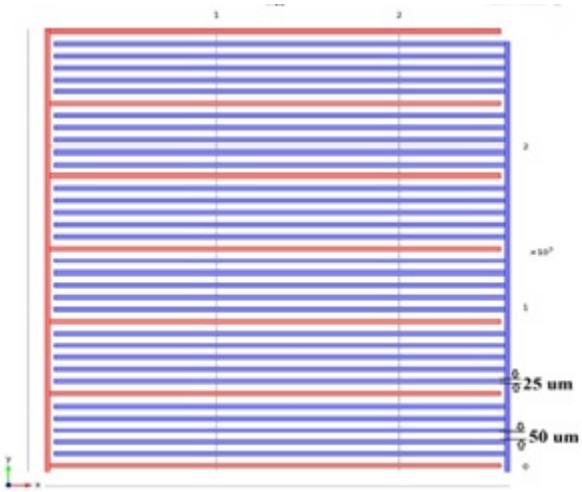

FIGURE 4.2: Sensor configurations (1-5-50)

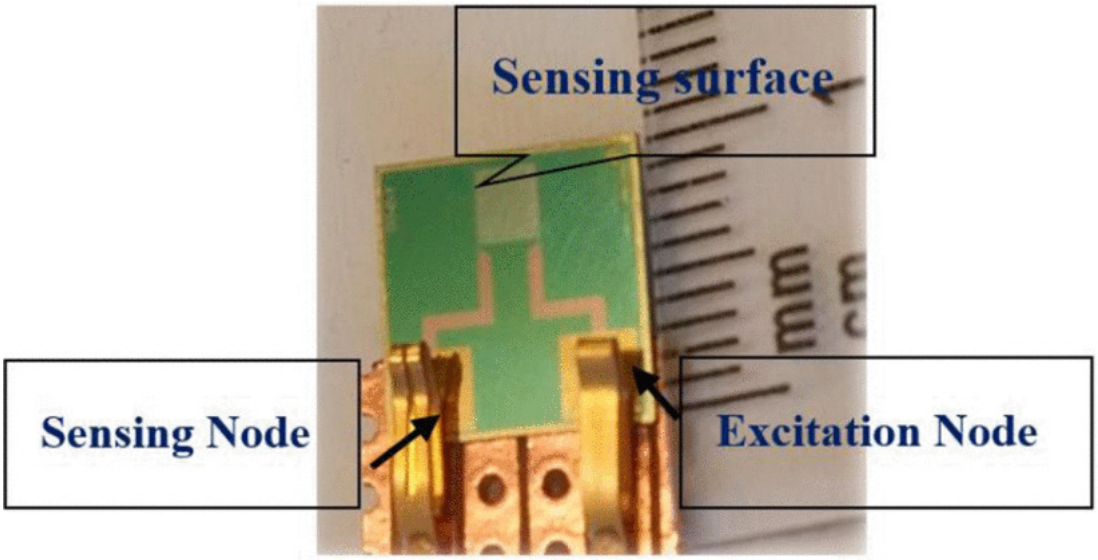

FIGURE 4.3: Interdigital sensor with Parylene Coating

4.3.2 Temperature Measurement

The impedance profile of water changes due to the change of temperature. Temperature also affects the mobility of ions in water [168]. Therefore, it is essential to measure the changing behavior of the sensor at different temperatures. Figure 4.4 shows the experimental setup

involving a high precision Hioki 3522-50 LCR meter, Hioki 4-terminal probe 9140, mercury thermometer, SCILOGEX MS 7-H550 Digital Hotplate and computer for data acquisition. The mercury thermometer was immersed in deionized water to obtain a continuous temperature reading. Meanwhile, the sensing surface was also immersed in water and collected data when the temperature reached a steady value. The frequency was swapped from 10 Hz to 10000 Hz, to characterize the sensor under different temperatures.

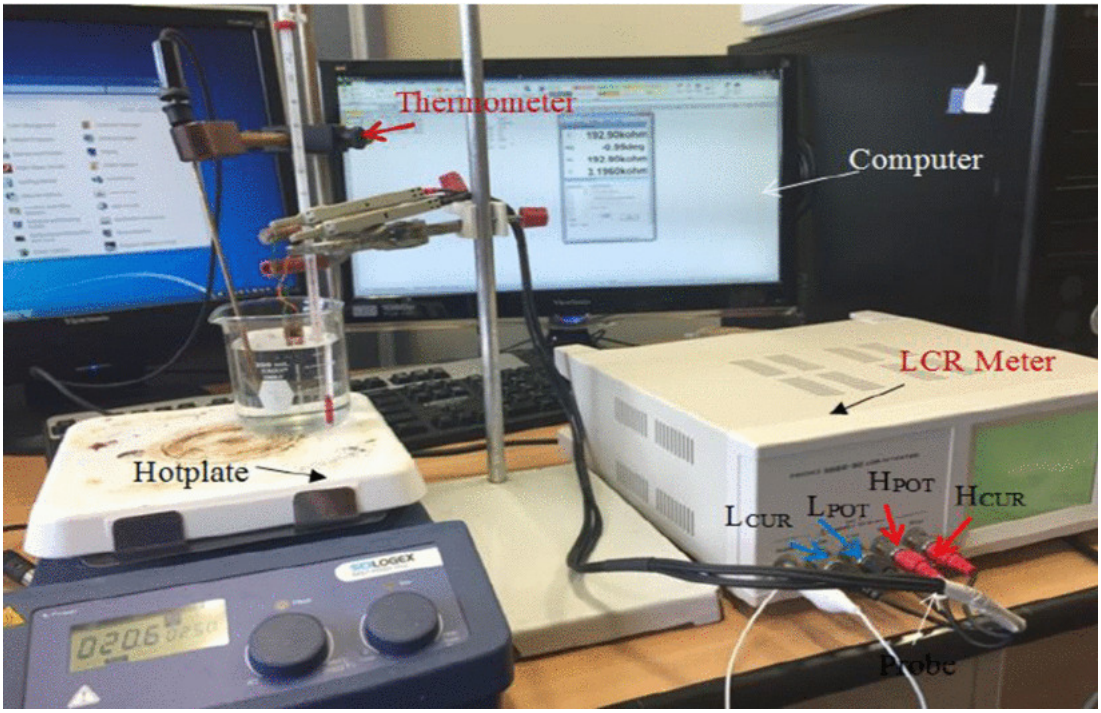

FIGURE 4.4: Experimental arrangement for temperature measurement

4.3.3 Nitrate Measurement

Figure 4.5 shows the experimental setup for nitrate-N concentration measurement. Experiments were executed at ambient conditions of temperature and humidity. The 12-Volt DC battery was used as a power source for the main circuit board, water pump, and solenoid valve. Arduino Yun was used to generating the sinusoidal waveform that was the input signal for the sensor and to performs data acquisition. The sensing part of the sensor was immersed into calibration standard samples with different $NO_3 - N$ concentrations to create references and later water samples collected from a stream near Palmerston North; New Zealand was tested based on the calibration plot obtained from the standard solution. The electronic circuit was designed to get the input and output voltage of the sensor and to detect the phase shift

between the incident and signal received through the sensor. The ions in the nitrate get polarized towards the plates according to their charge [141]. The experiments were conducted in laboratory conditions; two water pumps were used. The pumps were connected to the motor from one being used to pump the water sample into the container for measurement at every 15 minutes, and another one was used for discharging the sampled water from the container after one minute. The microcontroller calculated the sensor's impedance. The detailed explanation is described in the succeeding section.

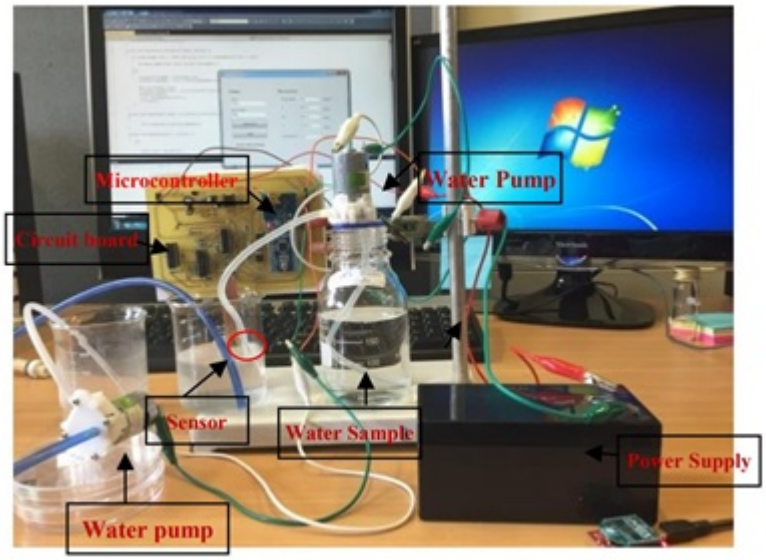

FIGURE 4.5: Experiment setup for nitrate detection

4.4 Sensing System

The sensing system was assembled, as a combination of different circuits performing required operations as described in the following sections.

4.4.1 Block Diagram of the Sensing System

Figure 4.6 shows the block diagram of the designed system. In this system, the sinusoidal waveform was generated by using PWM (pulse width modulation) output combined with a bandpass filter, which is based on the concept of the Direct Digital Synthesis (DDS) method. This method was implemented by breaking a waveform into discrete points digitally [169]. Two hundred and fifty-six (8 bits) points were used to produce a sinusoidal waveform that

gave a compromise between resolution and frequency. The operating frequency was fixed at 120 Hz.

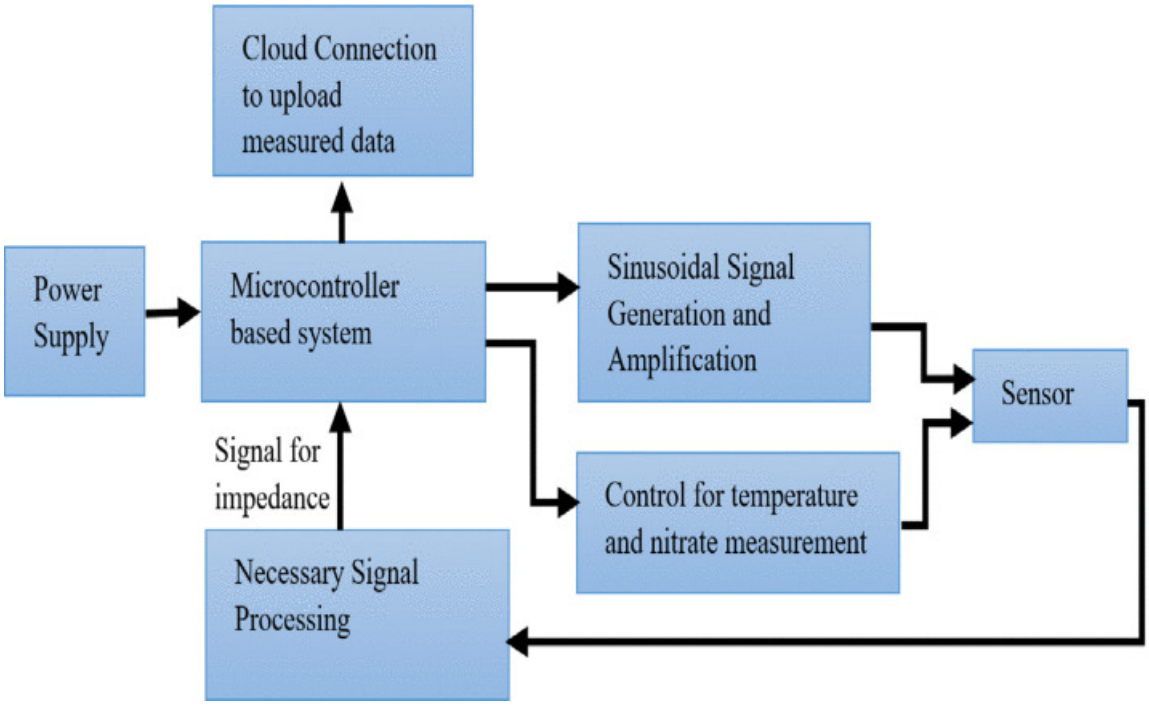

FIGURE 4.6: Block diagram of the designed system

4.4.2 The Signal Generator

The sinusoidal waveform was generated by using PWM output combined with a bandpass filter based on the concept of the Direct Digital Synthesis (DDS) method. DDS was implemented by breaking a waveform into discrete points digitally; the more points were taken and the higher precision of DAC [170]. 256 (8 bits) points were used to produce a sinusoidal waveform that gave a compromise between resolution and frequency. As resolution increased, the maximum achievable frequency decreased. With the full resolution (255), the maximum PWM frequency was reached. The duty cycle and the pulse width of the digital signal were optimized to generate different analog levels, [171]. By reading these points to generate a sinusoidal waveform, the value of Output Compare Registers (OCR0) was changed. The bandpass filter is shown in Figure 4.7 was employed to generate the smooth sine wave, and the cut-off frequency was set between 106Hz and 338Hz. After filtering, the smooth sine wave was generated, and its frequency was fixed at 120 Hz defined by the value of Output Compare Registers (OCR1A as Timer 1 used).

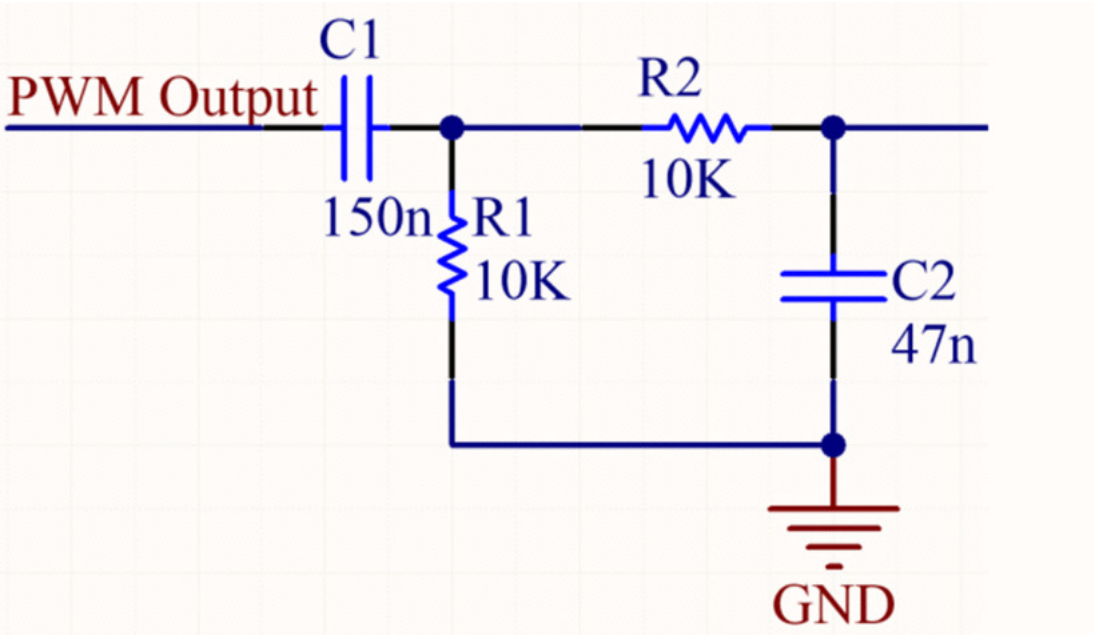

FIGURE 4.7: Band- Pass Filter connected to PWM output

4.4.3 Frequency Response Analysis Circuit

Due to the capacitive nature of the interdigital sensor, a resistor (R_s) was connected to the sensor in series to determine the output voltage across the sensor. The value of the series resistor is significantly small so that the effect of it can be negligible. Figure 4.8 illustrates the equivalent circuit diagram of the interdigital sensor. Based on Ohm's law, the current (I_s) flows through the sensor can be calculated by-

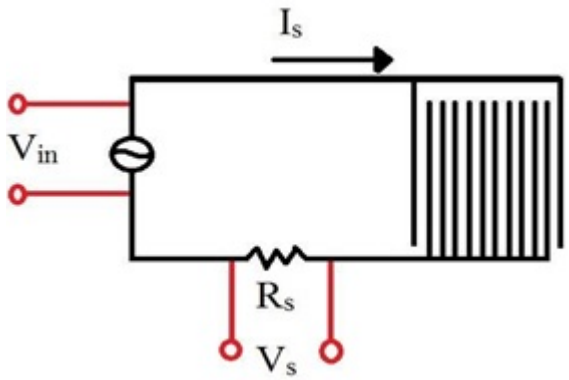

FIGURE 4.8: Circuit diagram of interdigital sensor

$$I_s = \frac{V_{in}}{Z} \tag{4.1}$$

where V_{in} is the voltage applied to the sensor, Z is the total impedance of the circuit. The

sensing voltage V_s which measured across the series resistance can be calculated by-

$$V_s = I_s R_s = \frac{V_{in}}{Z} R_s \tag{4.2}$$

where, R_s is the series resistance, used for measurement of sensing voltage. The active low-pass filter is shown in Figure 4.9 was employed to reduce the noise and amplify the signal with a gain of 11 by using $R20$ and $R21$. The buffer circuit is used in order to reduce the signal reflection from the load and transfer maximum power from the input.

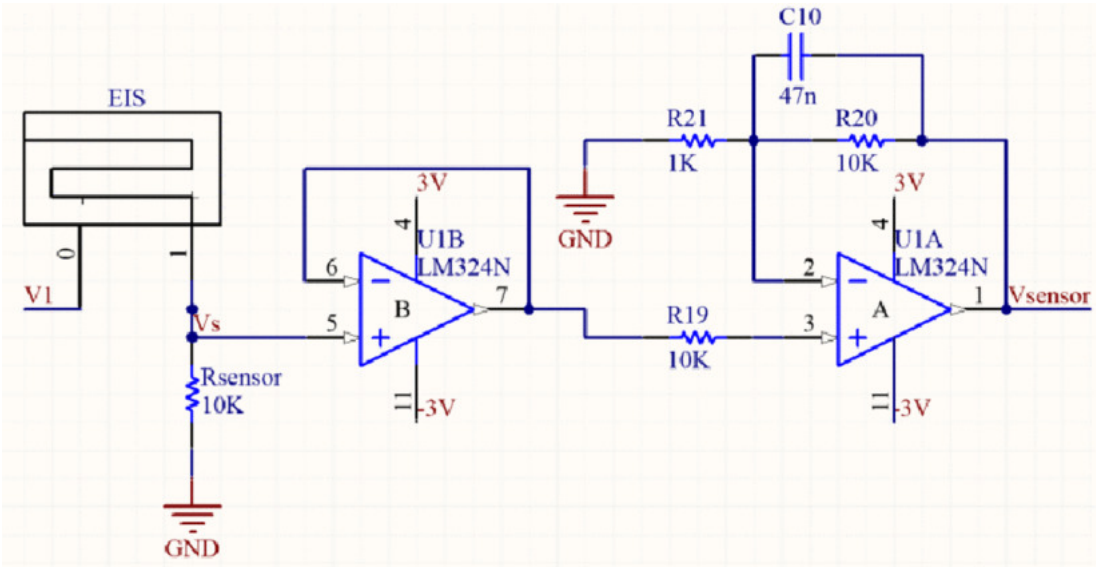

FIGURE 4.9: Amplification circuit

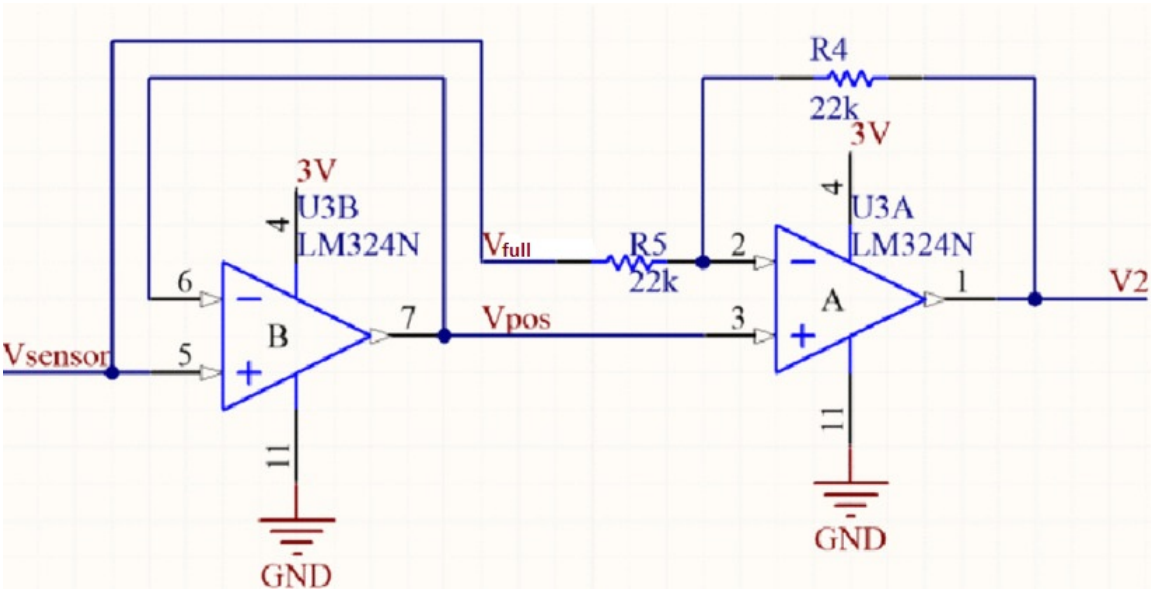

FIGURE 4.10: Full rectifier circuit

The impedance of the sensor can be calculated from the following relationship-

$$Z = \frac{V_{in}}{I_s} = \frac{V_{in}}{V_s} R_s \tag{4.3}$$

The voltage applied to the sensor V_{in}, and the voltages across the sensor V_s were measured, and micro-controller calculated Z. Series Resistor R_s was used at 10 kΩ, which is significantly small compared to Z. The precision rectifier is shown in Figure 4.10 was employed to reduce the voltage loss because the V_{sensor} was very small. The output voltage (V_{sensor}) was full sine wave fed into two operational amplifiers as shown in Figure 4.10. Only positive half waves were generated from the first op-amp. When $V_{sensor} > 0$, only positive half wave is generated from the first op-amp and $V_{pos} = V_{sensor}/2$. The second op-amp worked as a subtractor,$V_{pos} = V_{full}/2$ (where, $V_{sensor} = V_{full}$) when $V_{sensor} > 0$, $V_2 = V_{full} - V_{pos} = V_{full}/2$; when $V_{sensor} < 0$, $V_2 = 0 - (-V_{full}) = V_{pos}$; Therefore the output V_2 is full wave rectified and fed into the microcontroller. The R_s is a resistive element, so there is no phase difference between V_s and I_s. The phase angle between V_{in} and I_s is the same phase angle between V_{in} and V_s. To measure the phase angle (ϕ) between V_{in} and I_s, LM339 consisting of four voltage comparators was used as hysteresis comparator with zero reference voltage as seen in Figure 4.11. The purpose of using LM339 is to convert the V_{in} and V_s to square wave to calculate the phase angle in between them. It is also useful to reduce undesirable transitions caused by the noisy input signal.

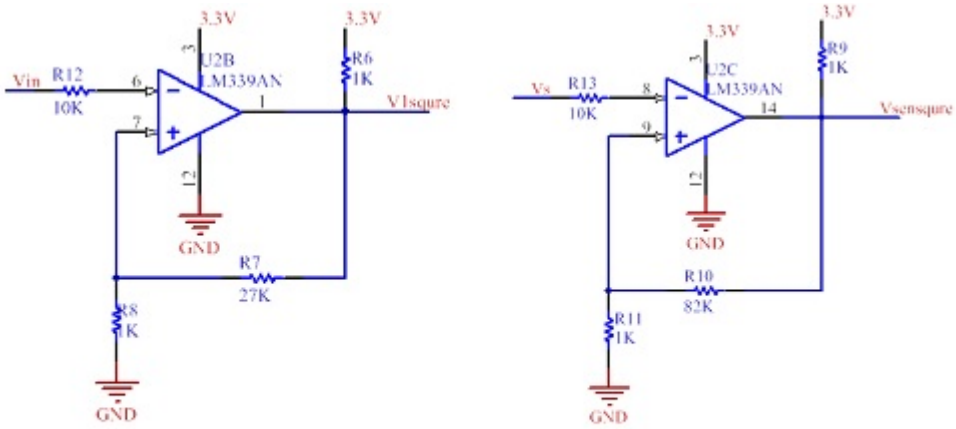

FIGURE 4.11: Zero-Crossing circuits

The real part (R) and imaginary part (X) of impedance can be calculated by:

$$R = Z \cos \phi \tag{4.4}$$

$$X = Z \sin \phi \tag{4.5}$$

where R and X are the resistance and reactance of the circuit. Therefore, the resistive part of the sensor (R_{sensor}) is calculated by:

$$R_{sensor} = R - R_s \tag{4.6}$$

To measure the phase angle (ϕ) between V_{in} and I_s, the Schmitt Trigger was used as zero crossing detector (ZCD). The Schmitt Trigger is based on the hysteresis comparator with zero reference voltage is shown in Figure 4.11. The purpose of employing the Schmitt Trigger was to convert the sinusoidal waveform to square waveform which can be easily read by the microcontroller and can reduce awkward transitions caused by the noisy input signal.

4.4.4 Controlling of Pump and Solenoid Valve

For field trial, it was planned to pump water into the sample container and to collect the impedance data. The water then was pumped out of the sample container. It was done to avoid the sensor to be continuously dipped in water. The water pump and solenoid valve were switched by two MOSFETs which were controlled by micro-controller signals shown in Figure 4.12 at certain time intervals. As the water pump required an input voltage of 5 volts, the PWM with 40 % duty cycle was applied to the microcontroller output pin and then provided 5-volt excitation to the water pump required for its operation.

4.4.5 IoT-based Smart System

The IoT [172] offers promising solutions to transform the operation and role of existing industrial technologies. IoT is already having an impact in the areas of agriculture, food processing, environmental monitoring, security surveillance and others [173]. The proposed Arduino Yun has integrated WiFi which can provide instant connectivity to the Internet. WiFi offers high bandwidth, large coverage area, non-line-of-sight transmission, easy expansion, cost-effectiveness, robustness and small distribution of Links [174]. An external antenna (2.4 GHz) is added to increase the transmission signal strength. The collected data is transmitted to Thingspeak [175] which is the open data platform for the IoT. HTTP POST [176] protocol has been used to send data directly to the specified server. Figure 4.13 shows the final IoT-based smart sensing system with a smart sensor which has been used to measure nitrate and upload the data on the designated website.

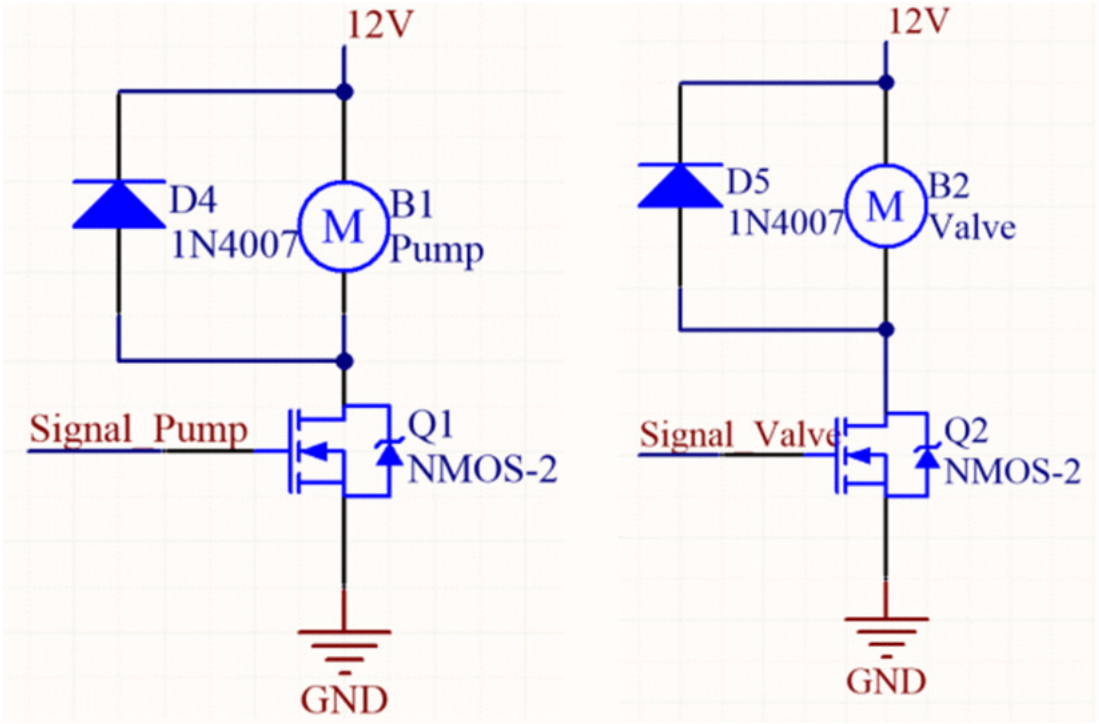

FIGURE 4.12: Water pump and solenoid valve for sample flow control

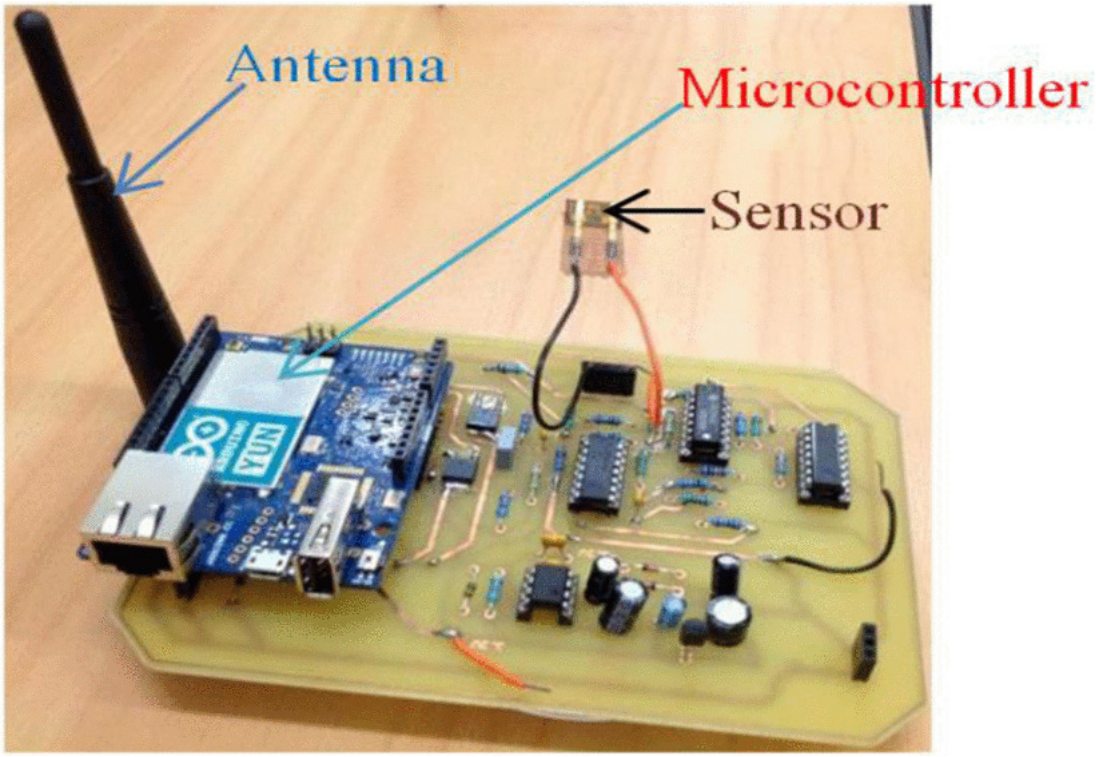

FIGURE 4.13: IoT enabled Smart sensing system

4.5 Results and Discussions

4.5.1 Measurement of Temperature

The same sensor was used to measure the temperature of water. The real impedance (Rs) and imaginary impedance (X) were evaluated and plotted in Figure 4.14. The X-axis shows the resistance part of impedance in ohms (Ω), and the Y-axis shows the reactance part of the impedance in ohms(Ω). The total impedance is decreased with the increase in temperature. The Nyquist plot (Figure 4.14 13) indicates the impedance at a specific frequency.

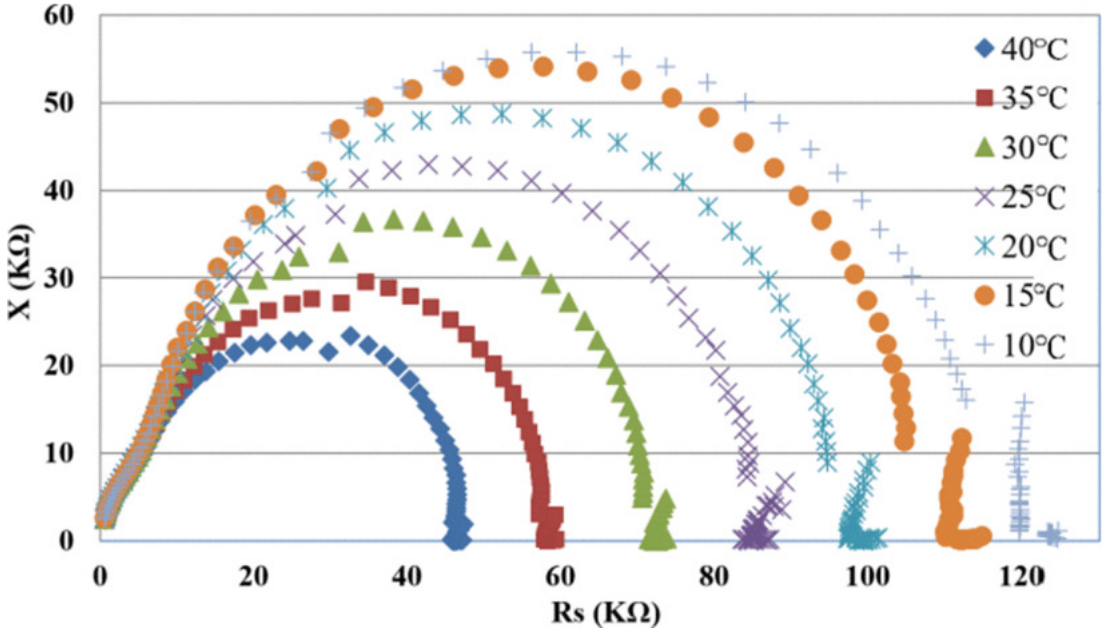

FIGURE 4.14: Nyquist plot of impedance at variable temperatures

Figure 4.15 shows the relationship between the real part of impedance and the frequency. It is seen from the figure that the resistance is decreased with increasing temperature, and the sensitive range is significant till 400 Hz. Figure 4.16 shows the imaginary part of impedance (X) of deionized water to changing temperature, plotted against frequency. The dielectric properties of the deionized water at different temperatures was measured by using this approach. The experiment was repeated five times to observe impedance behavior and to calculate average results. Figure 4.17 shows the measured resistance as a function of the ambient temperature, which is almost linear. The slope can be calculated by equation 4.7:

$$Slope = \frac{\Delta R}{\Delta T} = \frac{R_{40} - R_{10}}{T_{40} - T_{10}} \tag{4.7}$$

where, R_{40}: The resistance value measured at $40°C$, R_{10}: The resistance value measured

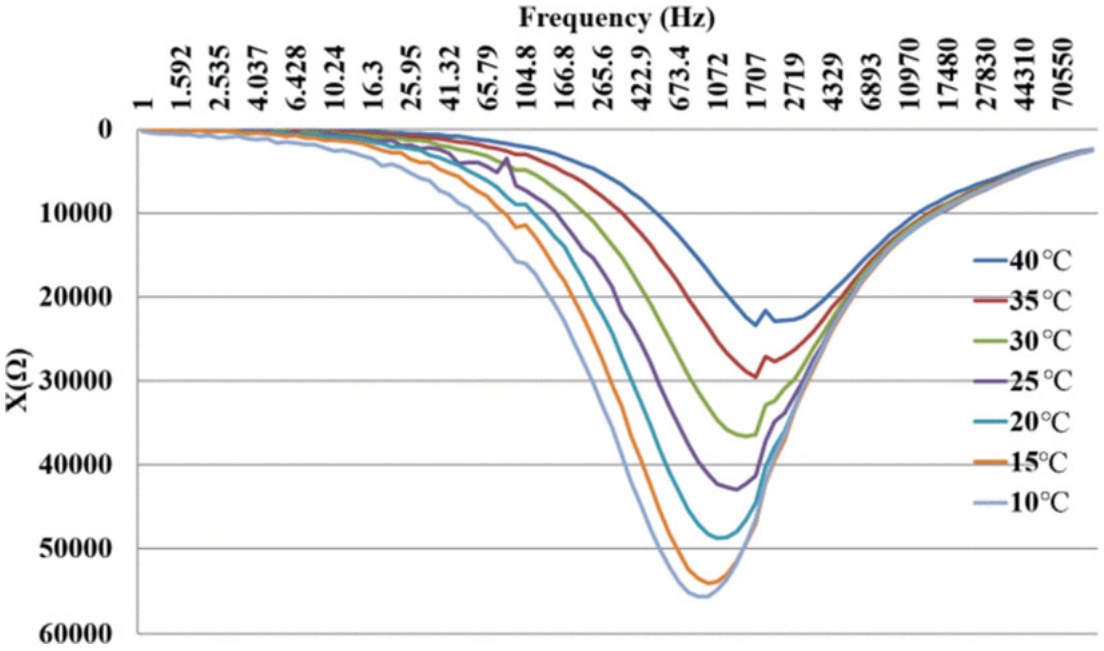

FIGURE 4.15: Imaginary part of impedance as a function of frequency

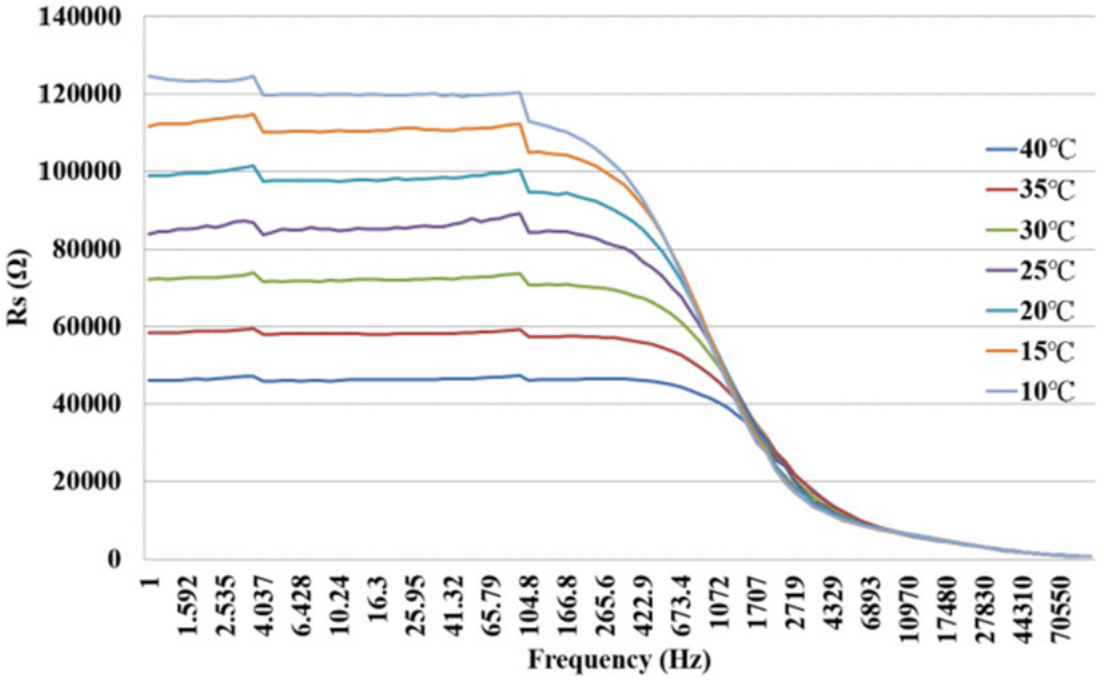

FIGURE 4.16: Real part of impedance vs. frequency under variable temperature

at $10°C$, T_{40}: The temperature at $40°C$, and T_{10}: The temperatures at $10°C$. Therefore, the slope for the resistance part is calculated as : $-\frac{42392.83-118037.76}{40-10} = -2521.498$. It is to be noted that all the resistance of impedance measurements are taken at the same frequency

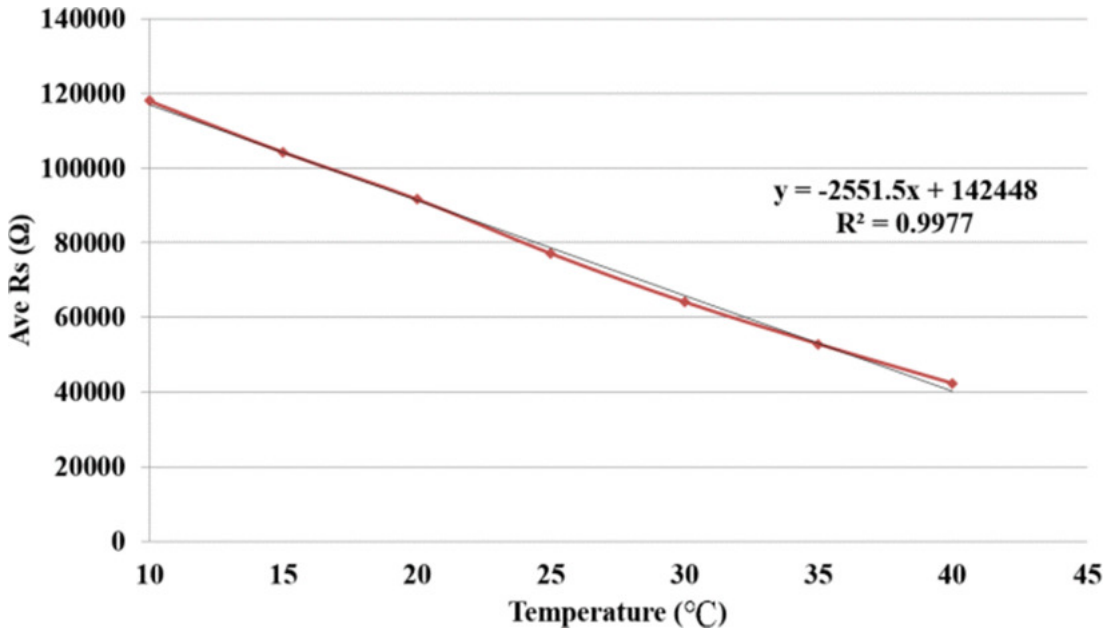

FIGURE 4.17: Resistance as a function of temperature at a frequency of 122.5 Hz

(122.5 Hz). Therefore, the temperature can be measured by the following equation:

$$T = \frac{R_T - R_{20}}{slope} + T_{20} \tag{4.8}$$

where, R_T is the measured resistance value, R_{20} is the resistance value at $20°C$ (which is the reference value), and T_{20} is the reference temperature at $20°C$. Figure 4.18 displays the correlation between the actual temperature and the calculated temperature. The calculated temperature is well correlated with the resistance ($R^2 = 0.99$) part and reactance part ($R^2 = 0.99$), respectively.

4.5.2 Nitrate Measurement and Standard Equation Development

The sensing system has been used to detect the concentration of nitrate in water. In the laboratory, samples of different concentrations of ammonium nitrate have been prepared by a serial dilution method with the concentration varying from 0.1 to 0.5 mg/L. The impedance of the sensor is measured using electrical impedance spectroscopy technique, and the results are plotted in the Nyquist plot (Figure 4.19) when the frequency is restricted to 100 KHz. The impedance of the sensor reduces with increased nitrate concentration. Figure 4.20 and Figure 4.21 shows the real part and imaginary part of impedance as a function of operating frequencies, for different nitrate concentrations. The real part of impedance shows a significant change in their value for different concentrations at low frequencies. The

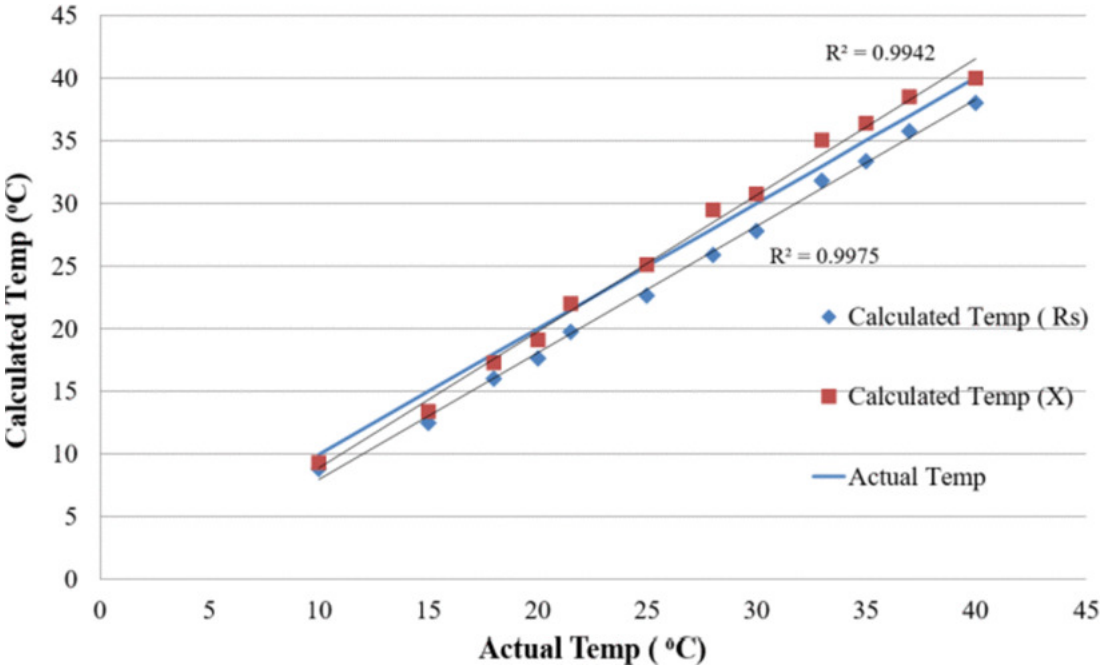

FIGURE 4.18: Comparison between the actual temperature and the measured temperature

imaginary parts do not show much change at low frequencies. Since ionic components play a significant role, the real part of impedance is used to determine the nitrate concentration. The following equation is considered as the standard curve:

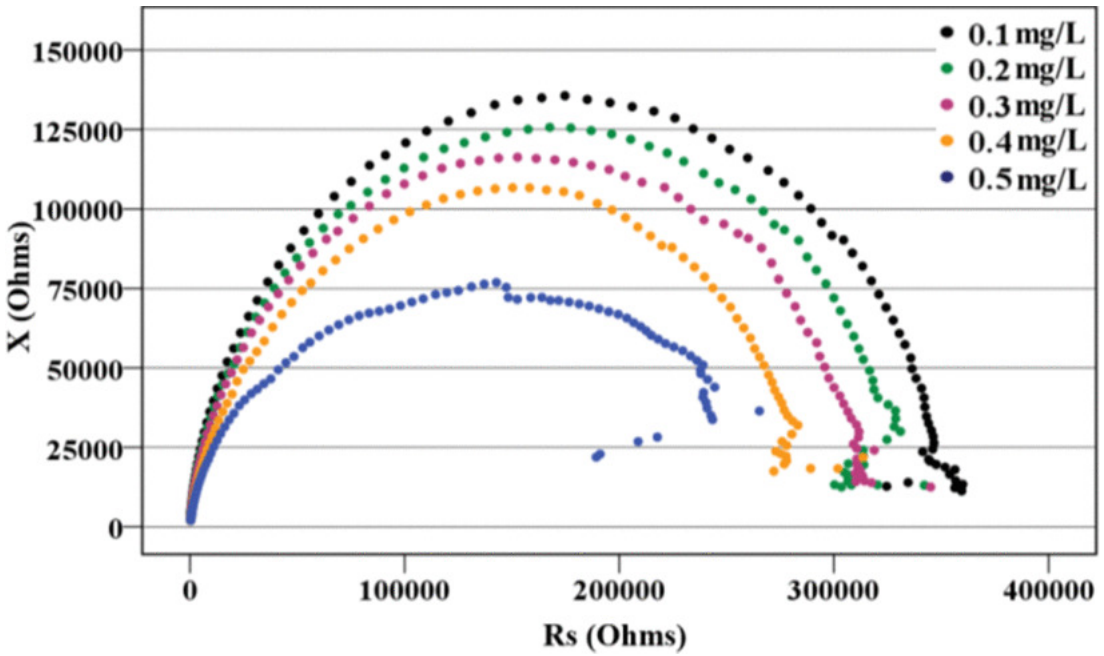

FIGURE 4.19: Nyquist plot for Ammonium Nitrate (NH4NO3) at different concentrations

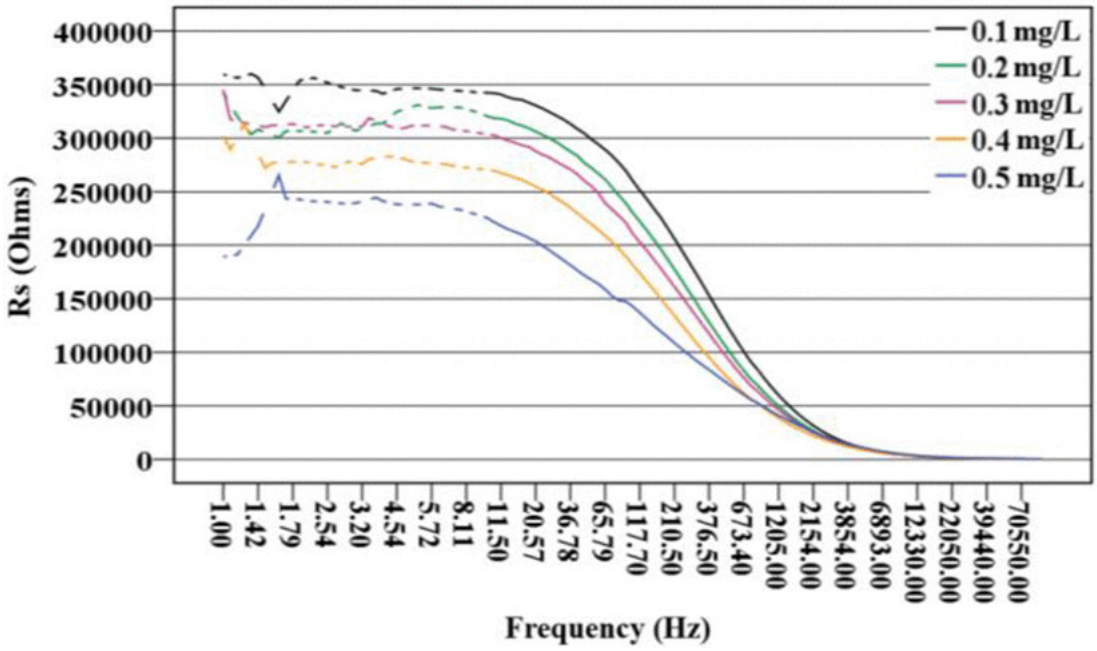

FIGURE 4.20: Real part of impedance as a function of frequency

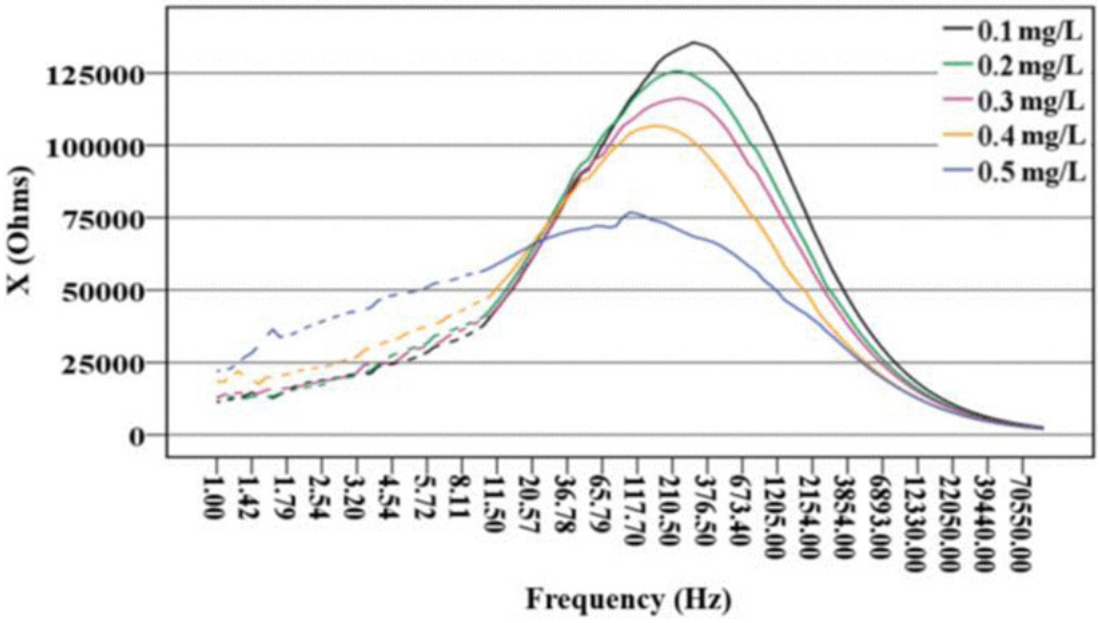

FIGURE 4.21: Imaginary part of Impedance as a function of frequency

$$C = \frac{R - R_{0.3}}{-115543} + C_{0.3} \tag{4.9}$$

where R is the real impedance of the sensor using water samples, $R_{0.3}$ is the real part of the impedance at 0.3 mg/L and $C_{0.3}$ represent the concentration of 0.3 mg/L, which is assumed as a reference. Substituting the value of $R_{0.3}$ and $C_{0.3}$, the concentration was calculated by:

$$C = \frac{R - 48056.78}{-115543} + C_{0.3} \tag{4.10}$$

Since the sensor is very sensitive to temperature change, the relationship between the resistance (R) and the temperature (T) can be used as a correction factor for the changing rate of R on changing T. Therefore, using the correction factor, the R_{actual} is modified by:

$$R_{actual} = R + \alpha(T - T_{20}) \tag{4.11}$$

where T_{20} is the temperature at $20°C$. R is replaced with R_{actual} to calculate the final computational formula of nitrate-N concentration. Therefore, the standard formula to calculate concentration with a correction factor for the Parylene coated sensor can be represented as follows:

$$C = \frac{R_{actual} - 48056.78}{-115543} + 0.3 \tag{4.12}$$

This equation has been used to estimate the nitrate concentration in an unknown sample.

4.5.3 Stream Water Testing

The next experiment was conducted with stream water samples using the developed sensing system. The water was collected from different streams and was analysed for nitrate using the spectrophotometric method in the laboratory. The developed standard formula in has been used to calculate the concentration using the designed system. Table 4.1 Comparison of nitrate concentrations measured by the sensor system and the spectrophotometric laboratory method shows the results from the designed system and the laboratory spectrophotometric method. The spectrophotometric method was taken as the standard laboratory measurement. The stream water samples not only contain nitrate, but also contain phosphates, ammonium, and other mineral salts. It explains the differences between these results. Despite this, the maximum error is less than 10% and is low, the reasons being (i) the calibration of the sensor was done based on nitrate measurement and (ii) the influence of other ions is not strong concerning the nitrate ions.

TABLE 4.1: Comparison of nitrate concentrations measured by the sensor system and the spectrophotometric laboratory method

Lab Number	Description	Spectrophotometric method (mg/L)	Sensor system (mg/L)
S202	Stream entering farm	0.50	0.53
S204	Stream entering wetland	0.49	0.53
S206	Stream paddock 9	0.47	0.51
S207	Stream paddock 10	0.47	0.52
S209	Stream exiting farm	0.50	0.55

4.5.4 Data in Cloud Server

In the fourth experiment, the interval time of pump in and pump out of the sample water was 10 minutes and initially deionized water was pumped out and then 0.5 mg/L Ammonium Nitrate (NH_4NO_3) solution was pumped out for the rest of the period. The microcontroller collects the data and sends the final measured data to the Thingspeak server. Figure 4.22 shows the real-time data which has been sent from the developed smart sensing system.

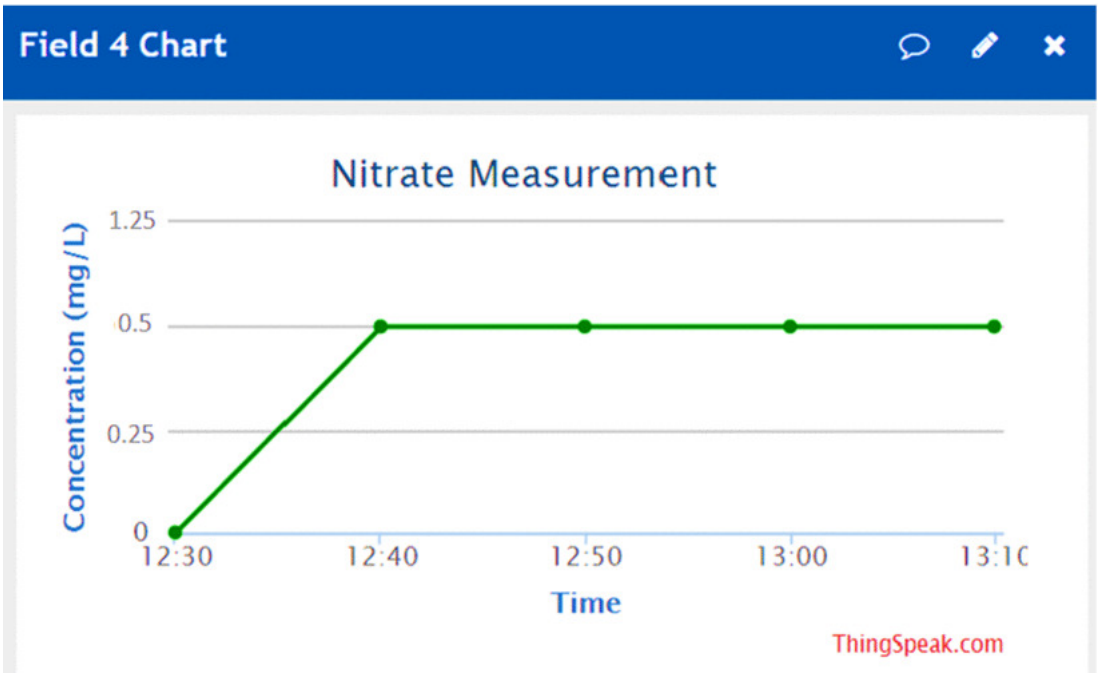

FIGURE 4.22: Final data to the cloud server

4.5.5 Comparison of Impedance Measurement by LCR and the Developed System

The fifth experiment was to compare the impedance measurement using the LCR meter and the developed system. Different known concentrations of Ammonium Nitrate (NH_4NO_3) between 0.01 and 0.5 mg/L were measured by the developed system and the LCR meter.

Figure 4.23 illustrates the test results (NH_4NO_3) from the designed system and LCR meter. When the concentration is increased in the sample, the real part of the impedance decreased accordingly. The corresponding impedance calculation was done inside the microcontroller, and the results of the impedance calculation from the system were very close to the impedance measured by the LCR meter. The designed system showed an excellent linear relation with $R^2 = 0.99$ which is very similar to the LCR impedance measurement. Figure 4.24 shows

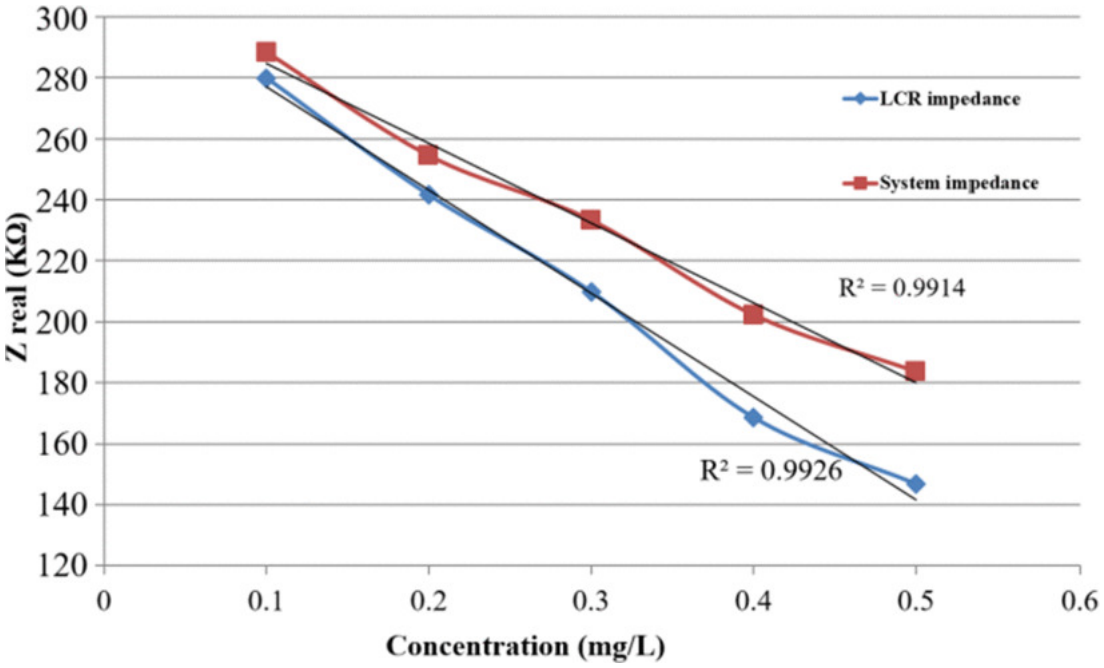

FIGURE 4.23: Comparison of the real part of impedance: by LCR and developed system

the comparison of the phase angle between the LCR and the sensor system measurement. During the impedance measurement, the phase angle of the different concentrations was measured. It should be noted that the system's measured phase angles are similar to the LCR measurement and the range of change of phase angle of the sensor system, is also similar to that of LCR measurement. The LCR meter has been used to measure the impedance of the Interdigital sensor for different applications. Therefore, it is important to compare both results to evaluate the system's performance. The system is capable of running the sensor

and recording the data continuously.

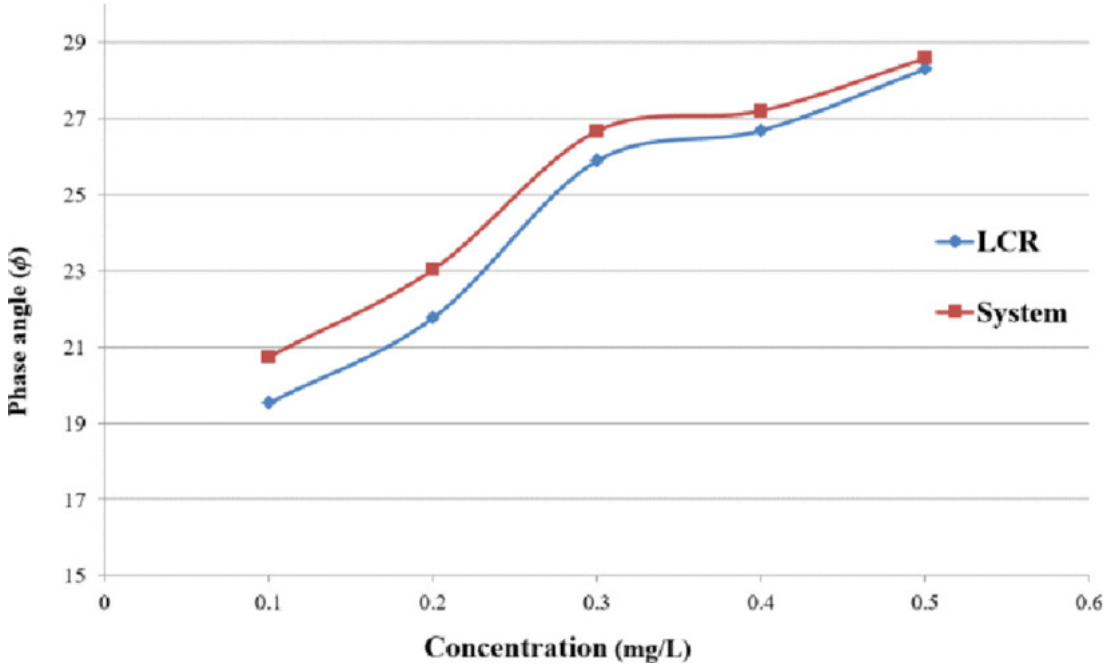

FIGURE 4.24: Comparison of phase angle by LCR and developed system

4.5.6 Improvement for Temperature Compensation

The last experiment was done to demonstrate the usefulness of the temperature compensation in the developed system. The temperature of the sample water was maintained at $30°C$. The concentration of nitrate was measured by the developed sensing system and laboratory spectrophotometric method. Table 4.2 compares nitrate concentrations measured before and after temperature compensation and calculated using equations 4.10 and 4.12, respectively. The error rate was higher (more than 20%) when the temperature change was not compensated in the developed system (Table 4.2).

4.6 Chapter Summary

A temperature compensated interdigital capacitive sensor has been developed in the current chapter to measure nitrate at low concentrations. A portable, novel sensing system has been developed that could be used on-site as a stand-alone device, as well as IoT-based remote monitoring smart sensor node, to measure nitrate concentration in surface and groundwater.

TABLE 4.2: Comparison of nitrate measurement before and after the temperature compensation.

Lab Number	Before Compensation (mg/L)	After Compensation (mg/L)	Spectrophotometric method (mg/L)
1	0.61	0.53	0.50
2	0.59	0.51	0.49
3	0.61	0.50	0.48
4	0.41	0.35	0.33
5	0.43	0.30	0.32

Electrochemical Impedance Spectroscopy was employed to detect and display nitrate concentrations, by evaluating the impedance change read by the interdigital transducer immersed in the surface water samples. The test samples were evaluated by commercial equipment (LCR meter) and the designed system. These results were also validated using standard laboratory techniques to assess nitrate concentrations in water samples. The designed system showed a good linear relationship between the measured nitrate concentrations (ranged from 0.01 to 0.5 mg/L) to those measured by the commercial equipment in the collected water samples. However, the current system has the potential to be used to estimate nitrate concentrations in water samples, in real-time. The system can upload the measured nitrate data on a website based on IoT. This system could be used to integrate water quality monitoring sites within farms, or between streams, rivers, and lakes. For the in-situ installation, a robust box containing the whole system would need to be installed at the monitoring site.

Chapter **5**

Graphene-PDMS Sensor for Nitrate Measurement

5.1 Introduction

This chapter is taken from one publication[1] . Low-cost nitrate-N sensors and smart sensing systems are necessary to develop a distributed network to monitor the quality of water in real time. This experiment presents the fabrication process of carbon printed sensors and the advantage of using a Graphene sensor to measure the concentration of nitrate-N in water. The sensor was characterised at different temperatures and with different nitrate-N concentrations in water. Electrochemical Impedance Spectroscopy (EIS) was employed to characterise the developed sensors. The calibration standard with the temperature compensation is also explained. UV-Spectrometry was used to validate all the results and the range of concentrations was 1-70 ppm. The sensing system has WiFi connectivity to transfer the data to a cloud server to monitor the data in real time. The sensor has shown good performance during measurements and the developed sensing system has very good potential to be a part of a distributed sensing network to monitor the data in real time.This chapter describes the fabrication and implementation of the second type of sensor patches developed from Aluminium (Al) and Polyethylene Terephthalate (PET). One distinct difference of the structure of these sensor patches are their formation from a single raw material. Due to this attribute, these sensor patches are different in terms of performance from other sensors. This also helped in curbing the complexity in the construction process of the sensor prototypes and so decreasing the

[1]**Alahi, Md Eshrat E.**, Anindya Nag, Subhas Chandra Mukhopadhyay, and Lucy Burkitt. "A temperature-compensated graphene sensor for nitrate monitoring in real-time application." Sensors and Actuators A: Physical 269 (2018): 79-90.

overall cost of fabrication. PET is a common polymer used as a substrate to develop flexible sensors for different strain [177], [178] and pressure [179],[180] sensing applications. The absence of any post-processing steps, high flexibility and smooth cut edges are some of the advantages of this polymer [181],[182]. Aluminium particles also have certain advantages which makes Aluminium a viable option for the electrode material [183]. Some of them are high corrosion resistance, high electrical and thermal conductivity, and flexibility [184]. Similarly to the CNT-PDMS sensors, laser cutting was used to develop the electrodes of these sensor patches. After fabrication and characterisation of the sensor patches in nitrate samples, they have used for nitrate detection to measure unknown sample in water.

5.2 Fabrication of the Printed Sensors

The fabrication of the sensor patches was done at fixed temperature and humidity conditions (temperature: 22°C, RH: 50%). Figure 5.1 shows a schematic diagram of the fabrication steps of the CNT-PDMS-based sensor. The Polydimethylsiloxane (PDMS) was cast on a Poly (methyl methacrylate) PMMA template to form the substrate for the sensor patch. PDMS was used to form the sensor patch due to its low cost, low Young's modulus (E), and hydrophobic nature. PMMA was used due to its non-toxicity and proper adherence to the cured PDMS. Then, a layer of nanocomposite (NC) formed by mixing Multi-Walled Carbon Nanotubes (MWCNTs) and PDMS was cast on the cured PDMS. MWCNTs were considered as the conductive material due to their high electrical conductivity, flexibility, high tensile strength and resistance towards a wide range of temperatures. The curing of the NC layer was followed by the laser cutting of the top layer to form the electrodes of the sensor patch. The individual fabrication steps are shown in Figure 5.2 . PDMS (SYLGARD ® 184, Silicon Elastomer Base) was formed by mixing a ratio of 10:1 between the base elastomer and the curing agent respectively. The height of the PDMS cast on the PMMA was adjusted by a casting knife (SHEEN, 1117/1000 mm) to around 1000 µm. The sample was then desiccated for 2 hours to remove any trapped air bubbles. After curing the sample at 80°C for 8 hours, a layer of NC formed by mixing MWCNTs (Aldrich, 773840-100G) and PDMS was cast on top of it. The weight value of the MWCNTs was optimised to have a trade-off between the flexibility of the sensor patch and the conductivity of the electrodes. The final optimised value of the CNTs chosen to form the NC was 4 wt%. Figure 5.3 (a) shows a Scanning Electron Microscope

(SEM) image of the optimised CNT in the NC. The black regions in the image represent the CNTs while the white spots define the PDMS in the NC. The height of the NC layer was again adjusted by the casting knife to around 600 µm. The sample was then again desiccated followed by its curing at 80° C for 8 hours to form the top layer of the sensor patch. Then the sample was taken for laser cutting to scan off the top part except for the design electrodes. A Universal Laser Systems (Model: OLS 6.75, CO_2 laser system, laser spot diameter: 150 µm) was used for laser cutting on the sample to form the electrodes. The design of the electrodes was done with the help of Corel DRAW as it was the design software available with the Universal Laser associated with the laser cutting system.

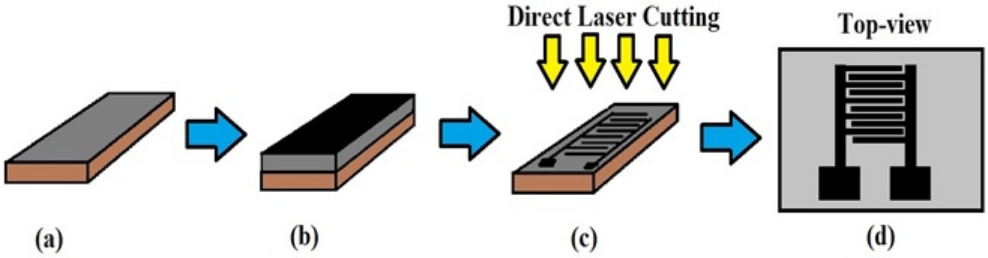

FIGURE 5.1: Schematic diagram of the CNT-PDMS-based sensor. (a) PDMS was cast on a PMMA template. (b) A layer of nanocomposite (NC) layer was cast on top of the cured PDMS. (c) The cured NC layer was laser cut to form the electrodes. (d) Final product used as a sensor.

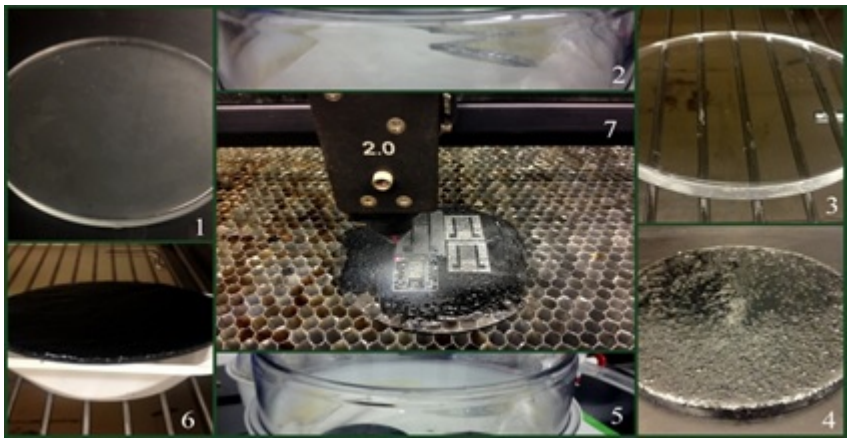

FIGURE 5.2: Individual fabrication steps followed to develop the CNT-PDMS sensor.

Three parameters, namely power (W), speed (m/min) and z-axis (mm) were optimised to achieve an optimal cut of reasonable quality. The power is defined as the power of the laser beam. The speed was used to control the movement of the laser nozzle over the sample. The Z-axis changed the height of the laser platform to adjust the focal point of the laser beam on

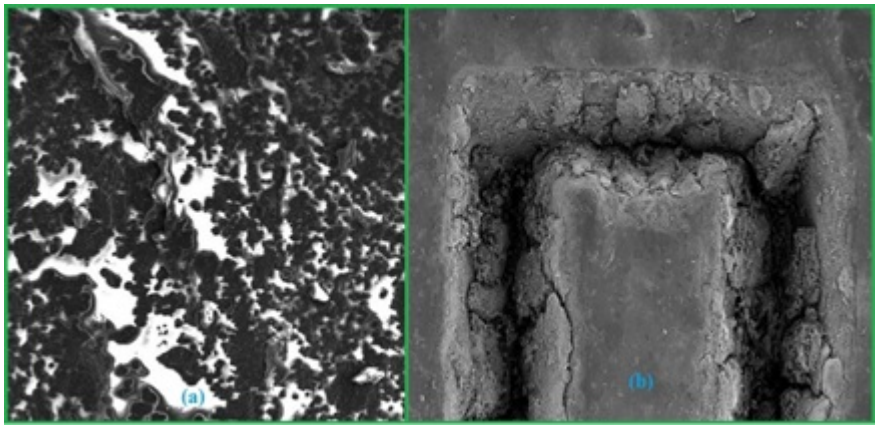

FIGURE 5.3: SEM image of the (a) CNT-PDMS mixture with the optimized CNT wt % and (b) formed sensor patch.

the sample. The optimized values of these three parameters were 24 W, 70 m/min and 1 mm. Figure 5.3(b) shows a SEM image of the finished product. The front and rear view along with the dimensions of the sensor patch are shown in Figure 5.4. There were four pairs of interdigitated electrodes with a width of 200 µm for each finger and a gap of 100 µm between two consecutive fingers. The length and width of the sensing area of the patch were 5 mm and 4.5 mm respectively. Two of the advantages of these sensor patches were their enhanced mechanical properties and the corrosion-resistant nature of the electrodes.

The schematic diagram of the second type of sensor is given in Figure 5.5. The electrodes of these sensor patches were developed from low-cost polyimide (PI) films by photo-thermal induction [185]. The laser cutting of the PI films was followed by transfer of the formed conductive material onto Kapton tapes by manually compressing the tapes over the induced graphene. The Kapton tapes with the transferred graphene were then used as sensor patches for experimental purposes. Figure 5.5 shows the individual steps of fabrication of the graphene sensor. After the design of the electrodes was provided to the laser cutting system, the PI films, of a thickness of around 100 µm, were taken to the platform for laser writing. The PI films were attached to a glass substrate to forbid movement during the induction process. The three laser parameters (power, speed, and z-axis) were again optimised to produce the conductive material from the PI films. The optimised values were 9 W, 70 m/min and 1 mm for the power, speed and z-axis respectively. The sp^3 hybridised carbon atoms of the PI films were photo-thermally converted to sp^2 hybridised carbon atoms of graphene. After the formation of graphene, Kapton tapes were laid over the designed electrodes to transfer the

induced conductive material. The transfer was done carefully by initially applying manual pressure over the sensing area of the patches, followed by transferring the bonding pads of the electrodes. Even though the PI film used to generate the graphene and the Kapton tapes used as a substrate of the sensor patches are of the same material, there are two reasons the laser writing was done on the PI film instead of doing it directly on the Kapton tapes. Firstly, the stickiness of the tapes would have coagulated the induced graphene, thus hampering the design. Secondly, the conductivity of the induced graphene would have been affected on the Kapton tapes. The conductivity of the conductive material was not much affected by the transfer as the difference was less than 20 mS/m between the induced graphene and the transferred graphene. Figure 5.7 shows SEM images of the top and side views of the electrodes of the electrode on the Kapton tapes. It is seen that the transfer came off clean with the edges almost of the fingers parallel to each other. Figure 5.8(a) shows the image of the sensor patch with its dimensions. Six pairs of electrode fingers were formed with each one having a length and width of 500 µm and 100 µm respectively. The interdigital distance between two consecutive electrode fingers was around 100 µm. Figure5.8(b) shows the equivalent circuit of the sensor patch. V_{in} is the input voltage and I_{in} is the current which is flowing through the electrodes. R_p and C_p are the electrical components, which are formed due to the influence of the electric field applied to the electrodes. R_p is the total resistance due to the conductive properties of the sample and C_p is the capacitance formed due to the dielectric properties of the medium of the sample [186].

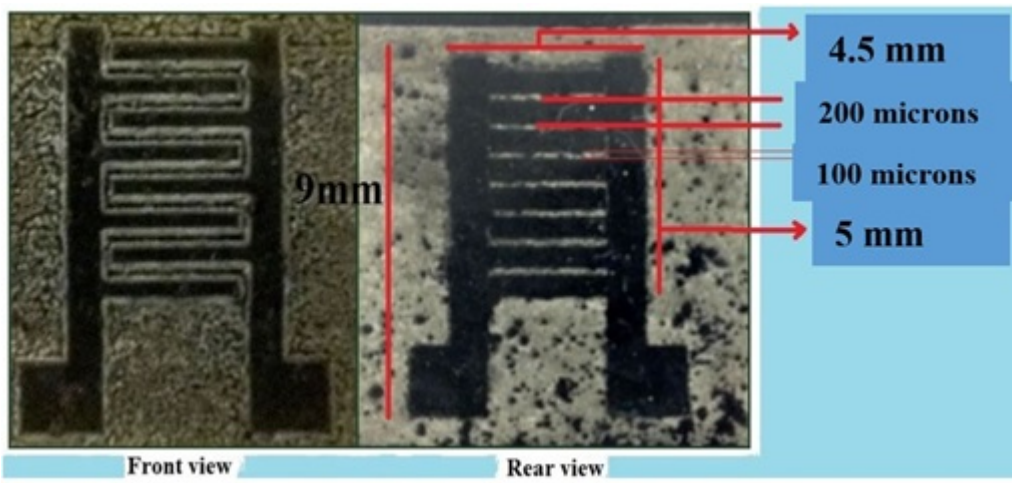

FIGURE 5.4: Front and rear view of the final sensor with its dimensions.

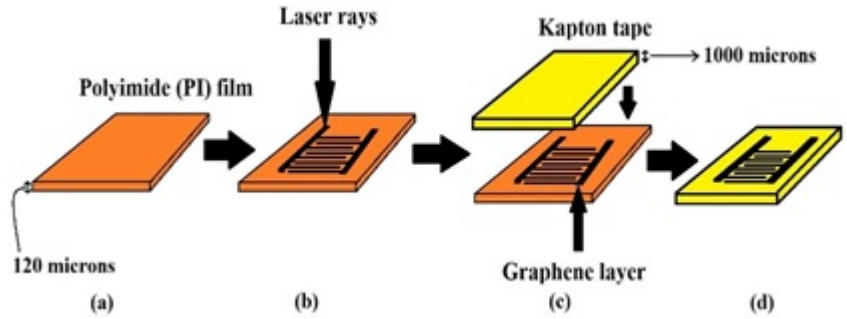

FIGURE 5.5: Schematic diagram of the graphene sensor. The polyimide (PI) film was taken (a) for laser writing on it (b). The induced graphene electrodes (c) were transferred to the Kapton tape to form the sensor patch (d).

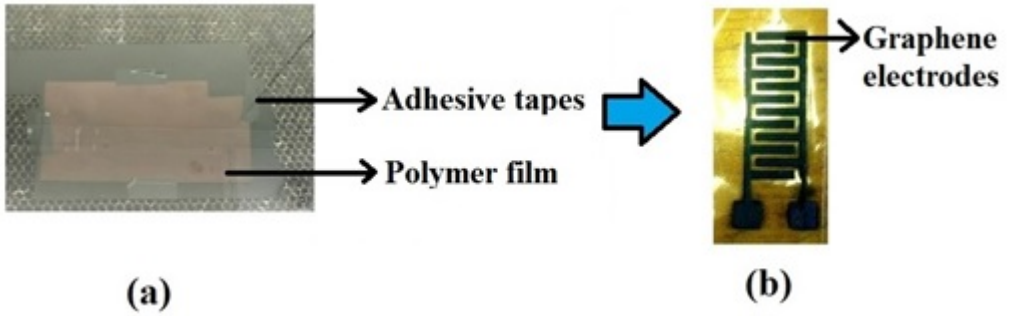

FIGURE 5.6: SEM image of the (a) CNT-PDMS mixture with the optimised CNT wt. % and (b) formed sensor patch.

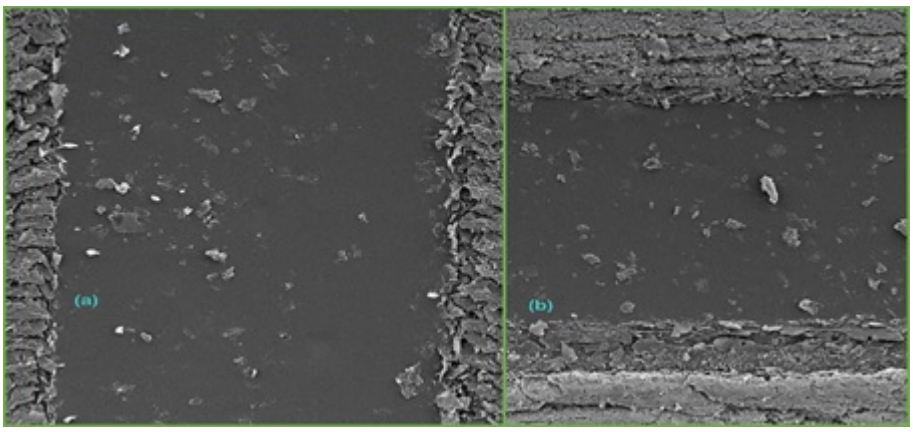

FIGURE 5.7: SEM image of the (a) side view and (b) top view of the transferred graphene on the Kapton tape.

5.3 Materials and Methods

5.3.1 Experimental Setup

Electrochemical Impedance Spectroscopy (EIS) is a highly sensitive method for an unsteady and variable system in equilibrium, and its instant impedance measurement is required

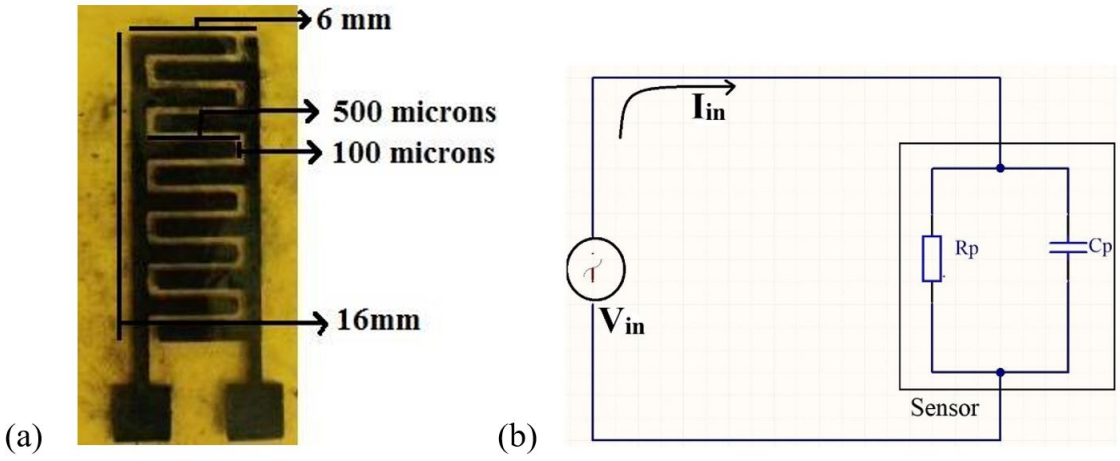

FIGURE 5.8: (a) Final product along with its dimensions that were used as a sensor patch, (b) The equivalent circuit of the Interdigital sensor.

for non-stationary systems. Different methods are available for impedance measurement, but the Frequency Response Analyser (FRA) is considered the de facto standard for EIS measurement. An FRA requires a single input sinusoidal signal with an amplitude of 5-15 mV. The frequency of the signal sweeps in a certain range on a direct current bias voltage. The signal is applied to the working electrode and a resulting voltage is taken from the sensing electrode. The measurement process is done in a certain frequency range to get a complete impedance profile. The following can be used to specify the impedance of a system:

$$Z = R + jX \tag{5.1}$$

where **Z** is the impedance (Ω) , **R** is the resistance (Ω), which is also the real part of the impedance, **X** is the reactance (Ω), which is the imaginary part of the impedance. The impedance profile data can be represented graphically as a Bode plot and a Nyquist plot, also called a Cole-Cole plot. The plot also reflects the electrochemical procedures taking place at the electrode-electrolyte edge. A clamp connects the sensor with the HIOKI IM 3536 LCR meter. 10 Hz to 100 kHz frequency sweeping was used to profile the sensor for EIS measurement. A standard temperature and humidity were maintained during measurement. Deionised water was used as a control solution. A standard nitrate-N solution was used to prepare the working solution for different concentrations. The average pH of the samples was 6.60. Initially, the sensors were characterised in air to extract the experimental reference curve. Then the deionised water and sample water were used to continue the experiments. Figure 5.9 shows the data-acquisition laboratory setup used for EIS measurements.

5.3.2 Comparative Analysis of Two Different Sensors

10-ppm Nitrate-N sample water was taken, and the real part of the impedance was measured for different sensors. The real part of the impedance of the deionised water was also measured. The temperature and humidity of the waters were identical due to the same laboratory environment. The pH of the water was also the same during the measurement. The sensor's response was calculated by using the following equation:

$$Sensor'sResponse(\%) = \frac{R_{milliq} - R_{sample}}{R_{milliq}} 100 \tag{5.2}$$

where, **R** indicates the real part of the impedance of the sensors.

5.3.3 Temperature and Nitrate Measurement

The graphene sensor was first used to measure temperature changes in water. Temperature changes the mobility of ions in water, therefore, it is important to measure the changing behaviour of the graphene sensor at different temperatures. An experimental setup similar to Figure 5.9 was used to measure the temperature. The GEX MS 7-H550 Digital Hotplate, mercury thermometer, LCR meter and the computer were used for data acquisition. The thermometer was immersed inside the deionised water to measure the temperature continously. The sensing surface of the graphene sensor was immersed inside the water and the frequency was swept from 10 Hz to 100 kHz to characterise the sensor, at various temperatures. 1, 10, 30, 50 and 70-ppm standard nitrate-N solutions were taken for another experiment, 100 mL in five beakers. 100 mL of deionised water was also taken as a control solution. The sensor was immersed in the sample waters until the completion of the measurements. The real and imaginary impedance were taken by the LCR meter. The measurement was taken five times and an average was presented in the final graph.

5.3.4 IoT-enabled Smart Sensing System

An Internet of Things (IoT)-enabled smart sensing system is proposed to collect the sensor data for nitrate-N measurement. An AD5933 [187] was used as an impedance analyser to measure the real part of the impedance of the graphene sensor. An Arduino Uno Wi-Fi [188] is used as a master microcontroller to collect the impedance data from the impedance analyser. It has an integrated Wi-Fi module, which is used to send data wirelessly to a cloud

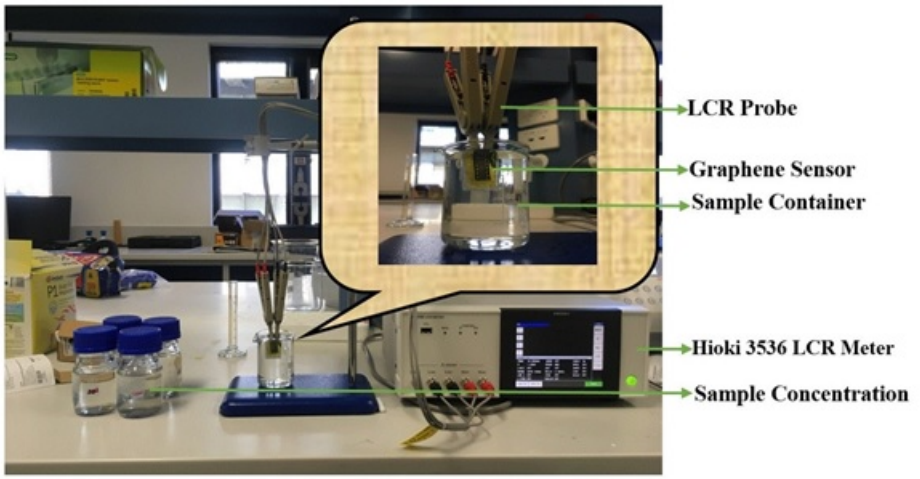

FIGURE 5.9: Experimental setup for nitrate measurement.

server. Thingspeak [175] is the IoT-based free web server to store the measured data and show it in real time. The Arduino Ciao [189] library was used to transfer the data to the designated private channel in Thingspeak. Ciao is a library which is capable of interfacing with system resources and communicating with the most common protocols such as (MQTT, XMPP, HTTP, SMTP, etc.). HTTP POST was used to send the measured concentration to the ThingSpeak cloud server. Security is an important issue in IoT research due to the large scale of the objects and the heterogeneity. It will be discussed in a future research article when the actual distributed network will be installed to monitor in real time.

The AD5933 is the impedance analyser which measures the impedance and the phase shift of the sensor. Before starting the measurement, the AD5933 had to be calibrated to get the gain of the impedance analyser. An ADG849 is used as a switch from a calibration resistor to the sensor, and the impedance is calculated by using that calibrated gain. The phase shift is also calculated from the impedance analyser. Frequency sweeping is not required as the final measurement depends on the single frequency. The I2C protocol is used to communicate to the impedance analyser to extract the real part of the impedance from the impedance analyser and store that in the main microcontroller. A data processing algorithm is used to convert that real part of the impedance into meaningful temperature and nitrate-N concentration values.

Finally, the temperature and nitrate-N data are send to the IoT-based cloud server to store for further processing. Some of the sample water, which was collected from different locations, is measured by the developed sensing system. Figures 5.9 and 5.10 show the

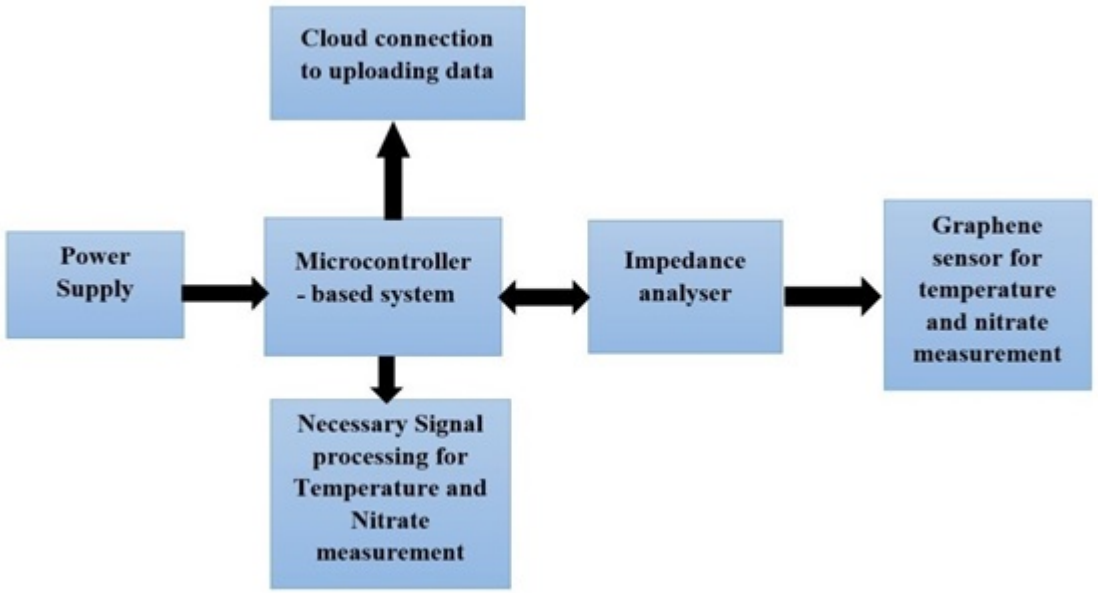

FIGURE 5.10: Block diagram of the smart sensing system.

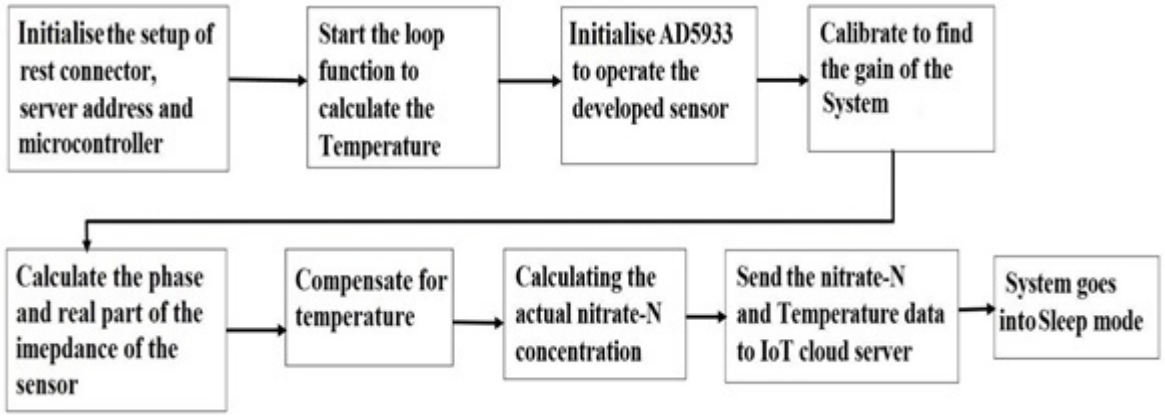

FIGURE 5.11: Software flow of the individual steps of the operating of the IoT-based system to calculate the nitrate concentration and transmit to the cloud server.

block diagram and software flow of the developed sensing system. Arduino Sketch was used to write the programming code. Initially the system starts, and the microcontroller is initialised the setup function to establish the rest connector, provided with the cloud-server API (Application Programming Interface) number which will be necessary to send the measured data to the designated IoT server. The impedance analyser is used to measure the phase and real part of the impedance of the sensor. The developed calibration standard for temperature measurement was used to measure the temperature of the deionized water. After that, the nitrate-N concentration was calculated, with the temperature compensation. The system communicates with the IoT cloud server to send the measured data. Finally, the

microcontroller goes into sleep mode to save power. Figures 5.11 and 5.12 show a schematic diagram of the conditioning circuit and the first prototype of the sensing system respectively. Circuit maker [190] was used to draw the circuit diagram of the sensing system.

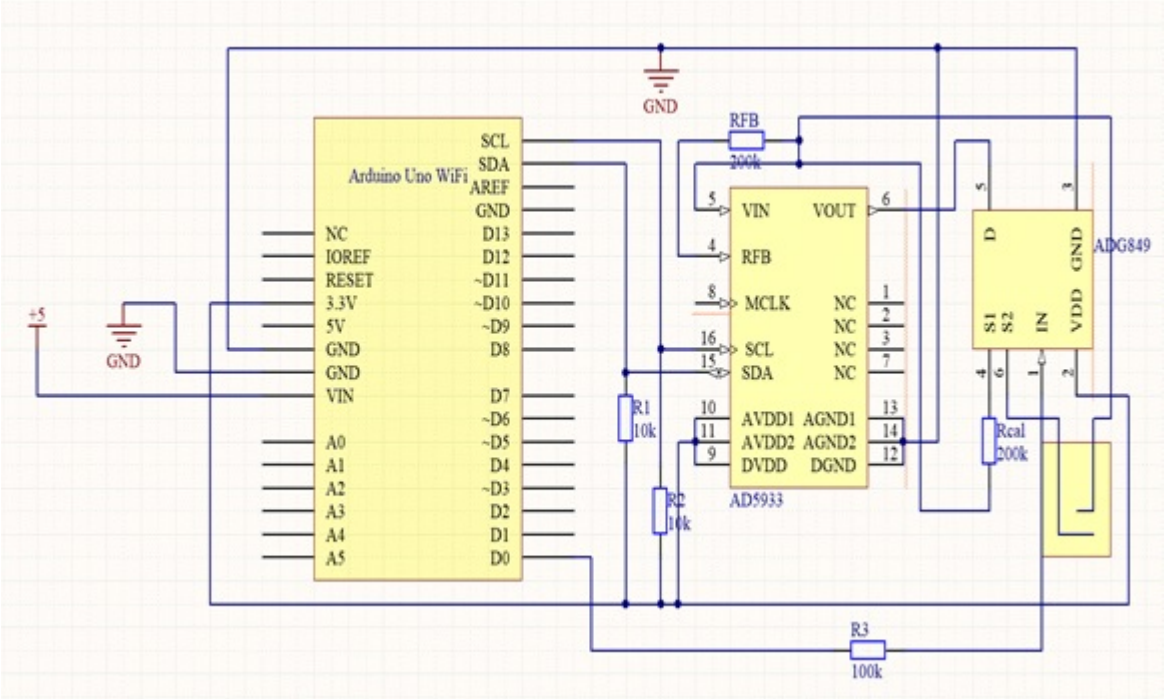

FIGURE 5.12: Schematic diagram of the smart sensing system.

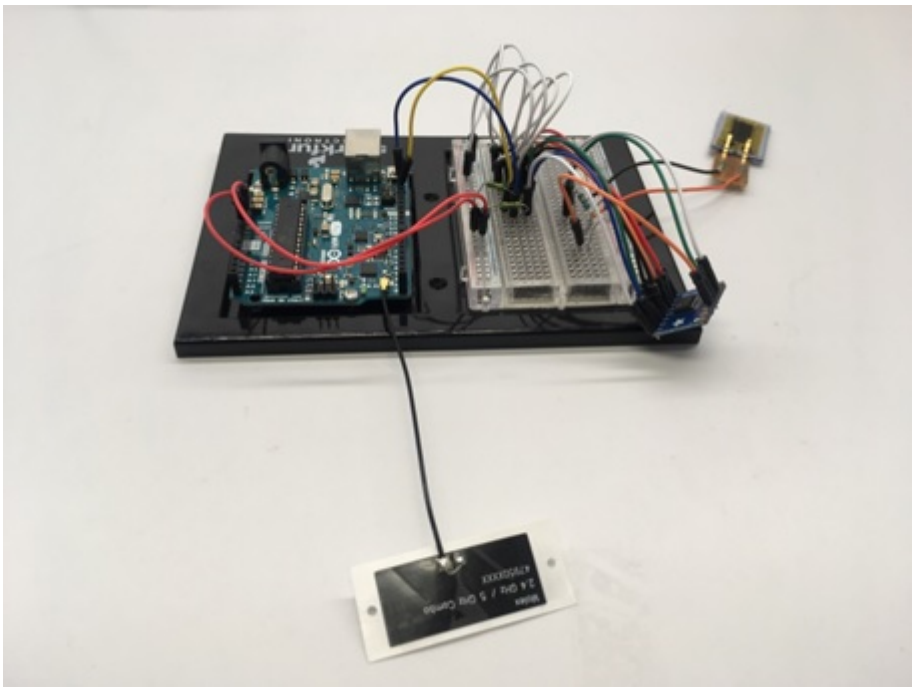

FIGURE 5.13: First prototype of the smart sensing system.

5.4 Results and Discussions

5.4.1 Comparative analysis

The sensor's response is calculated for two different sensors and plotted in fig. 5.14. It is seen from fig. 5.14 that the Graphene sensor has the maximum sensitivity compare to CNT PDMS sensor. The materials of the electrode have an impact on this sensitivity curve. The graphene has a good electrical conductivity compared to PDMS+CNT material. The electrical intensity, which generates from the positive electrode, can bulges through the sample water to the negative electrode. Therefore, Graphene sensor is showing better response compared to the other sensors. The response of the graphene sensor is also stable in all the frequency range. In the subsequent sections, all the experiments were done by using the Graphene sensor due to the higher response compare to the CNT PDMS sensor in this study.

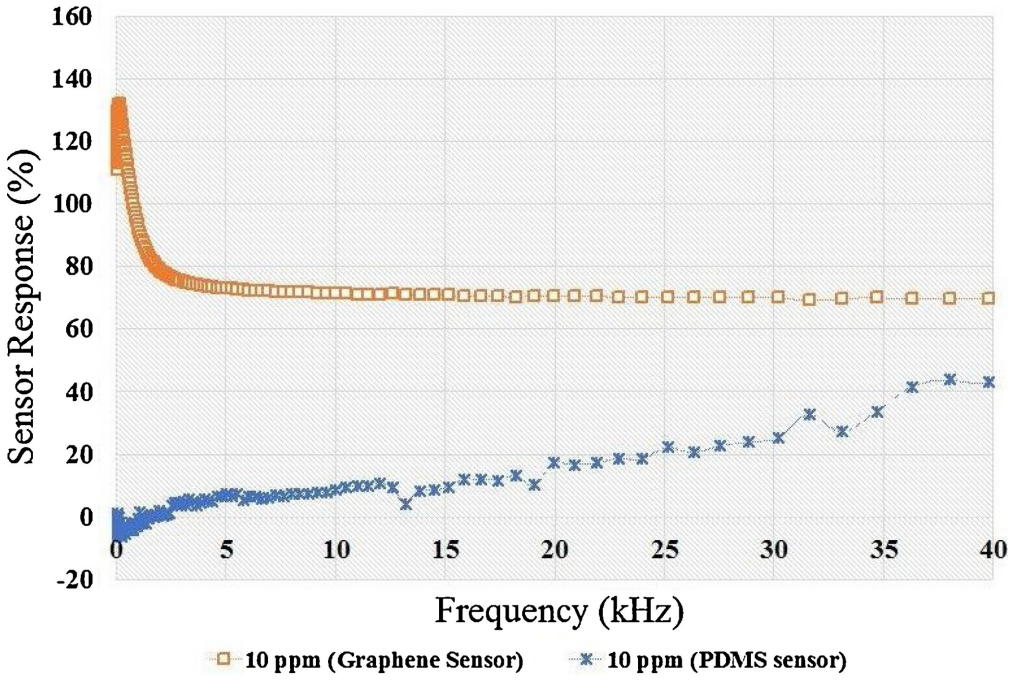

FIGURE 5.14: Comparison of the sensitivity of different sensors.

5.4.2 Nitrate Measurements

Figure 5.15 presents the real part of impedance for different concentrations with a frequency range from 1 Hz to 100 kHz. It is seen that the real part of the impedance is changing

due to the different concentrations of nitrate-N in the sample water. Due to the presence of nitrate-N ions in the water, the impedance profile changes for different concentrations due to the properties of the interdigital graphene sensor. It is observed that 1200-1700 Hz is the sensitive region for different concentrations. Of the real and imaginary parts of the impedance of the graphene sensor, the real part of the impedance shows the most change between the sample nitrate-N concentrations.

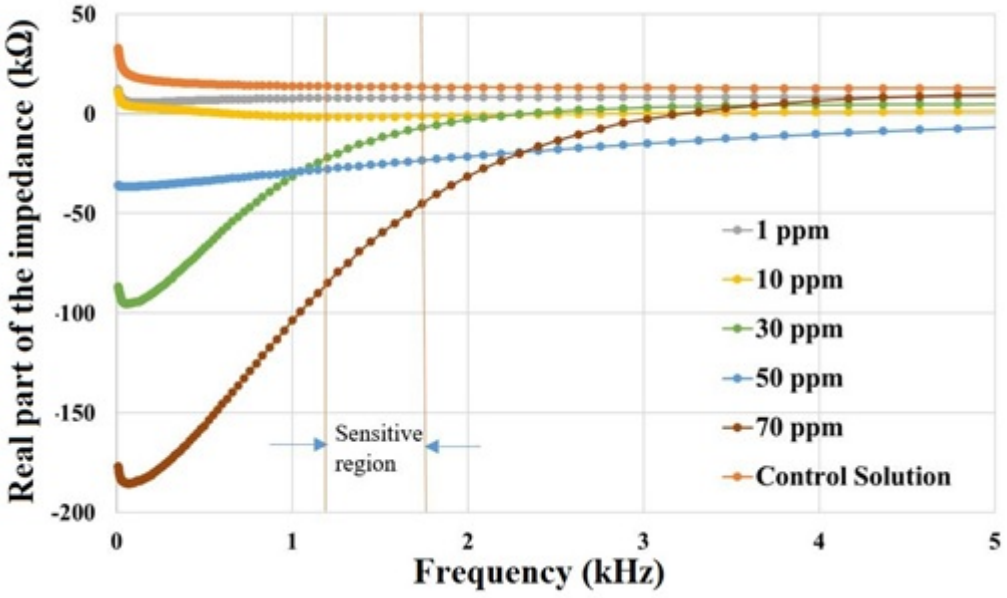

FIGURE 5.15: The change of real part of the impedance with respect to frequency.

5.4.3 Temperature Measurement

The dielectric properties of the deionised water were measured by this described method. The EIS measurement technique was used to measure the real and imaginary parts of the impedance of the sensor. The real part gives a more significant change than the imaginary impedance. The temperature was varied from 7 °C to 50 °C and the corresponding real part of the impedance was plotted on Figure 5.16. From linear regression analysis, it is seen that the temperature is well correlated with the real impedance ($R^2 = 0.99$) and can be calculated from 5.3:

$$T = \frac{R_T + 29153}{404.87} \tag{5.3}$$

where, R_T is the measured real part of the impedance for a certain temperature and T is the calculated temperature.The slope of the straight line indicates the change of the real part

of the impedance per unit change of temperature, which is α=404.87 Ω/°C. It is to be noted that the operating frequency of the graphene sensor of the temperature measurement was 1650 Hz. Figure 5.17 shows the temperature measured by the sensor and compares it with the actual temperature. It is seen that they are well correlated with each other and (R^2 = 0.99) which indicates that the sensor can quite accurately measure the temperature of sample water.

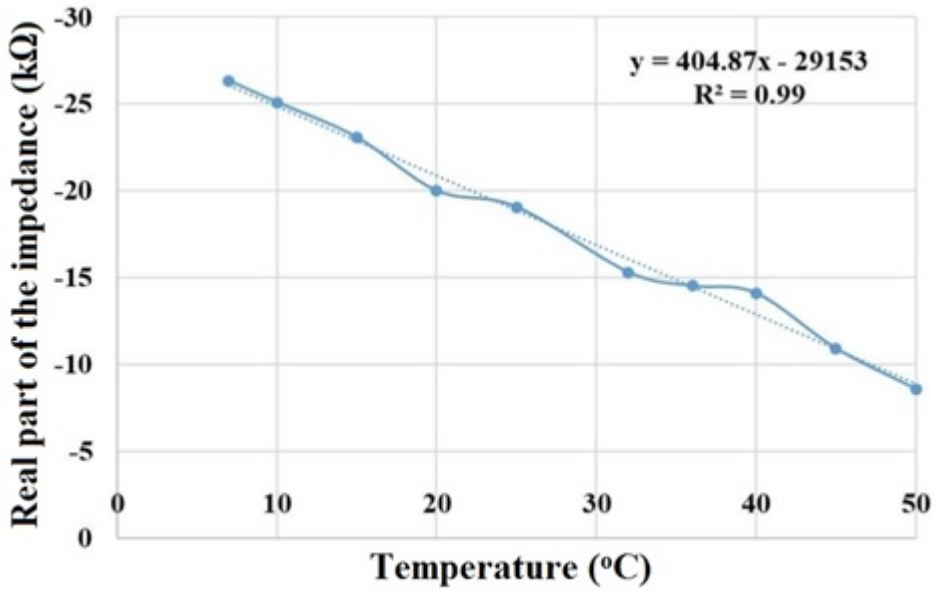

FIGURE 5.16: Real part of the impedance as a function of temperature.

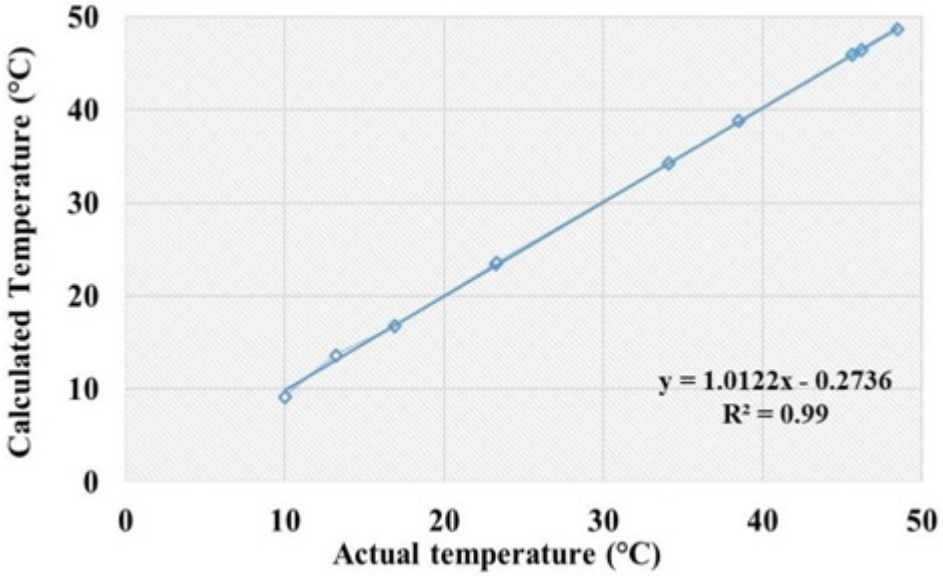

FIGURE 5.17: Comparison of actual and calculated temperatures.

1650 Hz was taken as the operating frequency to develop the calibration standard from a standard nitrate-N sample measurement. All the measured concentrations were considered as the x-axis and the corresponding real part of the impedance was considered as the y-axis. Figure 5.18 shows the final calibration standard for nitrate-N measurement.

$$C = \frac{R_{cal} - 9196.9}{-667.97} \tag{5.4}$$

where, C (ppm) is the actual concentration and R_{cal} (Ω) is the real part of impedance measured by the graphene sensor. 5.4 was used to calculate any unknown nitrate-N concentration in water. Since the sensor was sensitive to temperature and the ions mobility changes with temperature, the measured real part of the impedance was adjusted by a correction factor α . The R_{actual} is the modified real part of the impedance due to temperature and was calculated by equation 5.5:

$$R_{actual} = R_{cal} + \alpha(T - 25) \tag{5.5}$$

Therefore, the standard formula to calculate the actual concentration after applying a correction factor for the graphene sensor is represented as:

$$C_{actual} = \frac{R_{actual} - 9196.9}{-667.97} \tag{5.6}$$

where C_{actual} is the final concentration corrected for temperature. (5.6) was used to measure any unknown nitrate-N concentration, including temperature compensation. It is also seen that the sensitivity of the sensor is $667.97\Omega/ppm$, which will help to measure nitrate-N concentrations accurately.

5.4.4 Unknown Sample Measurement

To measure the unknown sample, different samples of water were collected from different sampling locations, such as river, lake, stream, tap water. Naturally, the concentration of nitrate-N level was not high. So, some nitrate-N samples were added to those water samples to elevate the nitrate-N concentration. The fabricated graphene sensor was used to measure the temperature, followed by a final measurement of nitrate-N. Among all the other samples, River water was taken as an example to show the calculation process and measure the nitrate-N concentration. The real part of the impedance was measured for deionised water and gave $R_T = -19750\Omega$. Therefore, from 5.4, the calculated temperature is T (°C) = 23.2 °C. The sensor was used to measure the sample concentration and the real part of the impedance was

found, $R_{cal} = -4568\Omega$. Using equation 5.6, R_{actual} becomes -5288.67Ω. Therefore, the final concentration is 21.69 ppm, which comes from that sample water measurement. This result was verified by the laboratory standard method of UV-spectrometry. Other sample waters are measured and compared with the laboratory standard method in Table 5.1. It is seen that the graphene sensor shows very good performance compared to the laboratory method. The error rate was less than 5%, which is an acceptable performance of the sensing system and the developed sensor. The error was considered as a measurement error due to the presence of other ions in the water. However, the accuracy of the sensor and sensing system was more than 95% and consistent.

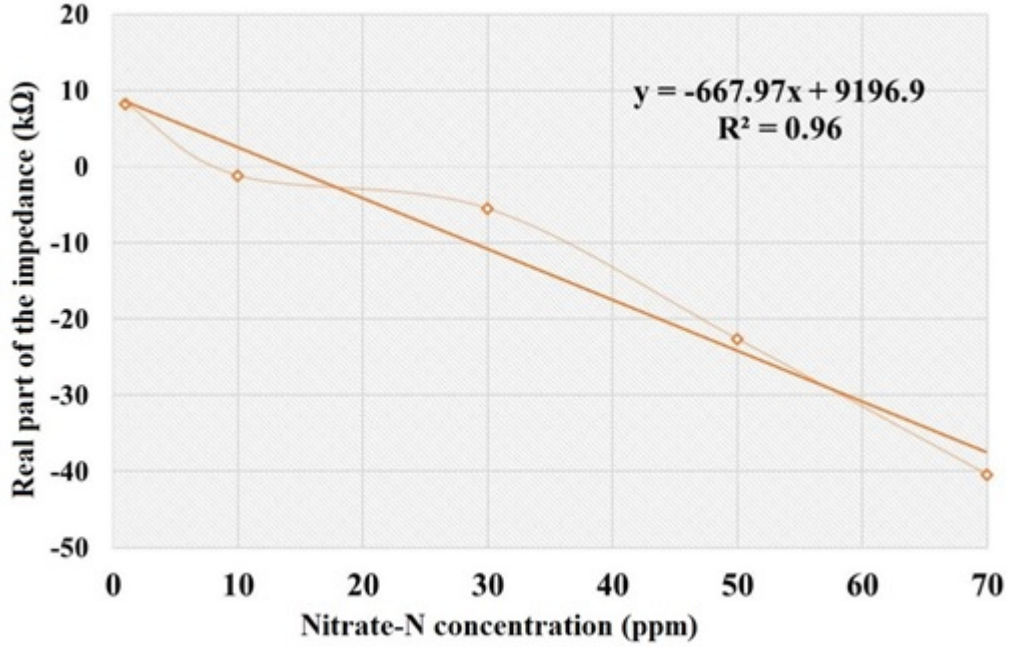

FIGURE 5.18: Calibration Standard of Nitrate-N concentration (ppm).

TABLE 5.1: Unknown Sample measurement (in ppm) compared with Laboratory standard method.

Serial No.	Sample	1st Run	2nd Run	3rd Run	4th Run	5th Run	Laboratory Run
1	River Water	21.69	21.56	21.54	21.63	21.35	21.5
2	Tap Water	5.25	5.1	5.35	5.15	5.75	5.5
3	Canal Water	56.75	56.7	56.6	56.65	56.55	56.5
4	Stream Water	65	65.2	65.1	65.3	65.15	65
5	River Water	32.35	32.65	32.55	32.45	32.62	32.5

5.4.5 Reusability and Data Transferring

The developed sensor is robust and maintains good repeatability. Figure 5.19 shows the reusability performance of the sensor and the sensing system. The sensor provides an almost identical result in each run of the measurement. Graphene is corrosion free [191] and protects the sensing electrodes from oxidation during the sample measurement, which helps when using the sensor in a repetitive manner. Mechanically it is also robust [192] and shows good performance during measurements.

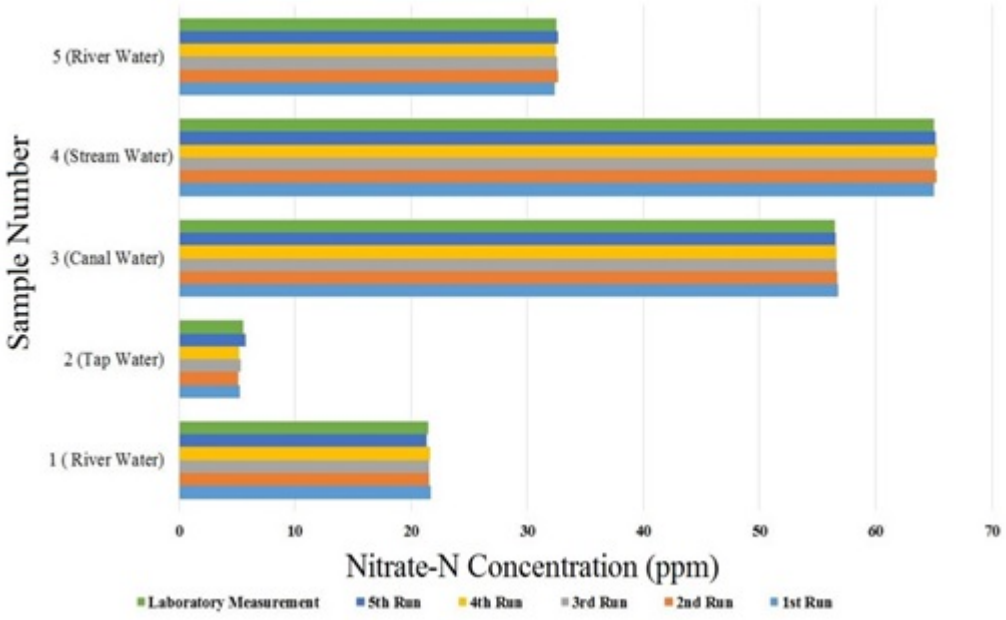

FIGURE 5.19: Repeated unknown sample measurements by smart sensing system.

Figure 5.20 shows the transfer of the data to the IoT-based cloud server. The concentration of nitrate-N was 25.5 ppm and the temperature were around 22 °C. The system was used for nearly three hours to monitor the actual data in real time. It was observed that the developed system was consistent in terms of monitoring continuous data at fixed intervals. They have transferred the data simultaneously, which would help to monitor the measured data in real time. There is a certain delay (30 seconds) from the ThingSpeak cloud server. The sensing system will also be useful to develop a distributed monitoring system to monitor the temperature and nitrate-N concentration in real time.

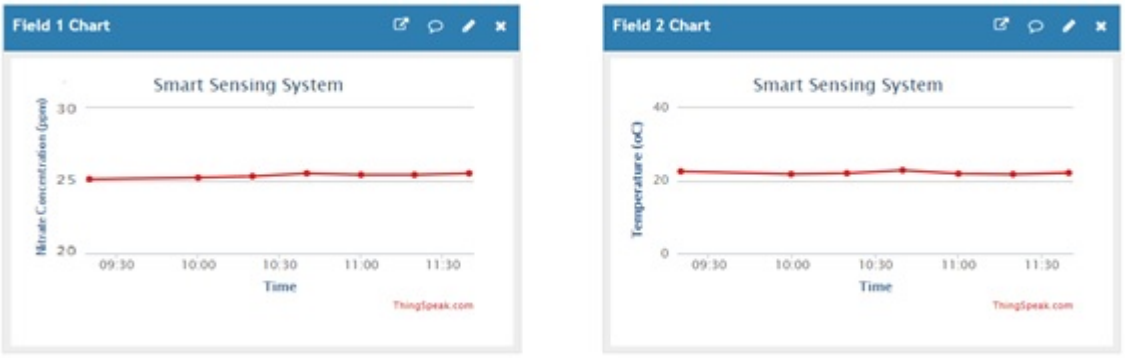

FIGURE 5.20: Data transferred to the IoT based web server.

5.5 Chapter Summary

This chapter explains the IoT-enabled sensing system for the detection of nitrate-N concentrations in water. Temperature compensation was included to improve the performance of the sensing system. The sensor performance was measured in terms of its ability to monitor different concentrations of nitrate-N in water samples. Due to the low fabrication cost of the sensor, it was easy to develop a low-cost sensing system to monitor the water in real time. The sensor was also robust, which helps the system to repeat measurements with good repeatability. The developed sensor and the smart sensing system can be used to monitor the real-time nitrate-N concentrations and develop a low-cost distributed network with adequate performance.

Chapter 6

Selectivity of Nitrate Sensor

6.1 Introduction

Most of this chapter is taken from these publications [1], [2], [3]. Chapter 4 and Chapter 5 explain two different sensors for nitrate measurement. Although they have shown good results, the nitrate sensors did not have any selectivity, which is an important parameter of sensor design. If a selective layer is exposed to a mixture of ions in water, it interacts with those ions for which the material is selective and rejects the other interfering ions. The selective layer of the sensor can be homogeneous or can contain specific binding sites for target ions. The Ion-Imprinting Polymerisation technique is used to develop the selective material which is explained in the next sections.

6.1.1 Ion Imprinting Polymerisation

Ion imprinting has become a fast-growing technology that has gained much attention recently, especially in the area of materials science. One of them is called ion-imprinted polymers (IIPs), synthesised on the principles of enzyme phenomena whereby a polymer is altered by a polymerisation [193], which takes place in the presence of a template that could

[1] **Alahi, Md Eshrat E.**, Subhas Chandra Mukhopadhyay, and Lucy Burkitt. "Imprinted polymer coated impedimetric nitrate sensor for real-time water quality monitoring." Sensors and Actuators B: Chemical 259 (2018): 753-761.

[2] **Alahi, Md Eshrat E.**, Nasrin Afsarimanesh, Subhas Chandra Mukhopadhyay, and Lucy Burkitt. "Development of the selectivity of nitrate sensors based on ion imprinted polymerization technique." In Sensing Technology (ICST), 2017 Eleventh International Conference on, pp. 1-6. IEEE, 2017.

[3] **Alahi, Md Eshrat E.**, Nasrin Afsarimanesh, Subhas Mukhopadhyay, Lucy Burkitt, and Pak-Lam Yu. "Highly selective ion imprinted polymer based interdigital sensor for nitrite detection." In Sensing Technology (ICST), 2016 10th International Conference on, pp. 1-5. IEEE, 2016.

later be removed to create cavities to recognise only the analyte of interest. This specific and selective affinity for the target species decreases the chances of competition with other different ions. Ion-imprinted polymers (IIPs) can be defined differently depending on the methods used to synthesise or fabricate them, the functions they play, or the materials used for their synthesis.

6.1.2 Types of Imprinting Process

The type of interactions involved in the imprinting technique defines the type of imprinted polymer generated and hence the method of imprinting employed [194]. The interaction is discussed in the following subsection.

Covalent Interaction

In this type of interaction, the template and the monomer are linked by unbreakable covalent bonds, though such bonds are limited in molecular imprinting [194, 195]. However, even though it provides a stable interaction between the monomer and template, it is highly inefficient as far as rebinding and reuse of the polymers to be synthesised are concerned. Figure 6.1 shows the processes involved in the covalent imprinting process.

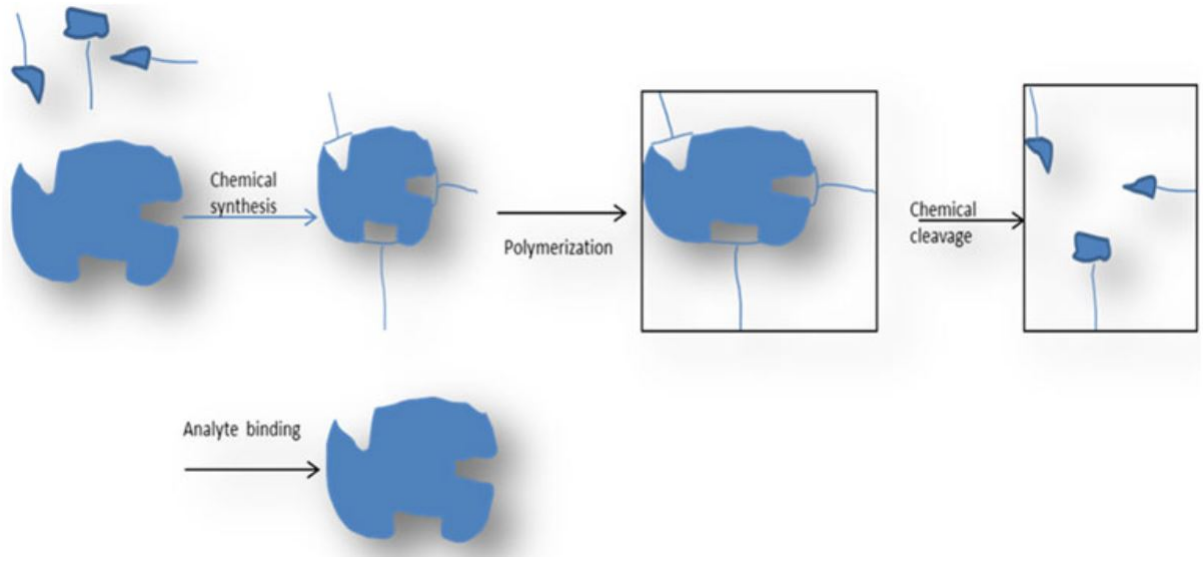

FIGURE 6.1: Covalent interaction of IIP

Non-Covalent Interaction

To achieve better rebinding kinetics and rapid template and monomer equilibrium, K. Mosbach [196] studied another generation of polymers based on non-covalent imprinting. In this method of imprinting, the template and monomer complex is formed by self-assembly. The monomer and template should be complementary, that is, the binding or completion is based on the union of these two by a number of mechanisms such as hydrogen bonding, hydrophobic interactions, salt bridges, ionic interactions, and van der Waals forces [194, 197]. Figure 6.2 is a diagrammatic representation of non-covalent imprinting.

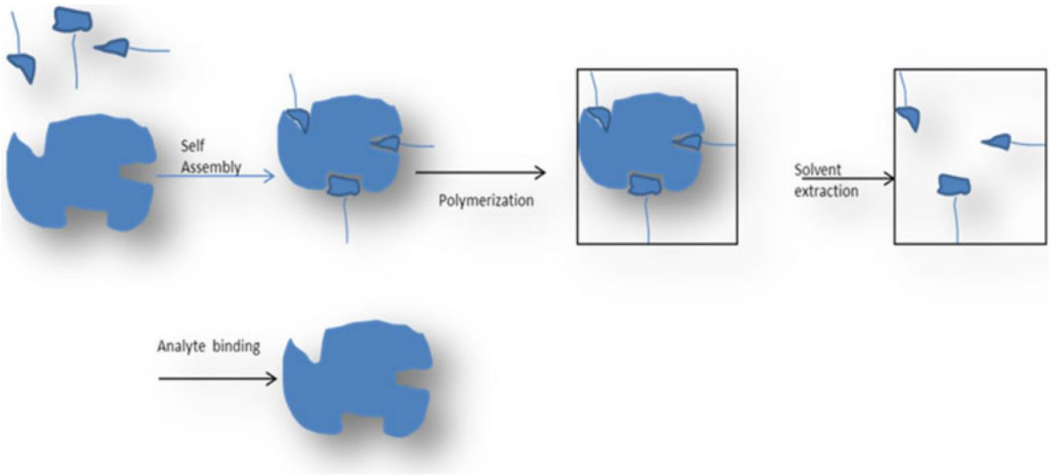

FIGURE 6.2: Representation of non-covalent imprinting

6.1.3 Monomers, Cross-linkers, Solvents and Initiator for the imprinting procedure

Monomers

The proper selection of monomer, cross-linker, and solvent affects the performance of the IIPs in their respective applications [198]. The performance is regarding shelf life, utility, rebinding abilities, and reuse [199]. In non-covalent imprinting, the durability of the polymer depends on the functional monomer and template interaction [197]. The monomer should have functional groups that will work towards strengthening the interaction between itself and the template and also the polymer matrix [200].

Cross-linkers

Cross-linkers play an important role in the imprinting process and create an environment whereby the orientation of the functional monomers and template favours formation of a rigid network where the template and, hence, the cavities are affixed [201]. The more stable these cavities are, the more useful the polymer will be. The cross-linkers should be in higher proportions in the final polymer, and highly branched, or high-molecular-weight crosslinkers have a tendency of producing such stable cavities [202].

Solvents

In most cases, solvents are used in the synthesis of IIPs. These include water, toluene, chloroform, acetonitrile, and many more [203]. A good solvent dissolves all the components of the polymerisation mixture and by extension contributes to the physical makeup of the polymer. The usability of solvents may depend on the hydrogen-bond parameter, dielectric constant, polarity, and solubility, which may increase or decrease the durability of that polymer [202, 204].

Initiator

The initiator is used to initiate the polymerisation process. It is a source of chemical species that reacts with a monomer to form a compound which is capable of linking with a large number of other monomers during a polymerisation process. Upon the exposure to heat or light, it generates free radicals or initiators. Figure 6.3 represents the chemical structure of various polymerisation components which are used in this research.

6.1.4 Polymerisation Methods

There are four different polymerisation methods generally used in the imprinting technique that have adequately been studied. Each has got some more attractive features than the others. They are-

Bulk Polymerisation

Bulk polymerisation has been preferred in recent times by most researchers [205]. They have limitations such as the non-uniform distribution of particle size, thermal instability,

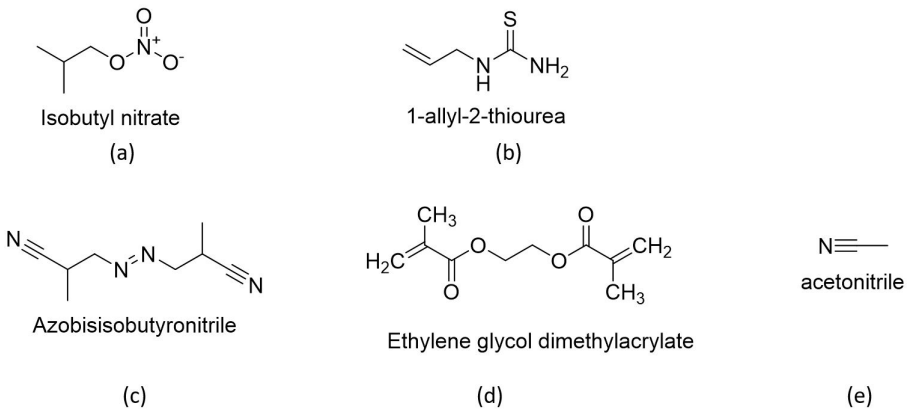

FIGURE 6.3: Chemical structure of: (a) Template molecule, (b) functional monomer, (c) initiator, (d) cross-linker and (e) solvent

wasting of the polymer at the grinding stage, and destruction of binding sites. They are easy to prepare. The synthesis of IIPs via the bulk polymerisation process includes mixing all the materials: template, monomer, cross-linker, and initiator in a reaction vessel; sometimes the polymerisation process is initiated by UV irradiation.

Precipitation Polymerisation

This type of polymerisation emerges as an excellent alternative to bulk polymerisation, having a high yield and also forming particles that are rigid and cross-linked, which helps them not to be easily coagulated; hence, it needs no stabilisers and, therefore, shows specific binding properties because the particles are free of stabiliser molecules. This method gives particles at the 0.3–10 μm range [206], and these particles, which are highly cross-linked, are formed with an excess amount of solvent [200].

Suspension Polymerisation

Generally, this is a complex process whereby the initiator is soluble in the monomer, and these two are insoluble in the continuous phase, which in most cases is water [200, 207]. This method produces micro-beads with a size distribution in the range of 0.5–10 μm [200], which are enhanced by the rate of stirring. Droplets of the monomer and initiator are suspended in the continuous phase, in the presence of a stabiliser, then polymerised. It is fast and reliable, and polymerisation of particles may be achieved in the space of two hours.

Surface (Emulsion) Polymerisation

The surface polymerisation is an excellent alternative to the other types of polymerisation and one of the highly used polymerisation methods. It annihilates the template and offers very rapid adsorption and desorption kinetics [200]. Surface polymerisation also possesses good stability in acidic conditions which is good for metal removal, as most metals are soluble in acidic conditions, which may imply that better removals may take place in those conditions. This method is also able to produce polymers of high molecular weight which helps in the stability of the polymer and is also easy to control and to remove heat.

6.2 Materials and Methods

6.2.1 Chemicals

Isobutyl Nitrate (IBN) $(C_4H_9NO_3)$, $1-Allyl-2-thioure$ (AT) $(C_4H_8N_2S)$, Ethylene glycol dimethacrylate (EGDMA) $(C_{10}H_{14}O_4)$, acetonitrile (ACN) (C_2H_3N) and 2,2-azobisisobutyronitrile (AIBN) $(C_8H_{12}N_4)$ were purchased from Sigma-Aldrich, Australia. Liquid acrylic resin was purchased from Briture Co. Ltd from Anhui, China. EGDMA and ACN were also purchased from Sigma-Aldrich, Australia as commercial reagents of the highest grade and distillation was not required before use. Deionised (DI) water was collected from a Millipore (18 Mohms cm) water system. A standard nitrate-N sample with a concentration of 100 (mg/L) was also purchased from Sigma-Aldrich. A NitraVer X Nitrogen-Nitrate Reagent Set was purchased from HACH, Australia.

6.2.2 Apparatus

A Hach DR/4000 Spectrophotometer was used to validate the concentrations generated using nitrate-N detection [208]. A Hioki IM 3536 LCR meter [209] was used to measure the impedance behaviour of the interdigital sensor. A Mettler Toledo Pro-ISM-IP67 pH meter was used to measure the pH level in the sample water.

6.2.3 Synthesis of Nitrate-Imprinted Polymer Coating

A conventional synthesis protocol for preparing the ion-imprinted polymer involved dissolving the following chemicals in acetonitrile (4.0 mL): Isobutyl nitrate (IBN) (1mmol), 1-allyl-2-thiourea (AT) (4.0 mmol), Ethylene glycol dimethylacrylate (EGDMA) (20 mmol) and Azobisisobutyronitrile (AIBN) (0.12 mmol). IBN and AT were used as the template molecule and functional monomer respectively, for preparing the nitrate derivative-imprinted polymers [220]. Figure 6.3 represents the chemical structure of the template molecule, functional monomer, initiator, cross-linker and solvent. The reaction mixture was purged with nitrogen gas for 10 minutes to remove oxygen. The mixture was polymerised in a water bath at 55°C for 16 hours, followed by 80°C for 3 hours, under a nitrogen environment. The polymer was washed with methanol to remove any unwanted particles. A mechanical mortar was used to grind the polymer and filtered to produce a particle size of 75 µm. The template molecule was removed from the polymer particle by washing with a mixture of 500 mL of methanol/triethylamine (4:1, v/v) solvent, followed by 500 mL of methanol for 24 h by soxhlet extraction equipment. After removal of the template molecule, deionised water was used to wash the polymer. Finally, it was desiccated in a nitrogen atmosphere at room temperature, scaled to measure the weight and kept in a closed container at 4°C. The same synthesis protocol was used without the template molecule to develop a non-imprinted polymer (NIP). Figure 6.4 illustrates the polymer synthesis process.

TABLE 6.1: Synthesis recipe of IIP and NIP polymerisation

Polymer Type	Template (mmol)	Functional Monomer (mmol)	EGDMA (mmol)	Acetonitrile (mL)
IIP	1.0	4.0	20.0	4.0
NIP	none	4.0	20.0	4.0

6.2.4 Functionalising the Polymer Coating

Acetone was used to remove any unwanted material on the sensing surface. 50 µL of acrylic resin, 250 µL of acetone and 400 mg of IIP polymer were mixed to prepare a suspension. PTL-MM01 Dip Coater was used to coat the sensing surface. The sensor was dipped in the suspension and was withdrawn at a rate of 200 mm/min to achieve a uniform coating on the

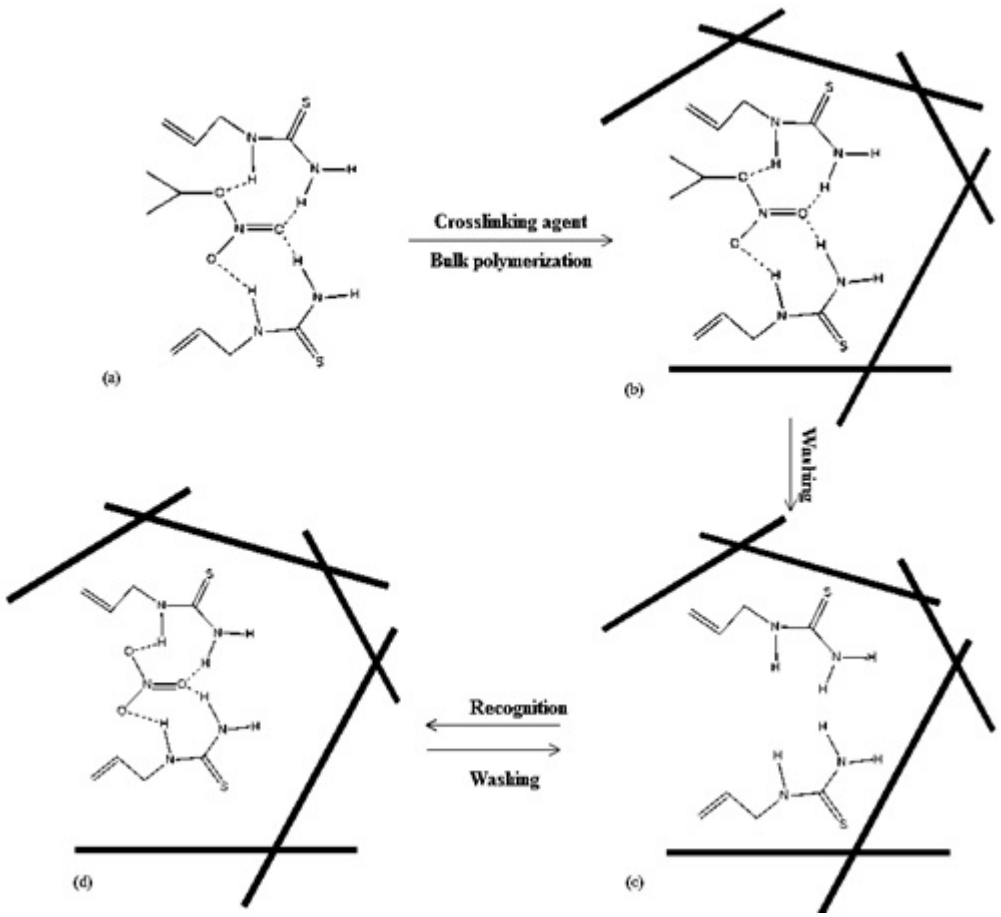

FIGURE 6.4: Graphic illustration of IIP with AT as a functional monomer. (a) IBN (template) and AT were mixed in solvent; (b) polymerisation with adding of EGDMA; black lines indicate the formation of polymer with target ions and functional monomer. EGDMA helps to form the polymer. (c) creating cavity for template molecule; (d) binding of nitrate ion. Table 6.1 gives the synthesis recipe of IIP and NIP polymerisation.

sensing surface. Due to evaporation of the acetone, the suspension became a solid coating on the sensing surface. Figure 6.5 shows the IIP polymer coating on the sensing area. The scanning-electron-microscope (SEM) images of Figure 6.6 (a) and (b) indicate the coating on the sensing area. The height of the coating surface is <150 μm, which is sufficient to measure the impedimetric behaviour of the sensor. The estimated cost of the imprinted polymer which was used on the coating surface is < $1 US.

6.2.5 Sorption Study

This study investigates the affinity of nitrate-N ions and measures the adsorption capacity with IIP and NIP. Ten mL of 1, 2.5, 5, 7.5, 10, 12.5, 15, 17.5 and 20 mg/L standard samples of nitrate-N were placed into nine different flasks. Ten mg of dried IIP polymer was added

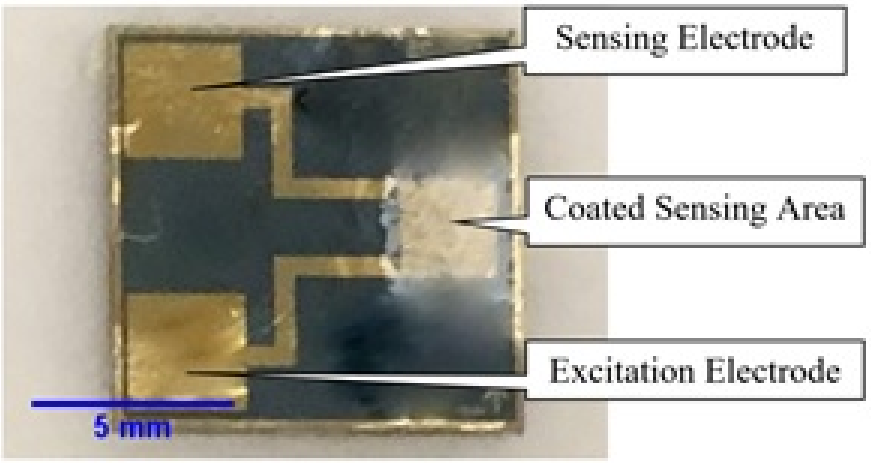

FIGURE 6.5: IIP Coating on the sensing surface.

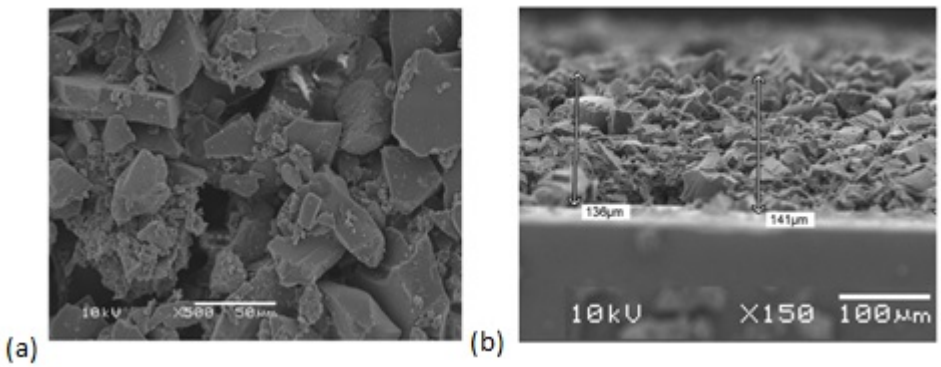

FIGURE 6.6: (a) top scanning-electron-microscope (SEM) view of the coating surface, (b) height of the coating as an SEM image.

to the sample solutions. The mixed solution was incubated by stirring in a shaker at 22°C for 1 hour. After incubation, the supernatant was sampled. The whole process was repeated with NIP polymer using similar standard samples. A 0.22 µm filter was used to filter out the samples. The final filtered solution was analyzed. The number of ions bound to the IIP was calculated using the following equation:

$$Q = \frac{(C_i - C_f)V}{m} \tag{6.1}$$

where, Q (mg/g) = Mass of nitrate adsorbed per gram of IIP, C_i (mg/L) = Initial concentration of nitrate-N; C_f (mg/L) = Final concentration of nitrate-N after adsorption. V (L) = Volume of the adsorption mixture, and m(g) = Mass of the polymer used.

6.2.6 Static Sorption Time

This study measures the binding kinetics of nitrate-N IIP and the time required to complete the binding. A 10 mL sample of 10 mg/L nitrate-N was added into six separate 50 mL glass flasks containing 10 mg of dried IIP. All the samples were stirred in a shaker (150 rpm) for 1,3,5,7,9,11,13 and 15 minutes at a similar temperature and humidity. Subsequently, all the mixtures were centrifuged, and the supernatant was analysed.

6.2.7 Selectivity Test

Fifty mg of IIP polymer was mixed with 50 ml of a solution of sodium nitrite ($NaNO_2$), potassium nitrate (KNO_3) sodium sulfate (Na_2SO_4) and DI water, where the concentration of nitrate-N, nitrite-N and sulfate was 20 mg/L respectively. The mixture was incubated for 1 hour with continuous stirring at room temperature. The samples were centrifuged after the incubation, and the supernatant was collected to analyse further for the selectivity test. Dionex 2000 Ion Chromatography was used to conduct the analysis.

6.2.8 Binding procedure of coated sensor

The polymer has imprinted cavities which adsorb the nitrate-N ions on the sensing surface from the aqueous medium. Figure 6.7 illustrates the adsorption process of nitrate ions. Ten µL of sample water was pipetted on the coated sensing area. Due to the hydrogen bond of the imprinted polymer, the nitrate-N ions were entrapped by the cavities. The sensor took seven minutes to absorb the maximum number of ions, and it took 30 minutes to dry the wet surface. After drying the coating surface, the EIS technique was applied to measure the changing behavior of the impedance data.

6.2.9 EIS Measurement of the Coated Sensor

Samples containing 1, 2.5, 5, 7.5 and 10 mg/L of nitrate-N were analysed, and the corresponding impedances were measured by an LCR meter. A Cole-Cole plot or Nyquist plot was created for impedance measurement, as shown in Figure 6.8 at the frequency range of 10 Hz-10,000 Hz. It is seen from Figure 6.8 that the radius of the plot decreases due to the increase in solution concentration. Figure 6.9 shows the change of reactance as a function of frequency. There is a significant difference in reactance between all the concentrations in

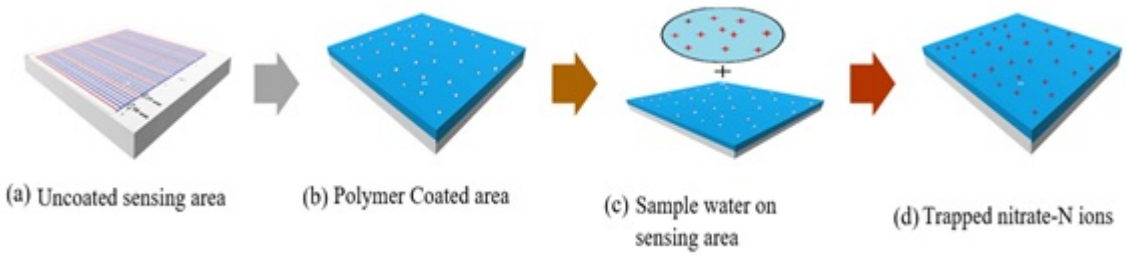

FIGURE 6.7: Diagram describing the adsorption process of nitrate-N ions: (a) uncoated sensing surface, (b) coated sensing surface, (c) sample water is added on the sensing surface, (d) ions are trapped on the sensing surface. White markers indicate the imprinted cavities on the polymer, and red markers indicate the nitrate-N ions.

the frequency range 40-220 Hz. The maximum difference of reactance was used to create the calibration curve, to measure the unknown sample for a specific frequency. The coated sensor was exposed in the water, and according to the imprinting polymer principle, the nitrate-N ions were trapped by the recognition sites. The sensor was exposed for 7 minutes to finish the entrapping. During the EIS measurement, the electrical intensity bulges through that imprinted polymer, and the corresponding impedance changed. The reactance or imaginary impedance is considered due to its significant change for different concentrations. The number of ions is different for different nitrate-N concentrations, which leads to different reactance as measured by the LCR meter.

6.2.10 Unknown-Sample Measurement

This experiment was conducted with different water samples, which were collected from various sampling locations in Sydney, Australia using the developed coated sensor. Additional nitrate was added to these samples to elevate the nitrate-N concentration to the desired concentration range, without changing the other parameters. An exception was sample 5, which did not have any nitrate-N added. The spectrometric method was used to validate the sensor measurements. The measurement was undertaken five times, and the results averaged for analysis.

6.2.11 Reusability Testing

It is required to use the sensor repeatedly with consistent performance to monitor the water in real time. Therefore, reusability testing is an important experiment, which was done for the developed coated sensor. The coated sensing surface requires cleaning to be

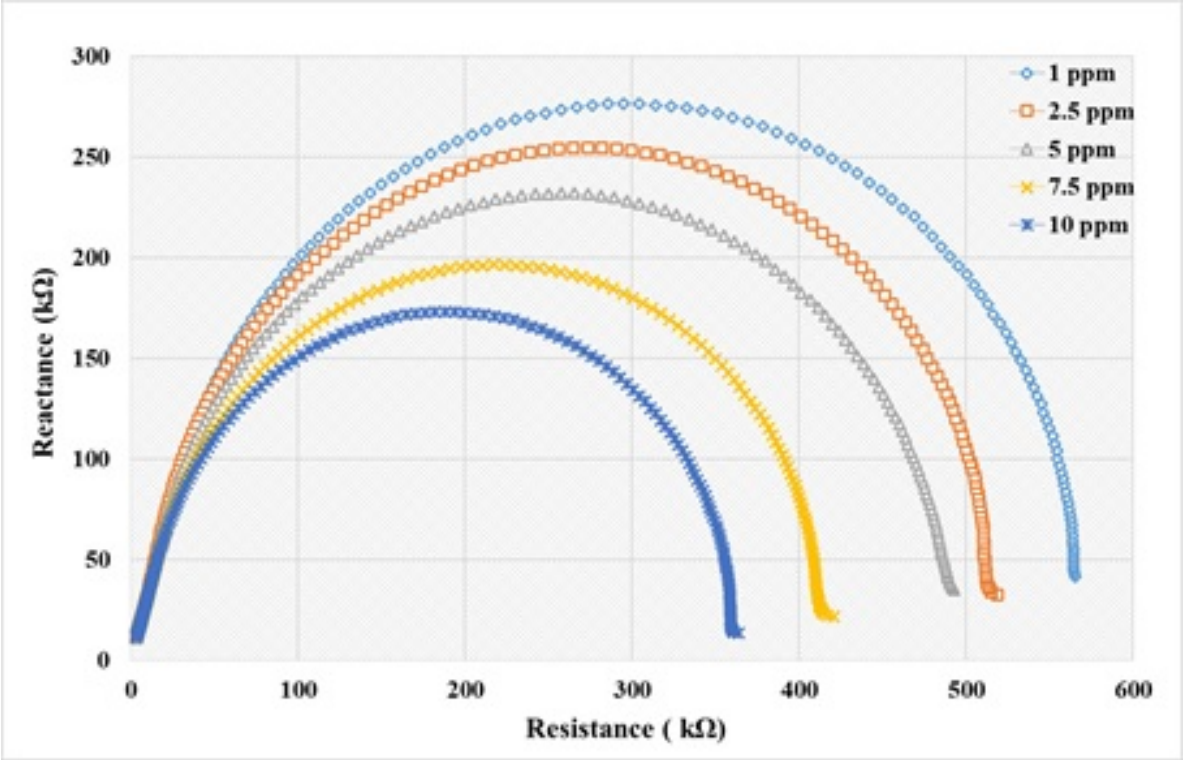

FIGURE 6.8: Nyquist plot for various concentrations

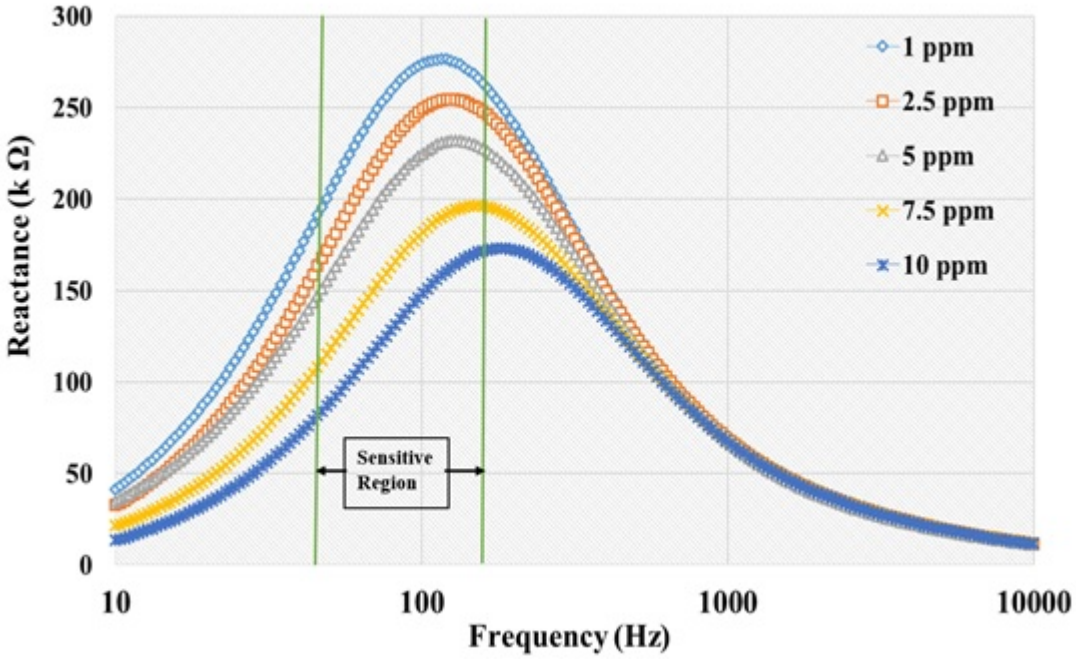

FIGURE 6.9: Reactance vs Frequency for various concentrations

used for continuous measurements. Ten µL of 10 mg/L nitrate-N was used as sample water for pipetting on to the sensing surface. A mixture was created with a ratio of Acetic Acid:

Deionized Water: Methanol = 1:20:2 (v/v) to remove the adsorbed ions from the sensing surface. The sensor was rinsed with the prepared mixture to remove the adsorbed ions from the coating surface. The process was performed five times to check the stability of the measurements.

6.2.12 Non-Linear Least-Square Curve Fitting

An EIS Spectrum Analyser [210] was used to analyse the impedance spectra. The algorithm of the electrochemical spectrum analyser was used for theoretical calculations to estimate the equivalent circuit parameters. The measured impedance from the sample solution and theoretically estimated values were matched by a complex algorithm, called the nonlinear least-square fitting technique. That complex algorithm also estimated the equivalent-circuit parameters. The statistical approach used to calculate the residual mean square r_c^2; it also explains the deviation in between the experimentally observed data and optimal solution. The proposed equivalent circuit with the corresponding mathematical model is used sometimes to optimise the solution to get the best-fitted curve. The residual mean square is the error, which estimates how well the model agrees with the equivalent circuit parameters and calculating those parameters with an error < 5

6.2.13 Comparison of Coated Sensor and ISE

Chapter 4 reported a smart sensing system which measured the impedance of an interdigital sensor. The smart sensing system is used to calculate the reactance or imaginary part of the impedance of the coated sensor. In order to calculate the imaginary part of the impedance of the sensor, the microcontroller calculates the phase difference between the input voltage and current. The calculated phase difference is used to calculate the reactance of the coated sensor. The details of the sensing system have been discussed in Chapter 4. The sensing system has been used to measure the concentration of nitrate-N in real water samples and these results compared with sensION + 9662 Nitrate Ion-selective electrode, which is a commercial sensor. Both results are compared with results from standard laboratory measurements to calculate a discrepancy. Compared to our earlier chapter (Chapter 4), An Arduino Uno Wi-Fi embeds the current sensing system. The sample data is also sent to an IoT-based web server to monitor the sensor data in real time.

6.3 Results and Discussions

6.3.1 Sorption Studies

It is required to investigate the affinity of nitrate-N ions with IIP and NIP. The adsorption studies of nitrate-N ions to IIP and NIP are shown in Figure 6.10 (a). This illustrates that the number of nitrate-N ions bound to IIP increased with increases in the sample nitrate-N concentration up to a concentration of 11 mg/L. Above 11 mg/L, the polymer became saturated, and the curve was parallel to the concentration axis. However, the amount of nitrate-N ions bound to NIP at equilibrium was 7 mg/L and reached saturation. The result showed that the amount of nitrate-N ions bound to IIP was higher than the NIP at higher concentrations because of the more specific binding sites of IIPs are generated due to the imprinting polymerisation. Countries which follows the acceptable drinking limit of the US EPA (Environmental Protection Agency) [211] can also accept this saturated limit, and the developed polymer material is useful for coating.

6.3.2 Uptake Kinetics Study

An adsorption kinetics study helps to measure the adsorption time, which is required to trap all the target ions on the developed IIP. Figure 6.10(b) shows the plot for the uptake kinetic study of nitrate-N to the IIP. The concentrations were chosen according to the experiment, which was undertaken in section 2.6. The results indicate that the nitrate-N IIP maintains fast trapped uptake kinetics, and the equilibrium of the binding was reached in almost 7 minutes. This time also counts as the response time of the coated sensor, due to the use of the polymer as a coating on the sensing surface. The EIS measurement of the sensor takes less than 5 seconds

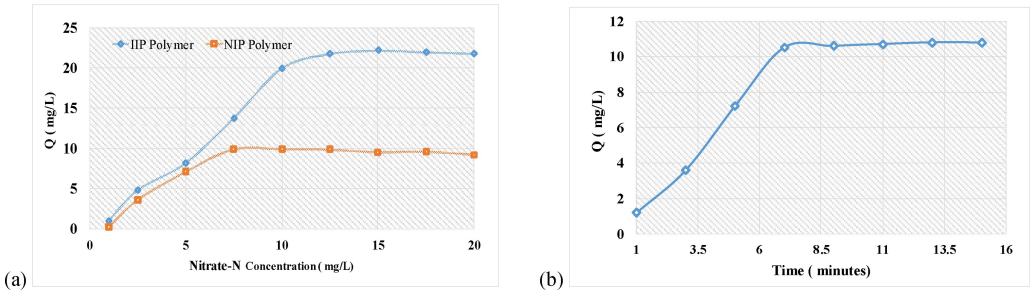

FIGURE 6.10: (a) Sorption study for IIP and NIP polymer, and (b) uptake kinetics study.

6.3.3 Study of Selectivity Test

Figure 6.11 illustrates that the peak area of the nitrate-N ions (retention time of 8.5 minutes) was distinctively reduced, compared to other ions (sulphate and nitrite). The retention time for nitrite and sulphate ions are at 5.39 and 6.58 minutes. The imprinted polymer has a high affinity for nitrate in aqueous media (pH 6.60). The binding of other analyte anions (nitrite and sulphate) have a relatively low affinity. Nitrite and sulphate are the other interfering ions which have a similar ionic structure to nitrate-N ions. With this in mind, a subsequent experiment was undertaken where 11 mg/L of nitrate-N, nitrite-N, and sulphate ions were placed into three different containers. From section 3.1, it is known that at nitrate-N concentrations of up to 11 mg/L the majority of the nitrate-N can be adsorbed by the IIP. Therefore, a similar amount of nitrite-N and sulphate ions are considered for the experiment. It is seen from table 6.2 that the IIP bound 90% of ions in the presence of nitrite and sulphate ions. In the absence of these additional ions, the IIP adsorbs 98% of the nitrate-N ions. This result suggests that the nitrate-N has a higher affinity towards the developed imprinted polymer compare to similarly structured ions. IBN has one functional group which is exactly similar to nitrate-N and removal of IBN from the imprinted polymer created the shape of nitrate-N which has a higher affinity of nitrate-N only. Nitrite-N and Sulphate ions have different shapes and sizes which makes the developed IIP specific for nitrate-N ions.

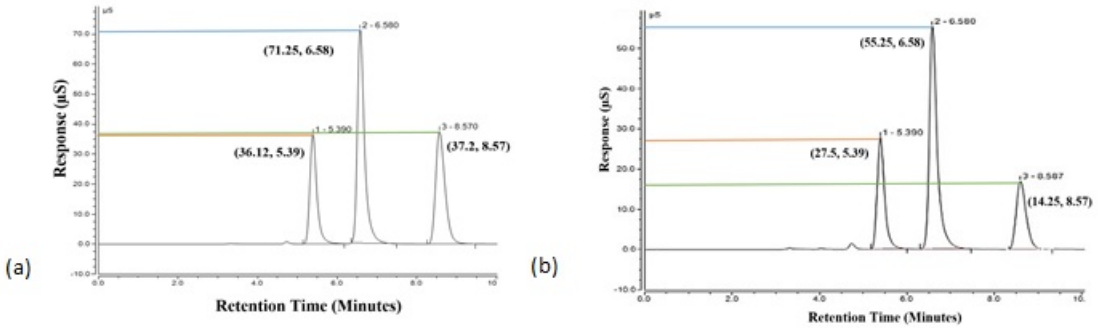

FIGURE 6.11: Chromatograms of sample mixture in the imprinted polymer, (a) mixed solution before incubation, (b) after incubation.

6.3.4 pH-Dependent Binding Profile

The performance of the IIP coated sensor was studied in different pH solutions to observe the effect of pH. The pH was varied by the standard buffer solution to cover a range of 3.0-8.0.

TABLE 6.2: Binding of nitrate-N in aqueous media

Type	Nitrate-N (%)	Nitrite-N(%)	Sulphate(%)
Mixture of Different Ions	90	6	4
Only Nitrate-N ions	98	-	-

The surrounding ionic strength of the polymer will change significantly when it is exposed to a pH solution. It has been reported [222] that an increase in pH usually increases the swelling of the polymer. This phenomenon can be observed on the developed IIP as well, and the results are illustrated in Figure 6.12. The number of ions bound by the sensor increased as pH decreased. As the pH increased, the number of ions bound reduced significantly. The sensor was operated at a pH value of 6.60, where the IIP-coated sensor bound nearly 90% of the ions which is acceptable in New Zealand water.

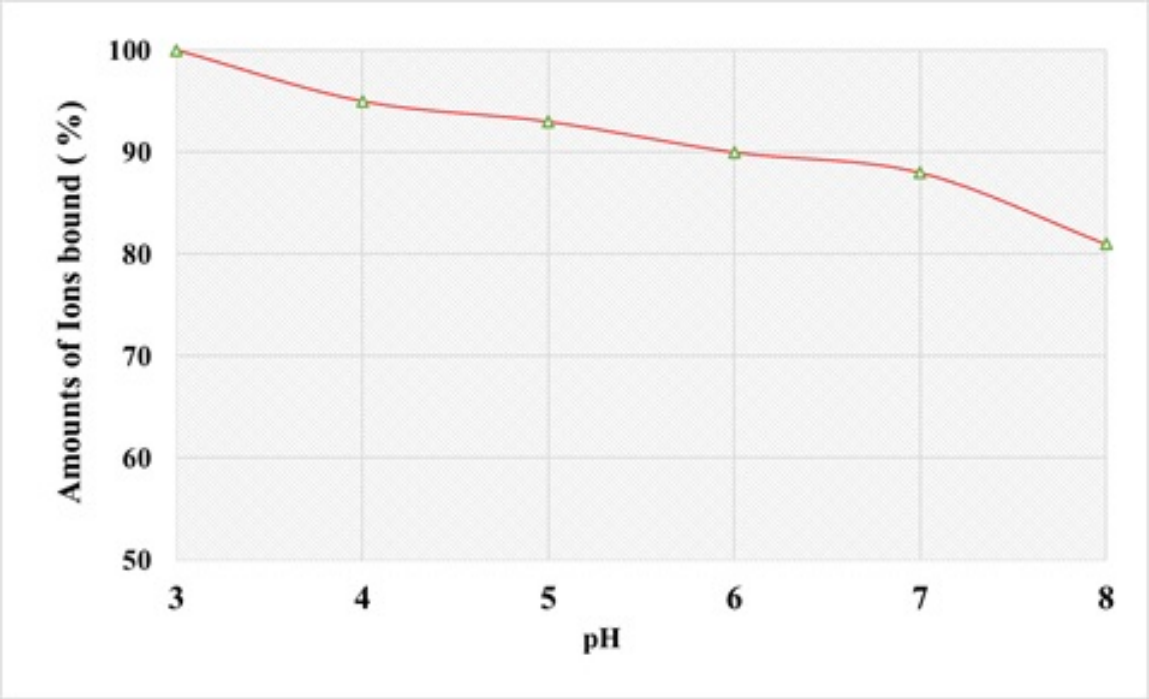

FIGURE 6.12: Effect of pH on the measurement

6.3.5 Calibration Standard

It is seen from Figure 6.13 that, at 110 Hz, the difference of the reactance change for various concentrations is at a maximum. Therefore, the reactance for various concentrations is taken at that frequency to develop the calibration curve to measure an unknown sample. The nitrate-N concentration is represented on the x-axis, and the corresponding reactance is represented on the y-axis. Figure 6.13 indicates the developed calibration graph which is linear ($r^2 = 0.99$). This calibration standard will be used to measure the nitrate-N concentration of any unknown water sample. The final formula to calculate the unknown sample-

$$C = \frac{X - 289418}{-12811} \tag{6.2}$$

Where, C is the unknown sample in mg/L and X is the measured reactance (Ω) from EIS measurement. This standard is applicable when the coated sensor operates at 110 Hz. The LOD and limit of quantification (LOQ) were 1.06 mg/L and 3.21 mg/L, respectively. Therefore, 1.06 mg/L is the lowest concentration, which can be measured by the developed coated sensor, and 3.21 mg/L can be measured reliably at the specific constant temperature and humidity.

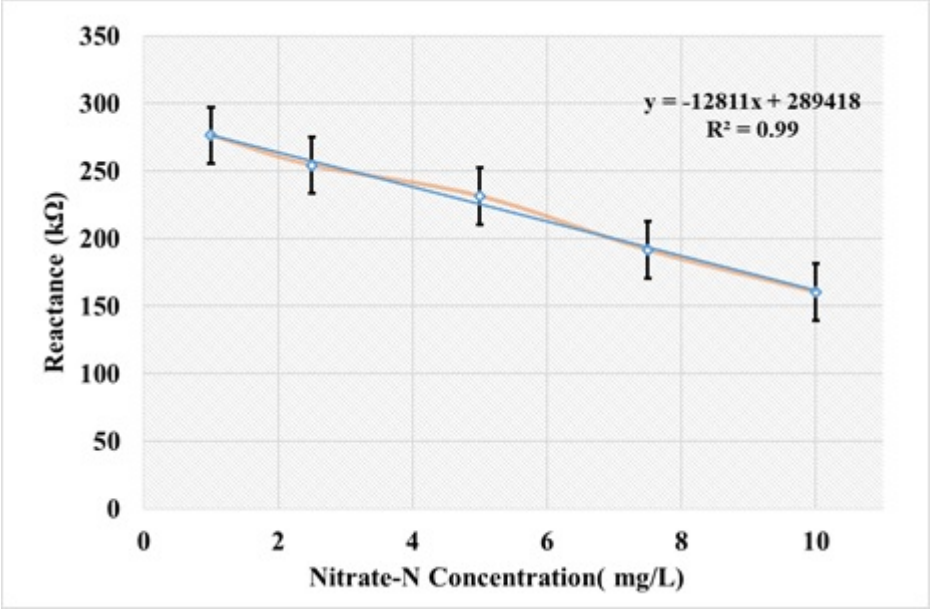

FIGURE 6.13: Calibration standard for nitrate-N measurement.

6.3.6 Unknown Sample Measurement

6.2 is used to measure an unknown sample by the developed coated sensor. Sample 5 was taken as one of the unknown samples, and the coated sensor was used to measure the concentration. It was found that the reactance of the sample was $X = 275325.9\ \Omega$. The measured X was used in 6.2 and the final concentration was$C = 1.1mg/L$. Table 6.3 shows that the coated sensor accurately measured the sample concentration across a wide range of nitrate-N concentrations, with an error rate of less than 1%, when the concentration was more than 3 mg/L. This supports the statement that the LOQ of the sensor is $3.21mg/L$. When the concentration is on the lower side $(1 - 3mg/L)$, the errors are closer to 5%, which is still acceptable for this measuring purpose. In New Zealand and Australia, the concentration of nitrate-N in surface water covers this range, and the coated sensor can measure this range with a reasonable amount of error, which will be acceptable statistically.

TABLE 6.3: Comparison of nitrate-N concentration (mg/L) measured by the coated sensor and using the spectrometric method.

Sample Number	Coated Sensor (mg/L)	Lab Measurement (mg/L)	Error Rate(%)
Lake Water	3.57	3.6	0.83
Stream Water 1	2.47	2.5	1.19
Stream Water 2	8.5	8.55	0.58
River Water	9.96	10.0	0.4
Canal Water	1.1	1.15	4.34

6.3.7 Reusability of the Sensor

The number of ions bound on the sensing surface was measured and plotted in Figure 6.14. This showed that the sensor could be reused accurately five times before measurement errors occur. More than 95% of the nitrate-N ions can be rebound by the IIP coating surface for the first five measurements. After five measurements, the sensor recorded errors of >10%. It is likely that some of the recognition sites were damaged due to the washing of the sensing surface repetitively. Therefore, some of the ions are not bound by the recognition sites, which were binding earlier. It is also seen that the repetitive measurements were also stable.

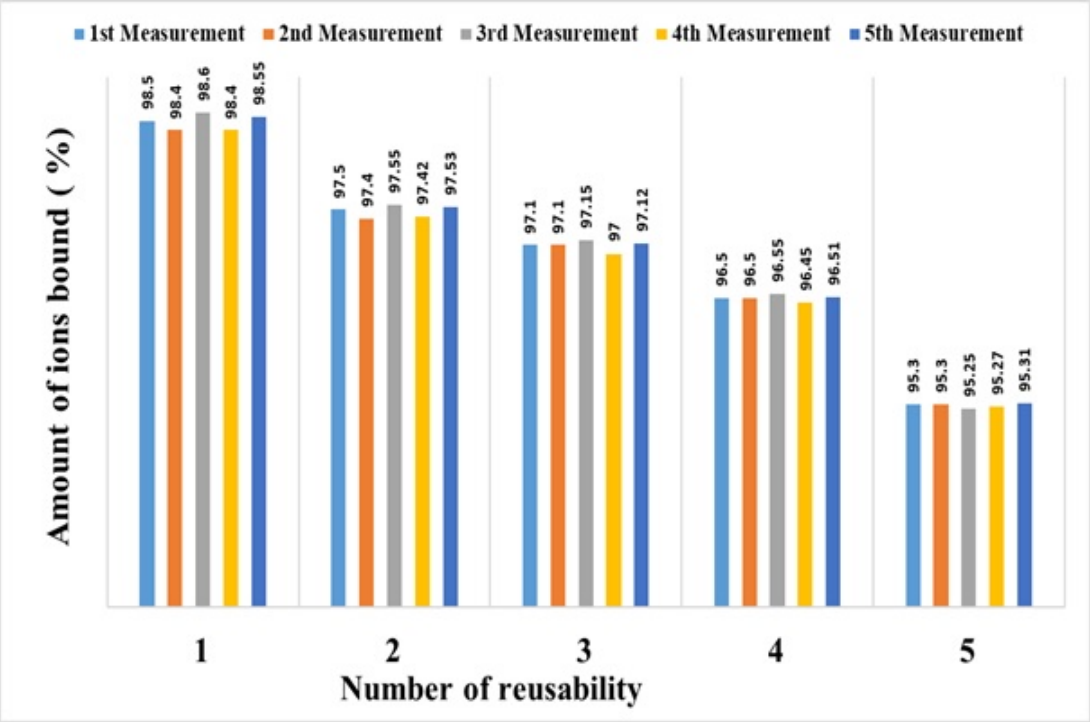

FIGURE 6.14: Calibration standard for nitrate-N measurement.

6.3.8 Comparison of Coated Sensor and ISE

Table 6.4 and 6.5 compares results from the coated sensor combined with the sensing system to those from the ISE sensor, and provides a measurement of error (%). The coated sensor combined with the sensing system measured nitrate-N with an error rate of less than 5%. The ISE sensor recorded higher measurement errors than the laboratory measurements. Sample 4, which was collected from a lake, was used to transfer through the developed sensing system with the integrated WiFi to an IoT based web server and the real-time data are shown in Figure 6.15. Therefore, the developed sensor can measure the nitrate-N concentration in the actual sample and transfer the measured data through a low-cost device, which can be used as a part of a distributed network in the future.

6.3.9 Non-Linear least-square curve fitting

The estimated circuit parameters and the model are given in Table 6.6. The fitted curve and the simulated results are shown in Figure 6.16 (a) and (b). In Figure 6.16 (a) the red markers are experimentally obtained results, and the solid green line represents the fitted curve for the equivalent circuit. It is also seen that the curve nicely fits with the experimentally obtained

TABLE 6.4: Comparison of measurement between the coated sensor and lab measurement

Sample Number	Concentration (mg/L)	Error rate (%)	Lab Measurement (mg/L)
1 (Tap Water)	1.22	1.67	1.20
2 (Stream Water 1)	1.67	1.76	1.7
3 (Stream Water 2)	2.12	1.39	2.15
4 (Lake Water)	2.35	2.17	2.3
5 (River Water)	1.80	2.70	1.85

TABLE 6.5: Comparison of measurement between the Ion Selective Electrode and lab measurement

Sample Number	Concentration (mg/L)	Error rate (%)	Lab Measurement (mg/L)
1 (Tap Water)	1.26	5	1.20
2 (Stream Water 1)	1.73	1.76	1.7
3 (Stream Water 2)	2.20	2.32	2.15
4 (Lake Water)	2.34	1.73	2.3
5 (River Water)	1.75	5	1.85

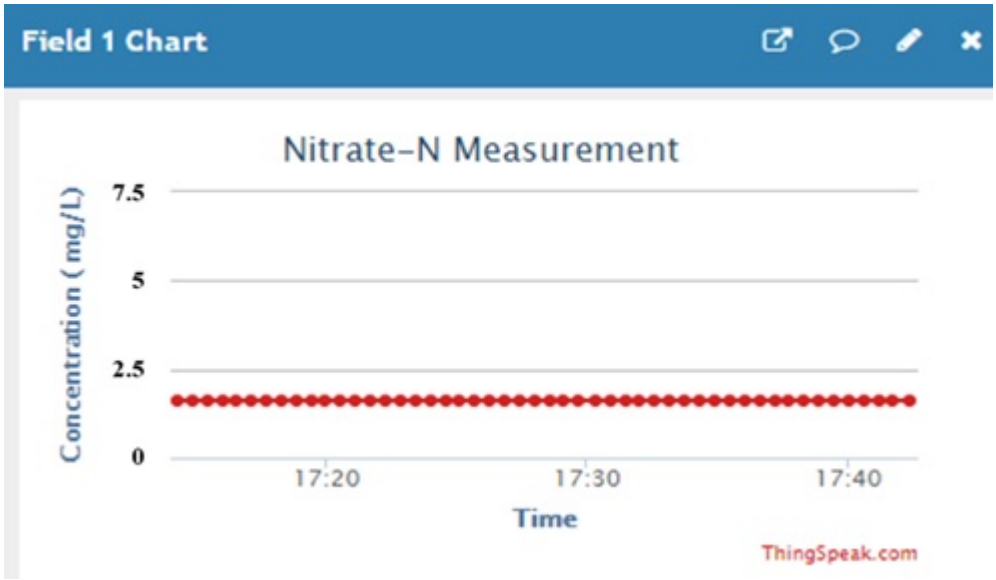

FIGURE 6.15: Real time data transferred to an IoT server

results. Figure 6.16 (b) represents the fitting of simulated results (blue markers) from the developed model, which is also matched with the measured or experimental results. Figure 6.16 (a) also shows the equivalent circuit parameters which are imposed on the fitted curve for

the coated sensor. C_1 is the double layer capacitance, which formed on the interface between an electrode and its surrounding electrolyte. This double layer is formed as ions from the solution adsorb onto the electrode surface. The positive and negative electrodes are parted from the charged ions by an insulating space, often about angstroms. R_1 is the charge transfer resistance. In this study, the double layer capacitance and charge transfer resistance are the key electrical parameters in determining impedance change, when analyzing system kinetics.

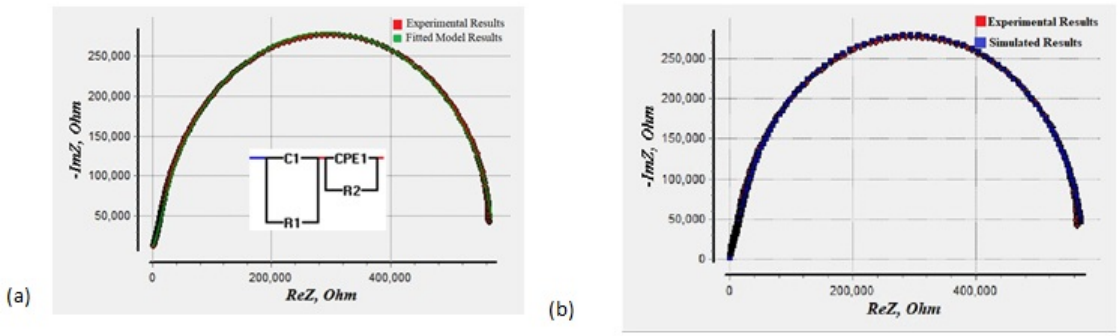

FIGURE 6.16: (a) Experimental results and fitted model results are fitted together; (b) Experimental results and simulated results are fitted together from the developed model

TABLE 6.6: The coated sensor with the equivalent-circuit parameters in different concentration

Concentration (mg/L)	C_1 (nF)	R_1 Ω	R_2 Ω	P_1 $(nano)$	n_1
1	2.4171	556020	17328	7.51	0.91
2.5	2.4078	508490	14433	6.13	0.93
5	2.4827	472890	14513	1.07	0.88
7.5	2.5135	397430	17904	9.14	0.89
10	2.4366	348340	14544	6.78	0.92

Figure 6.17 is the calibration standard developed from R_1 of Table 6.6. One of the equivalent-circuit parameters was used to develop this calibration standard which is linear ($r^2 = 0.98$). This calibration standard can be used to measure any unknown sample, and is not frequency-dependent. The earlier calibration standard is frequency-dependent, whereas is the calibration standard from CNLS analysis was frequency-independent. A nonlinear curve fitting method requires large computation memory and time, which forces to use the earlier developed frequency dependent calibration curve with a smart sensing system, to measure the nitrate-N concentration from an unknown sample.

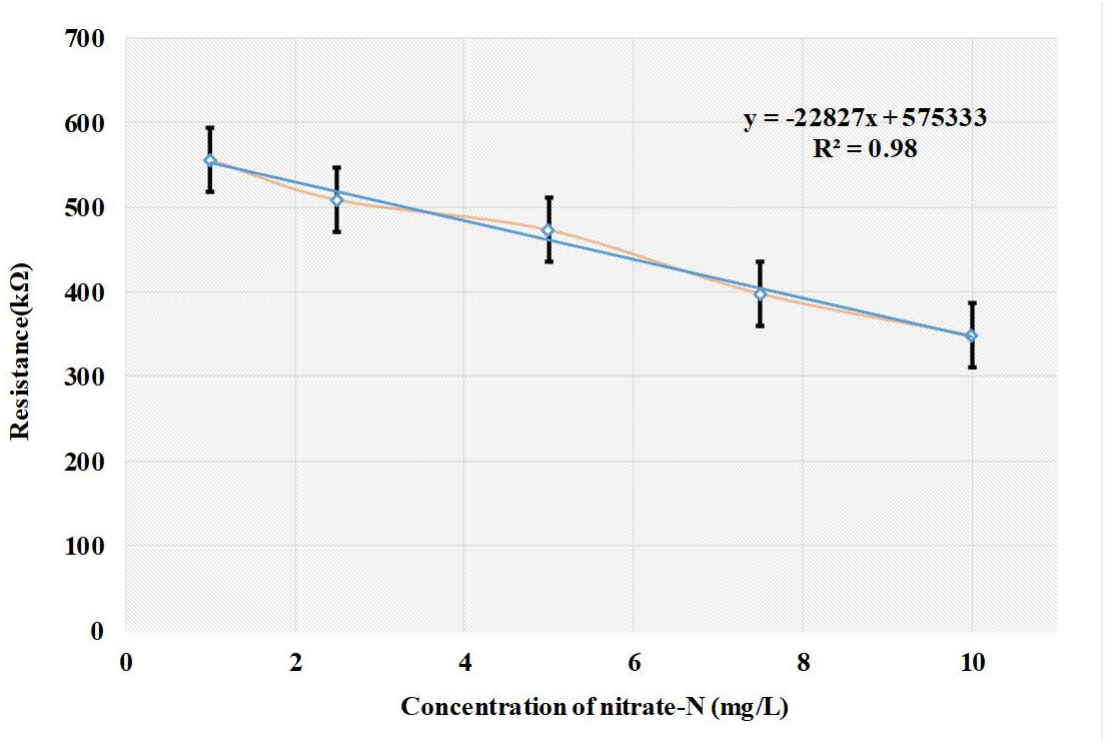

FIGURE 6.17: Calibration standard from CNLS analysis

6.4 Chapter Summary

An ion-imprinted polymer-based nitrate-N adsorber has been developed and used as a coating material on the sensing surface. The interdigital capacitive sensor has been used for detection purposes, where the detection limit is 1-10 mg/L. The sensing surface was functionalised by an acrylic resin with an embedded coating material to introduce selectivity for nitrate-N. A calibration curve has been developed to measure an unknown sample. The measurement of unknown water samples has shown good results, with an error of <5 %. The sensor can be reused up to 5 times before the error rate becomes unacceptable. CNLS curve fitting was also applied to interpret the experimentally obtained impedance spectra. An earlier developed sensing system was also used to measure the nitrate-N concentration in real time and transfer the data to a web server, which has great potential to develop a large distributed network. Future research will focus on increasing the reusability of the sensor so that it will be more useful for real-time water monitoring.

Chapter 7

IoT enabled Smart Sensing System

7.1 Introduction

Most of this chapter is taken from this publication[1] . Monitoring nitrate concentration in the field is an excellent ability for a water-monitoring study. In this chapter, we have explained an Interdigital FR4-based capacitive sensor, which is characterised for nitrate concentrations of 0-40 ppm (mg/L). Different unknown samples were measured and validated with standard UV-Spectrometry. A smart sensing node has been developed which can collect water from a lake, stream, or river, measure the instantaneous nitrate concentration, and transfer the data through the gateway to a user-defined cloud server. The system is completely autonomous and solar powered, robust, and trialled in the field successfully. A simple moving-average algorithm is used to smooth the collected data in the cloud side. The LoRa protocol and WiFi protocol are compared in terms of power consumption. The proposed system is trialled in the field continuously and the result validated with standard UV-Spectrometry. The developed smart system can be easily deployable and friendly to use, and offers new possibilities for both spatial and temporal analysis for nitrate concentration.

7.2 Materials and Methods

7.2.1 Interdigital Sensor

The working principle of the interdigital sensor is explained in Chapter 3. An FR4-based interdigital sensor(Figure 7.1) is used in this experiment. The dimensions of the sensing area

[1] **Alahi, Md Eshrat E.**, Najid Pereira-Ishak, Subhas Chandra Mukhopadhyay, and Lucy Burkitt. "An Internet-of-Things enabled Smart Sensing System for Nitrate Monitoring." IEEE Internet of Things Journal (2018).

are 33mm17mm, which is easy to dip into water. Tin oxide is layered as a coating material on the copper electrodes to keep them from corrosion free.

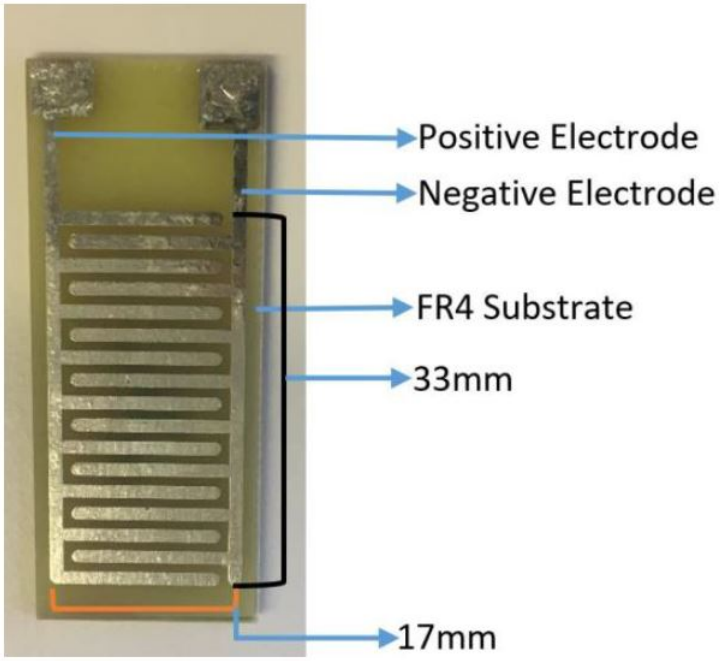

FIGURE 7.1: FR4 interdigital sensor and dimensions

7.2.2 Experimental Setup

The sensor was characterised by a Hioki IM 3536 LCR meter, where the frequency was swept from 10 Hz to 100 kHz. Standard laboratory temperature and humidity were maintained throughout these experiments. 1, 10, 20, 30, 40 ppm nitrate solutions were taken as standard solutions. Deionised water was taken as a control solution. The average pH of the solution was 6.71, which is also maintained in creek water. Figure 7.2 shows the laboratory setup for EIS data acquisition. Initially the sensor was characterised to get the impedance profile and develop the calibration standard for nitrate measurement. All experiments were repeated five times to observe the impedance behaviour, and average results were calculated.

7.2.3 System Description

A smart sensing system is proposed to carry out the in-line nitrate analysis as per Figure 7.3. Figure 7.4 shows the circuit diagram of the developed system. Arduino Uno and Arduino Uno Wi-Fi were used as the main microcontroller. An AD5933 is used to get the impedance

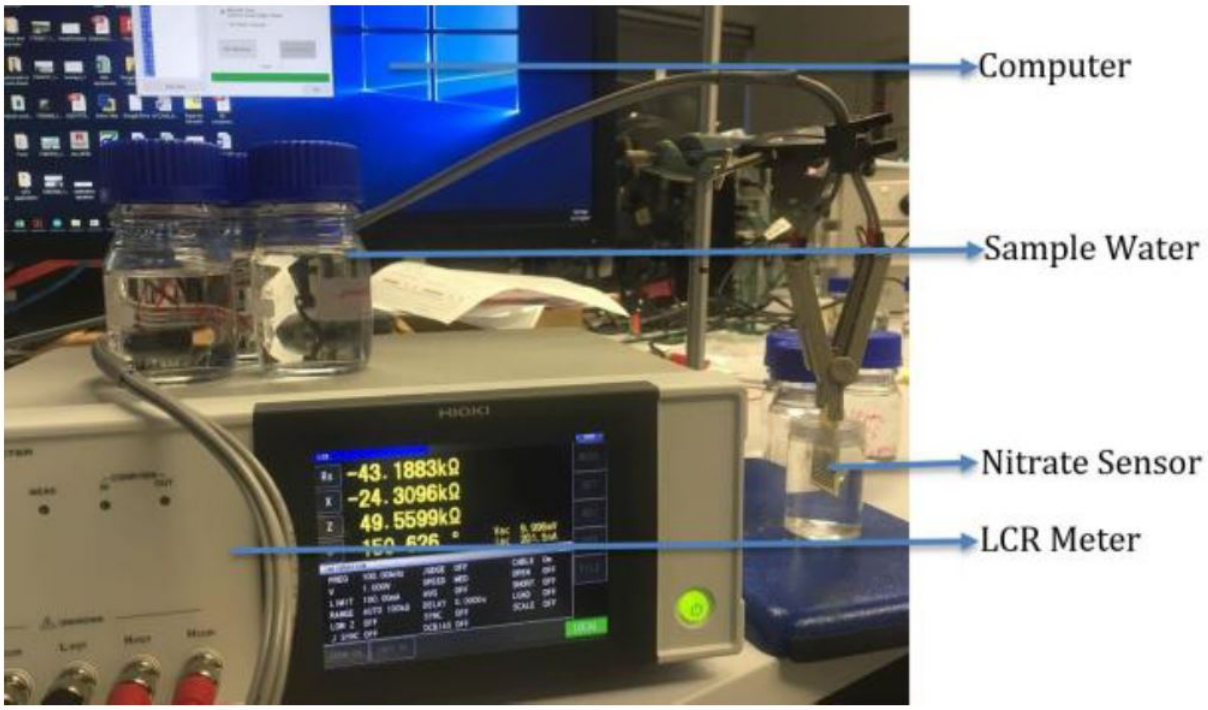

FIGURE 7.2: EIS measurement in laboratory conditions

data from the sensor. The impedance analyser gets the impedance and the phase shift of the sensor. The impedance analyser has the ability to sweep the frequency, though this is not required in the current application. The operating frequency is fixed and each measurement is done five times. Only the average nitrate concentration is sent to the IoT cloud server.

A Dragino LoRa shield is used as a long-range transceiver to communicate with the gateway. It allows sending data and reaching an extremely long range with low data rates. It is based on the RFM95W/RFM98W and used for 915 MHz transmission/reception. An L298N is used as a motor driver to control the inlet and outlet pumps. The inlet pump brings the water into the reservoir and the outlet pump empties the reservoir after the measurement.

LG01S is used as the LoRa/Wi-Fi gateway to communicate between the sensing node and the cloud server. The gateway is also responsible to send the data to the cloud server. Thingspeak is used as an IoT-based cloud server, which is free to use and can easily store data. WiFi and LoRa, both communication protocols, were used to examine the durability of the sensor nodes. The Arduino Uno WiFi has a WiFi module, which is responsible for transmitting and receiving data through the gateway. An LG01S is also used as a WiFi gateway. All the microcontrollers, sensor, inlet and outlet pumps, rechargeable battery, solar charge controller, and water reservoir are contained in a steel box which is robust and easy

to install. Figure 7.5 indicates the materials which are used in the sensing node. Figure 7.6 shows the inside of the steel box.

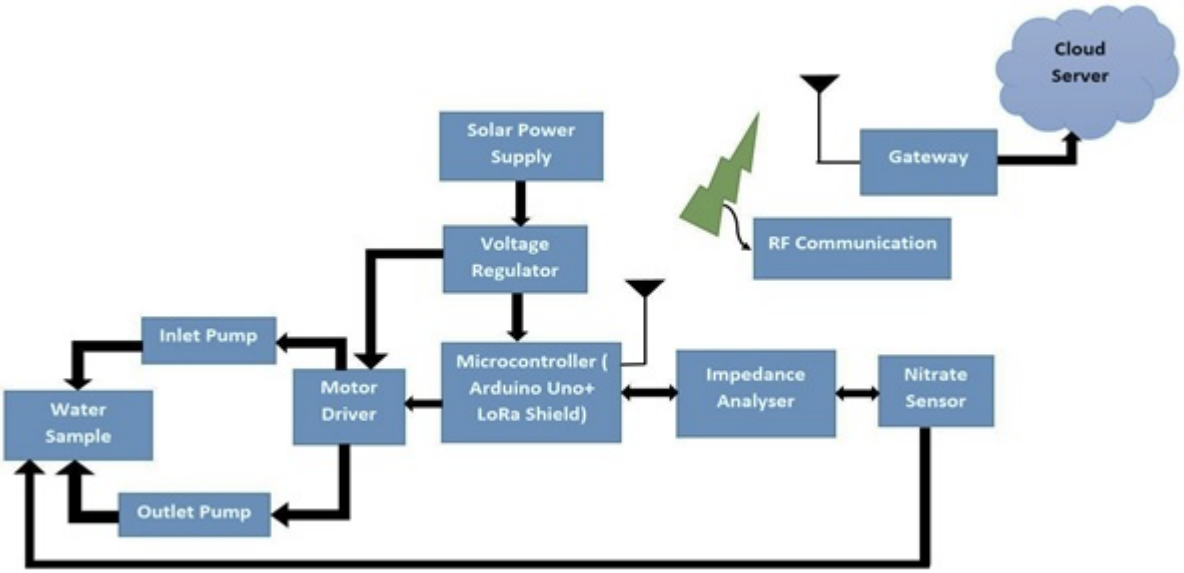

FIGURE 7.3: Block diagram of the data transmission

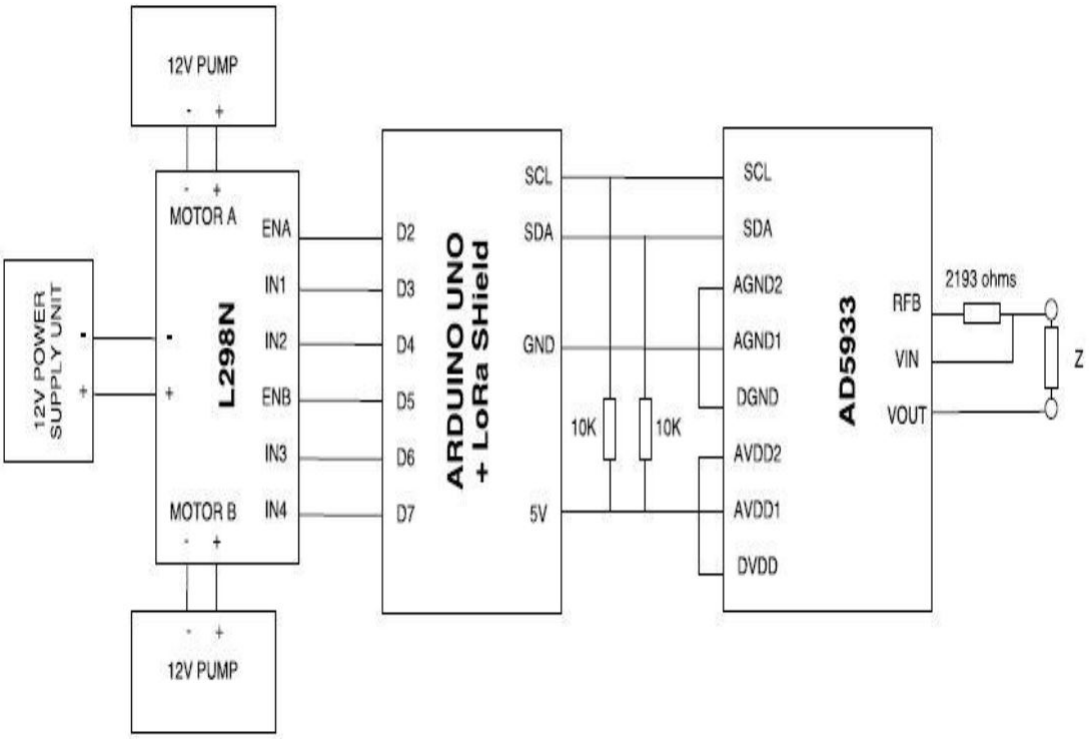

FIGURE 7.4: Circuit diagram of the sensing system

7.2.4 Energy-harvesting Technique

A solar panel (Model: ZM-9051), solar charge controller (MP-3750), and a sealed rechargeable battery (12 V, 12 AH) were used to provide energy continuously without any human intervention. All through the day the system is controlled from the microcontroller in various operation modes (active, sleep, transmitting/receiving). Due to the steel structure, the microcontroller had some difficulty communicating with the gateway to send the data from the sensor node with the existing antenna. Therefore, a VERT900 omni-directional antenna was used and extended through the steel box. Finally, it was installed near the study location as per Figure 7.7.

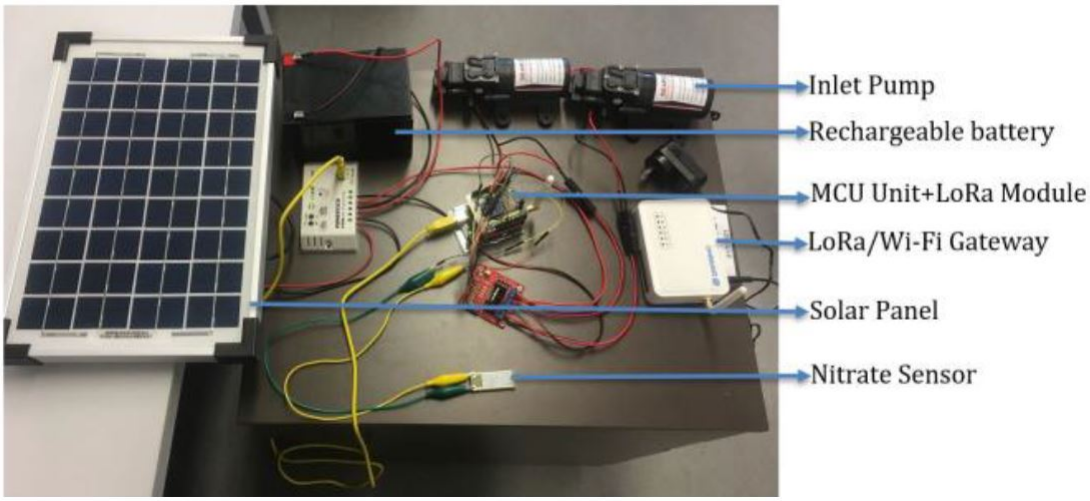

FIGURE 7.5: Different parts of the proposed system

7.2.5 Study Location

The study location is in Macquarie University near a small creek. As is seen from Figure 7.8, that sensor node is installed 340 m from the gateway. The gateway is installed in such a way that the sensor node has a clear line of sight and there is no obstacle to data transmission. The blue marker in the map indicates the gateway location and the green marker indicates the sensor node's location.

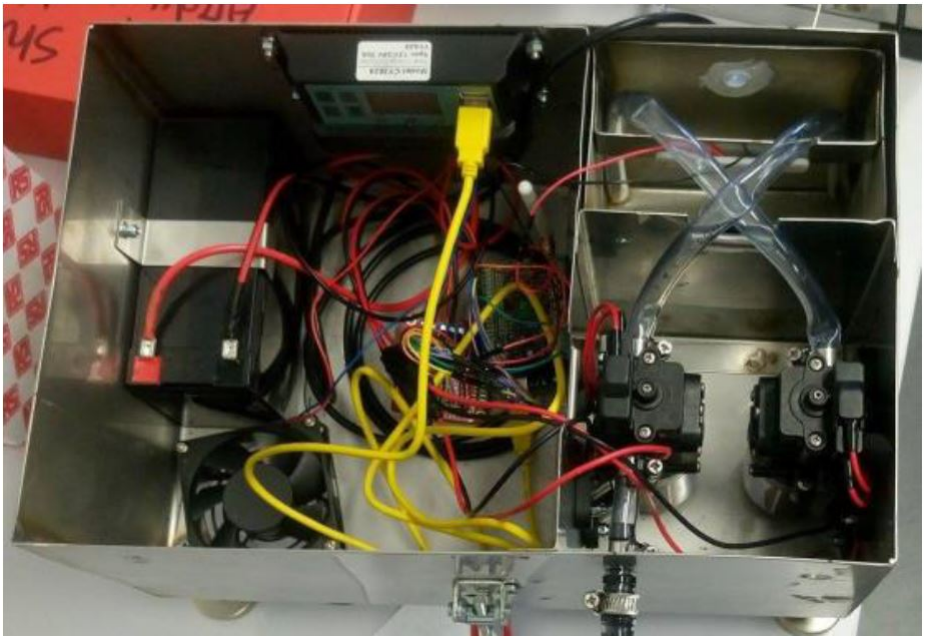

FIGURE 7.6: Inside of the sensor node

FIGURE 7.7: Field installation of the smart sensor node

7.3 Results and Discussion

7.3.1 EIS Measurement for Nitrate Concentrations

The impedances of different concentrations of nitrate sample are measured during an EIS measurement and plotted as Figure 7.9. It is seen that the bode plots for concentrations of 1, 10, 20, 30, and 40 ppm are different from each other due to the impedance change.

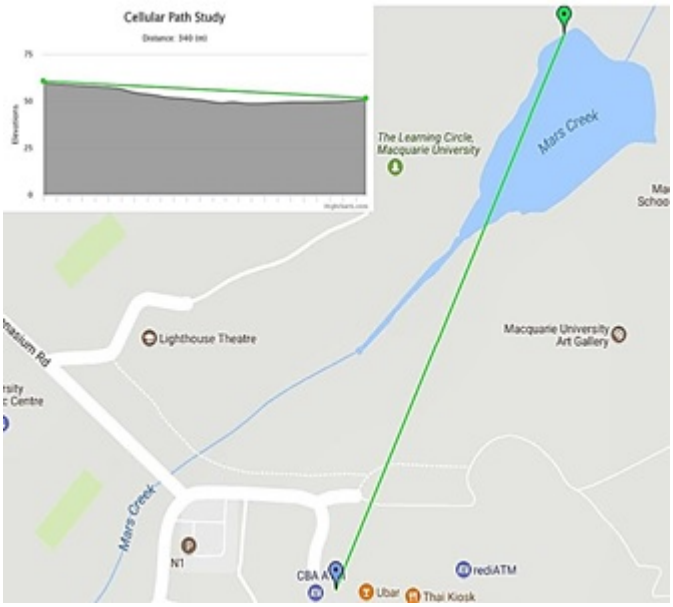

FIGURE 7.8: Study location and distance between gateway and the sensor node

The number of ions for different concentrations are different from each other. Therefore, the electric field from the positive electrode bulges more or less through the ions in the aqueous medium on the path towards the negative electrode. The dielectric properties of different concentrations are different which is reflected on the bode plot. The real impedance and imaginary impedance are plotted with respect to frequency, and it is noted that the real impedance has a more significant change than the imaginary part of impedance(Figure 7.10). The change is stable and consistent when the frequency is more than 500 Hz.

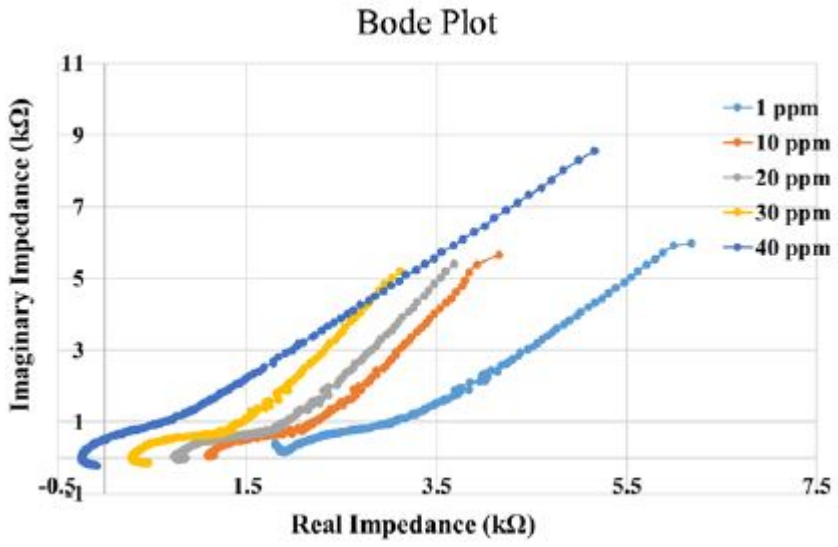

FIGURE 7.9: Bode plots for various nitrate concentrations

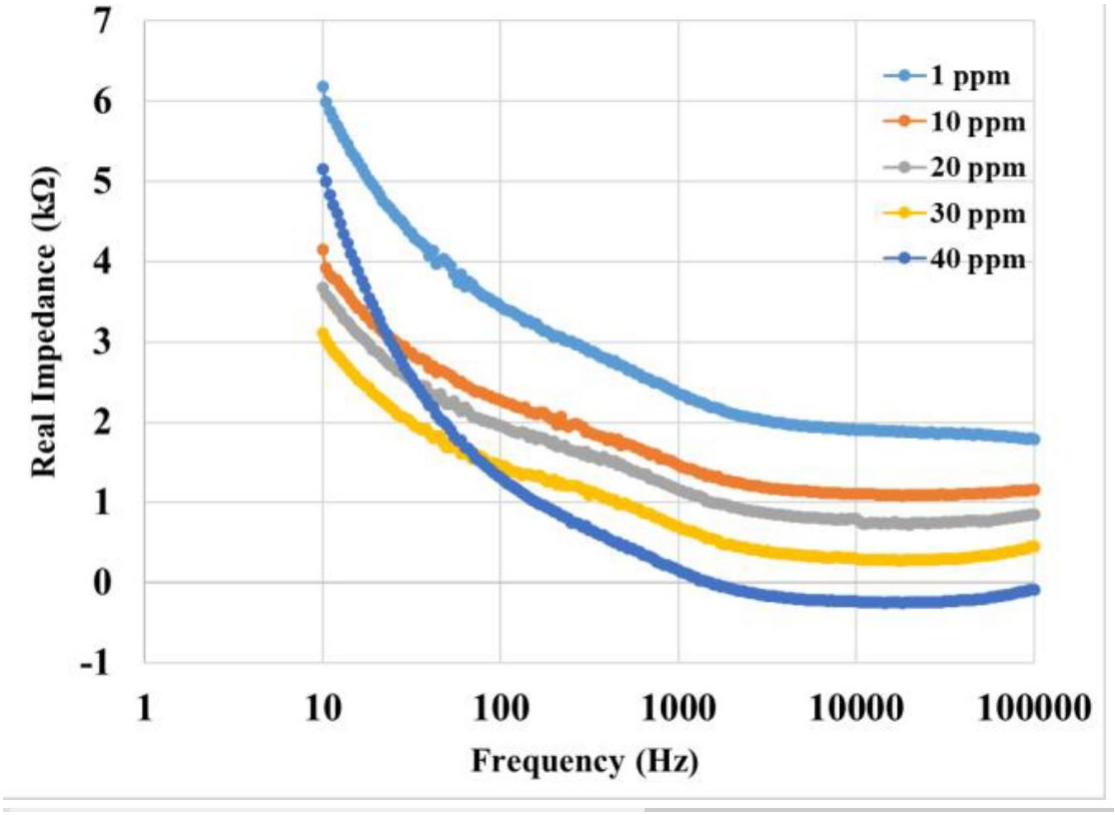

FIGURE 7.10: Frequency vs real part of impedance for various nitrate concentrations

7.3.2 Calibration Standard

It is seen from Figure 7.10 that the sensitive region for various concentrations is 500 Hz to 100 kHz. There is a significant change in the real part of impedance in that frequency range for various nitrate concentrations. 1000 Hz is chosen as the operating frequency to develop a calibration standard to measure unknown nitrate concentrations. At 1000 Hz, the real part of impedance for 1, 10, 20, 30, and 40 ppm of nitrate concentrations were used to develop a calibration standard to measure any unknown concentration. In Figure 7.11, with the nitrate concentrations plotted on the x-axis and the corresponding real part of impedance plotted on the y-axis,they follow a straight line, and the regression co-efficient is $R^2 > 0.98$, which is adequate to calculate any unknown impedance using the straight line. Therefore, the calibration standard for an unknown sample concentration is

$$C = \frac{R - 2212.2}{-51.77} \tag{7.1}$$

where **C** is the concentration (ppm), and **R** (Ω) is the measured real part of impedance from an unknown sample. It is seen that the sensitivity of the sensor is -51.77 Ω/ppm.

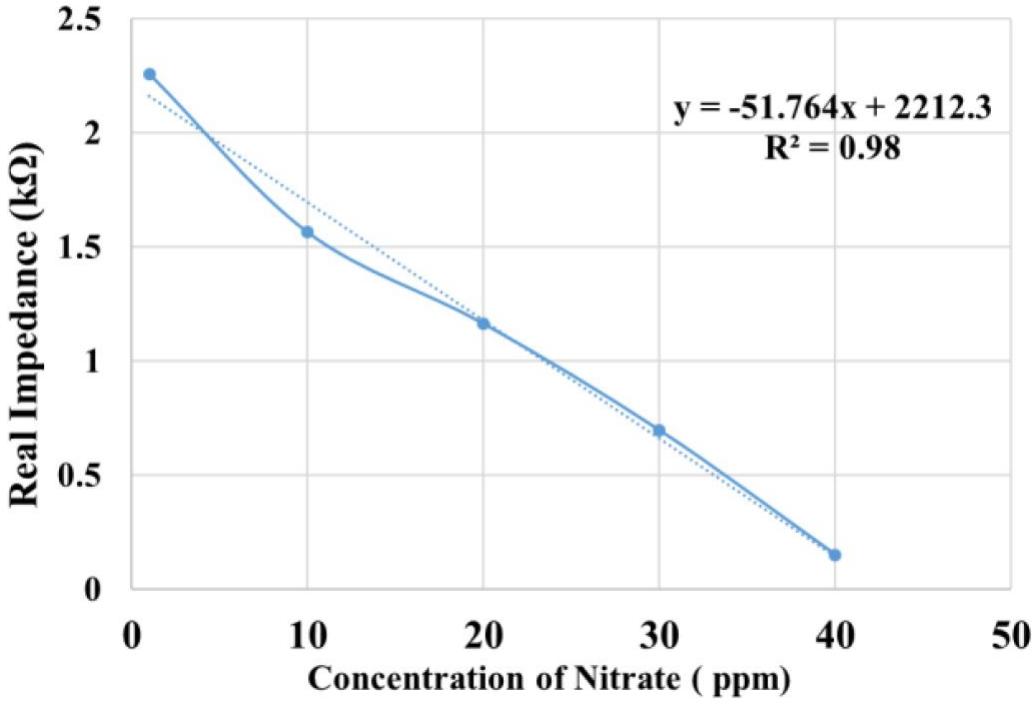

FIGURE 7.11: Calibration standard to measure any unknown nitrate concentration

7.3.3 Unknown Sample Measurement

To measure any unknown sample, different sample waters are collected from different sampling locations, such as river, lake, stream, tap water. The concentration of nitrate was not high enough to measure the range to high concentrations. Therefore, a nitrate sample was added to elevate the concentration of nitrate. The FR4-based sensor and sensing system were used to measure the nitrate concentrations and compared with the laboratory standard method. Equation 7.1 was used to measure the unknown nitrate concentrations. It is observed that the sensor and the developed system can measure the nitrate concentration with an error of less than 5%. When the concentrations are on the higher side, the error is smaller than with lower nitrate concentrations (Table 7.1).

7.3.4 Data Transfer to the Cloud Server

Figure 7.12 shows the measured nitrate concentration transferred from the field location during the field trial. Seven days of sampling data are collected without any interruption and the sampling interval was 13 minutes. Though this was a very dense data collection, the sampling interval could be easily controlled through the software programming. In 24

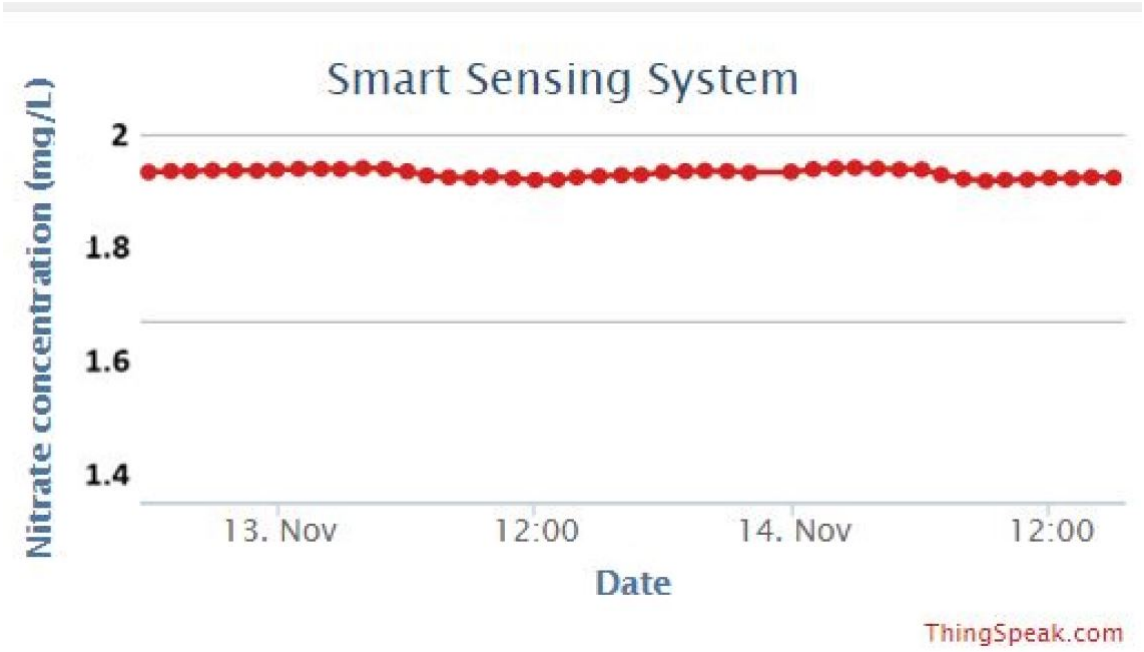

FIGURE 7.12: Nitrate concentration from Thingspeak server

TABLE 7.1: Unknown sample measurement compared to laboratory standard method

Sample Number	Smart Sensing node (*ppm*)	UV-Spectrometry method (*ppm*)	Error (%)
River Water	15.60	15.80	1.27
Tap Water	26.40	26.97	2.11
Canal Water	35.45	36.01	1.56
Stream Water	8.65	8.70	0.57
Creek Water	2.01	2.10	4.29

hours, 112-113 batches of sampling data could be collected with sampling every 13 minutes. Table 7.1 shows the average nitrate concentration and compares the data with laboratory measurements. Every morning, afternoon and evening, sample water was collected from the creek and measured in the laboratory immediately. In a single day, the sampling water was collected and measured in the laboratory to maximise the accuracy. It is obvious that this sampling frequency is not similar to the developed smart system, but is also observed that the sampling data from the developed system is close to the (quite accurate) laboratory measurements, with an error of less than 5%. A similar thing is also seen from Figure 7.13.

Figure 7.14 illustrates the single-day nitrate concentrations for each sample time. It varied between 1.8 and 1.9 ppm while the average nitrate concentration of that single day was 1.9

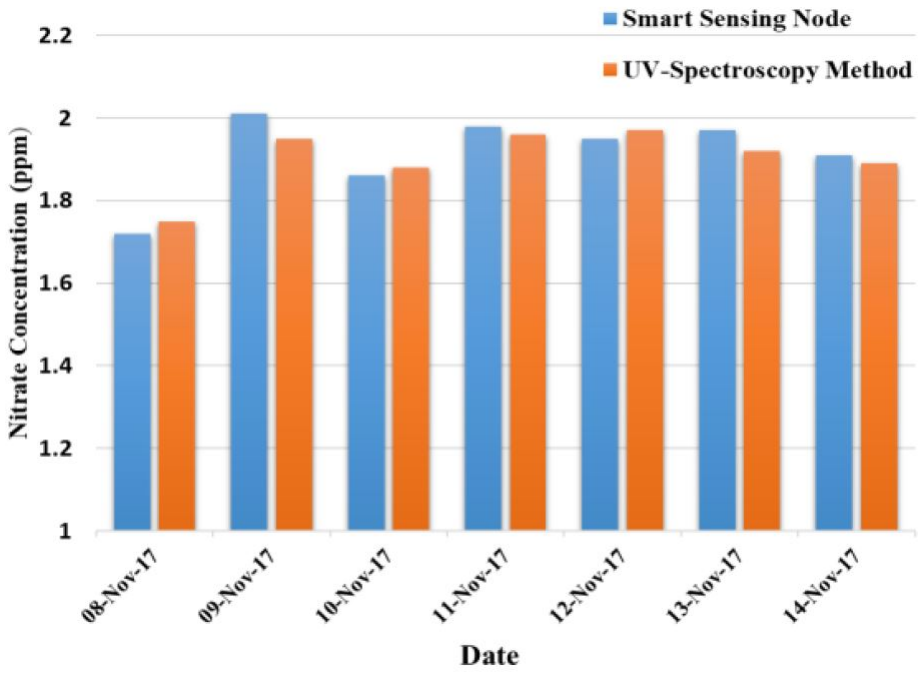

FIGURE 7.13: Comparison of daily evolution of nitrate concentration with standard method

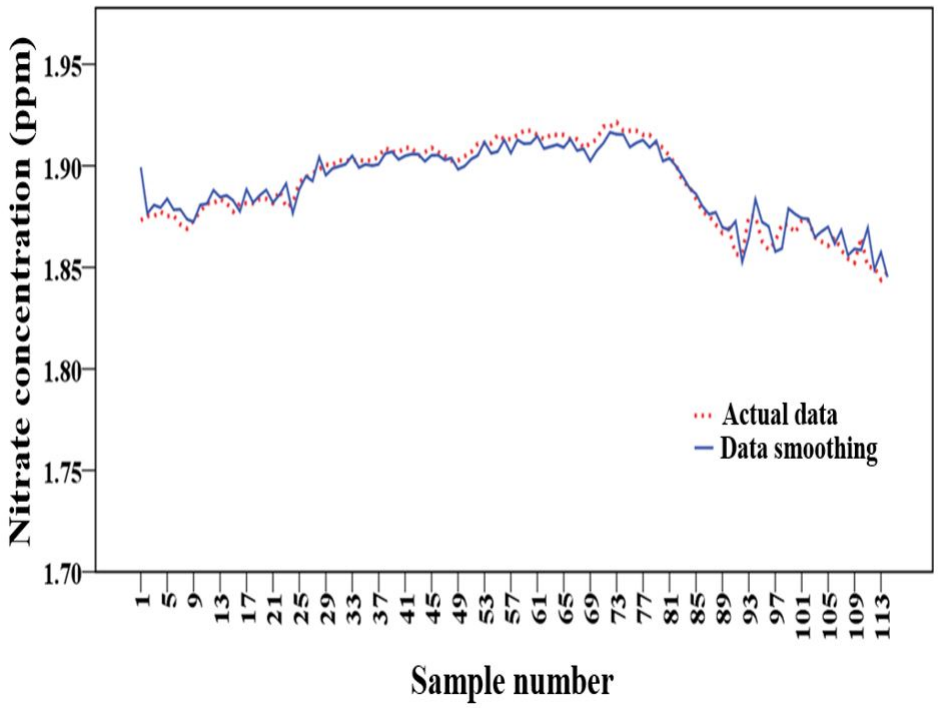

FIGURE 7.14: Nitrate concentration over a single day

ppm. In addition, the collected data have been smoothed with a simple moving-average algorithm. The smoothed data can provide the trend of nitrate concentration, which might be useful over a longer time. The creek does not carry a high level of nitrate concentration

as it is located inside the University and the administration of the University control all kind of pollution (air, water, environment) very carefully. Table 7.2 shows the average nitrate concentration of the study location which is compared with the laboratory standard method for validation.

TABLE 7.2: Average nitrate concentration of the study location compared with laboratory standard method

Date	Smart Sensing node (*ppm*)	UV-Spectrometry method (*ppm*)	Error (%)
8th Nov 2017	1.72	1.75	1.71
9th Nov 2017	2.01	1.95	3.07
10th Nov 2017	1.86	1.88	1.06
11th Nov 2017	1.98	1.96	1.02
12th Nov 2017	1.95	1.97	1.01
13th Nov 2017	1.9	1.92	2.60
14th Nov 2017	1.91	1.89	1.05

7.3.5 LoRa protocol over Wi-Fi protocol

Components for remote IoT applications must draw as little power as possible to maximise battery life. The difference of The LoRa protocol over the WiFi RF protocol was to reduce the overall power consumption during sleep mode to less than half. It also allows transmissions to penetrate obstacles and allows the data to travel larger distances, whilst consuming less power than the standard WiFi protocol. It optimises the data exchange with the gateway, allowing for lower power consumption as compared to WiFi. The current drain from each component for each stage, comparing WiFi and LoRa, can be observed in Table 7.3. It is observed that the LoRa protocol is consuming less current, which helped to conserving the energy for longer time. The consumption of energy for pumps and motor drivers are similar for both the system. However, WiFi enabled microcontroller consumes 2.22 times more energy than the LoRa enabled microcontroller. Therefore, a LoRa enabled sensing system was used to do the necessary field trial.

TABLE 7.3: Comparison of WiFi and LoRa driven sensing system

Mode of Operation	WiFi (per second)	Lora (per second)	Per Sample (13 min)
Arduino (5V)			
Sleep	0.119 A	0.039 A	550 s
Motor 1 (Inlet)	0.124 A	0.066 A	35 s
Motor 2 (Outlet)	0.124 A	0.066 A	1.02 s
Impedance Analyzer	0.124 A	0.046 A	1.01 s
Data Transmission	0.124 A	0.095 A	2.60 s
Motor Driver (12V)			
Motor 1 (Inlet)	1.8 A	1.8 A	35 s
Motor 2 (Outlet)	1.8 A	1.8 A	66 s

7.4 Chapter Summary

An IoT-enabled smart nitrate sensor and sensing system is proposed to monitor nitrate concentration in real-time. An FR4-based interdigital sensor is characterised and is extremely useful for robust use during nitrate monitoring. The system is autonomous and was trialled in the field for seven days without any interruption. The LoRa protocol was used to run the system over longer periods than for the WiFi protocol. The LoRa protocol is a low-power energy-saving protocol, which was implemented successfully. The system's collected data were also validated through the UV-spectrometry method. The collected data shows that few data have been lost during transmission, and 98% of data are successfully collected through the gateway to the cloud server. The results show that the proposed smart sensing system can be very useful to develop a WSN to monitor nitrate concentration in real time. It also shows that, without human interaction, changes of both temporal and spatial evolutions of nitrate concentration can be monitored successfully.

Chapter 8

Conclusions and Future Work

8.1 Conclusion

Regular measurement of nitrate is extremely important to keep the water safe for all purposes. In this research, Iot enabled smart sensors and sensing system were developed to measure nitrate concentration in water. The sensing system can be installed any sampling location and the system can measure the nitrate concentration and transfer it to the cloud server for further analysis. The purpose of this research can be concluded in the following manner.

Chapter 4 explains a temperature compensated interdigital capacitive sensor to measure nitrate at low concentrations. A portable, novel sensing system has been developed that could be used on-site as a stand-alone device, as well as IoT-based remote monitoring smart sensor node, to measure nitrate concentration in surface and ground water. Electrochemical Impedance Spectroscopy was employed to detect and display nitrate concentrations, by evaluating the impedance change read by the interdigital transducer immersed in the surface water samples. The test samples were evaluated by commercial equipment (LCR meter) and the designed system. These results were also validated using standard laboratory techniques to assess nitrate concentrations in water samples. The developed system has the potential to be used to estimate nitrate concentrations in water samples, in real-time. The system can upload the measured nitrate data on a website based on IoT. This system could be used to integrate water quality monitoring sites within farms, or between streams, rivers, and lakes.

Chapter 5 explains and highlights the fabrication process of a newly developed CNT-PDMS and Graphene sensor. It also explains the IoT-enabled sensing system for the detection of nitrate-N concentration in water. The graphene based sensor is easy to fabricate and easier to use for measurement purpose.The sensor is also robust which helps to duplicate measurements with good repeatability. The developed sensor and the smart sensing system

can be used to monitor real time nitrate-N concentration and develop a low-cost distributed network with effective performance.

Chapter 6 explains the ion imprinted polymer based nitrate-N has been developed and used as a coating material the sensing surface. The interdigital capacitive sensor has been used for detection purposes where the detection limit is 1-10 mg/L. The sensing surface was functionalized by an acrylic resin with an embedded coating material to introduce selectivity for nitrate-N. A calibration curve has been developed to measure an unknown sample. The measurement of unknown water samples has shown good results, with an error rate of <5 %. The sensor can be reused up to 5 times before the error rate becomes unacceptable. CNLS curve fitting was also applied to interpret the experimentally obtained impedance spectra.

Chapter 7 explains an IoT-enabled smart nitrate sensor and sensing system to monitor the nitrate concentration in real-time. An FR4-based interdigital sensor is characterized and is extremely useful for robust use during nitrate monitoring. The system is autonomous and was trialed in the field for seven days without any interruption. The LoRa protocol was used to run the system over longer periods than for the WiFi protocol. The LoRa protocol is a low-power energy-saving protocol, which was implemented successfully. The system's collected data were also validated through the UV-spectrometry method. The collected data shows that few data have been lost during transmission, and 98% of data are successfully collected through the gateway to the cloud server. The results show that the proposed smart sensing system can be very useful to develop a WSN to monitor nitrate concentration in real time. It also shows that, without human interaction, changes of both temporal and spatial evolutions of nitrate concentration can be monitored successfully.

8.2 Future Work

A satisfactory performance of the sensor and sensing system have been achieved in this research, still a few of the following improvements in the sensor and sensing system can make it even better.

1. The reuse of the sensor is important parameter which needs to be improved.

2. There are other heavy metals and concerned ions are available in water. A sensor array can be developed to monitor other water parameters.

3. Many IoT enabled sensing systems need to be installed to monitor nitrate concentration in real-time.

Appendix

Bibliography

[1] A. L. Souto, V. M. de Oliveira, V. C. da Silva, M. V. Correia, W. P. da Silva, M. A. G. Trindade, and C. M. Rodrigues. *Analytical strategies using chromatographic methodologies to analyze lignocellulosic feedstocks and their value-added compounds in biorefinery processes*. In *Analytical Techniques and Methods for Biomass*, pp. 197–234 (Springer, 2016).

[2] E. Berner and R. Berner. *The global water cycle prentice hall*. New Jersey (1987).

[3] J. Gaillard. *February 1995*. Lecture on Nitrogen Cycle .

[4] W. H. Organization. *Nitrate and nitrite in drinking-water.* . http://www.who.int/water_sanitation_health/dwq/chemicals/nitrate-nitrite-background-jan17.pdf (2016). [Online; accessed 28-July-2018].

[5] H. H. Comly *et al. Cyanosis in infants caused by nitrates in well water*. Jama **129**(2), 112 (1945).

[6] H. H. Comly. *Cyanosis in infants caused by nitrates in well water*. Jama **257**(20), 2788 (1987).

[7] P. F. Swann. *The toxicology of nitrate, nitrite and n-nitroso compounds*. Journal of the Science of Food and Agriculture **26**(11), 1761 (1975).

[8] C. S. Bruning-Fann and J. Kaneene. *The effects of nitrate, nitrite and n-nitroso compounds on human health: a review.* Veterinary and human toxicology **35**(6), 521 (1993).

[9] J. Davis, K. J. McKeegan, M. F. Cardosi, and D. H. Vaughan. *Evaluation of phenolic assays for the detection of nitrite*. Talanta **50**(1), 103 (1999).

[10] M. Friedberg, M. Hinsdale, and Z. Shihabi. *Analysis of nitrate in biological fluids by capillary electrophoresis*. Journal of Chromatography A **781**(1-2), 491 (1997).

[11] P. N. Bories, E. Scherman, and L. Dziedzic. *Analysis of nitrite and nitrate in biological fluids by capillary electrophoresis*. Clinical biochemistry **32**(1), 9 (1999).

[12] G. Ellis, I. Adatia, M. Yazdanpanah, and S. K. Makela. *Nitrite and nitrate analyses: a clinical biochemistry perspective*. Clinical biochemistry **31**(4), 195 (1998).

[13] A. Azmi, A. A. Azman, S. Ibrahim, and M. A. M. Yunus. *Techniques in advancing the capabilities of various nitrate detection methods: A review.* International Journal on Smart Sensing & Intelligent Systems **10**(2) (2017).

[14] P. Brimblecombe and D. Stedman. *Historical evidence for a dramatic increase in the nitrate component of acid rain*. Nature **298**(5873), 460 (1982).

[15] G. R. Hallberg. *Nitrate in ground water in the united states*. In *Developments in Agricultural and Managed Forest Ecology*, vol. 21, pp. 35–74 (Elsevier, 1989).

[16] G. Hallberg and D. Keeney. *Nitrate, regional groundwater quality, wj alley, ed* (1993).

[17] D. Behm. *Ill waters: The fouling of wisconsin's lakes and streams*. The Milwaukee Journal Sentinel pp. 5–10 (1989).

[18] M. A. M. Yunus, S. Ibrahim, W. A. H. Altowayti, G. P. San, and S. C. Mukhopadhyay. *Selective membrane for detecting nitrate based on planar electromagnetic sensors array*. In *Control Conference (ASCC), 2015 10th Asian*, pp. 1–6 (IEEE, 2015).

[19] C. Wardak. *Solid contact nitrate ion-selective electrode based on ionic liquid with stable and reproducible potential*. Electroanalysis **26**(4), 864 (2014).

[20] R. K. Mahajan, R. Kaur, H. Miyake, and H. Tsukube. *Zn (ii) complex-based potentiometric sensors for selective determination of nitrate anion*. Analytica chimica acta **584**(1), 89 (2007).

[21] E. Andreoli, V. Annibaldi, D. A. Rooney, K.-S. Liao, N. J. Alley, S. A. Curran, and C. B. Breslin. *Electrochemical conversion of copper-based hierarchical micro/nanostructures to copper metal nanoparticles and their testing in nitrate sensing*. Electroanalysis **23**(9), 2164 (2011).

[22] S. Aravamudhan and S. Bhansali. *Development of micro-fluidic nitrate-selective sensor based on doped-polypyrrole nanowires*. Sensors and Actuators B: Chemical **132**(2), 623 (2008).

[23] F. Can, S. K. Ozoner, P. Ergenekon, and E. Erhan. *Amperometric nitrate biosensor based on carbon nanotube/polypyrrole/nitrate reductase biofilm electrode*. Materials Science and Engineering: C **32**(1), 18 (2012).

[24] S. S. Hassan. *Ion-selective electrodes in organic functional group analysis: Microdetermination of nitrates and nitramines with use of the iodide electrode*. Talanta **23**(10), 738 (1976).

[25] M. O. Mendoza, E. P. Ortega, O. A. de Fuentes, Y. Prokhorov, and J. G. L. Barcenas. *Chitosan/bentonite nanocomposite: preliminary studies of its potentiometric response to nitrate ions in water*. In *Sensors (IBERSENSOR), 2014 IEEE 9th Ibero-American Congress on*, pp. 1–4 (IEEE, 2014).

[26] C. Li and L. Li. *Prediction of nitrate and chlorine in soil using ion selective electrode*. In *World Automation Congress (WAC), 2010*, pp. 231–234 (IEEE, 2010).

[27] L. Nuñez, X. Cetó, M. I. Pividori, M. V. B. Zanoni, and M. Del Valle. *Development and application of an electronic tongue for detection and monitoring of nitrate, nitrite and ammonium levels in waters*. Microchemical Journal **110**, 273 (2013).

[28] T. A. Bendikov and T. C. Harmon. *A sensitive nitrate ion-selective electrode from a pencil lead. an analytical laboratory experiment*. Journal of Chemical Education **82**(3), 439 (2005).

[29] L. Zhang, M. Zhang, H. Ren, P. Pu, P. Kong, and H. Zhao. *Comparative investigation on soil nitrate-nitrogen and available potassium measurement capability by using solid-state and pvc ise*. Computers and Electronics in Agriculture **112**, 83 (2015).

[30] A. Calvo-López, E. Arasa-Puig, M. Puyol, J. M. Casalta, and J. Alonso-Chamarro. *Biparametric potentiometric analytical microsystem for nitrate and potassium monitoring in water recycling processes for manned space missions*. Analytica chimica acta **804**, 190 (2013).

[31] S. S. Hassan, H. Sayour, and S. S. Al-Mehrezi. *A novel planar miniaturized potentiometric sensor for flow injection analysis of nitrates in wastewaters, fertilizers and pharmaceuticals*. Analytica chimica acta **581**(1), 13 (2007).

[32] P. T. Kissinger and T. H. Ridgway. *Small-amplitude controlled-potential techniques*. Laboratory Techniques in Electroanalytical Chemistry, Revised and Expanded p. 141 (1996).

[33] R. A. Wallingford and A. G. Ewing. *Capillary zone electrophoresis with electrochemical detection*. Analytical chemistry **59**(14), 1762 (1987).

[34] S. Sloss and A. G. Ewing. *Improved method for end-column amperometric detection for capillary electrophoresis*. Analytical Chemistry **65**(5), 577 (1993).

[35] J. Wang. *Analytical electrochemistry* (John Wiley & Sons, 2006).

[36] N. G. Carpenter and D. Pletcher. *Amperometric method for the determination of nitrate in water*. Analytica chimica acta **317**(1-3), 287 (1995).

[37] X.-l. Zhang, J.-x. Wang, Z. Wang, and S.-c. Wang. *Improvement of amperometric sensor used for determination of nitrate with polypyrrole nanowires modified electrode*. Sensors **5**(12), 580 (2005).

[38] J. R. C. da Rocha, L. Angnes, M. Bertotti, K. Araki, and H. E. Toma. *Amperometric detection of nitrite and nitrate at tetraruthenated porphyrin-modified electrodes in a continuous-flow assembly*. Analytica Chimica Acta **452**(1), 23 (2002).

[39] J. E. Newbery and M. P. L. de Haddad. *Amperometric determination of nitrite by oxidation at a glassy carbon electrode*. Analyst **110**(1), 81 (1985).

[40] M. A. Stanley, J. Maxwell, M. Forrestal, A. P. Doherty, B. D. MacCraith, D. Diamond, and J. G. Vos. *Comparison of the analytical capabilities of an amperometric and an optical sensor for the determination of nitrate in river and well water*. Analytica chimica acta **299**(1), 81 (1994).

[41] J. C. Gamboa, R. C. Pena, T. R. Paixão, and M. Bertotti. *A renewable copper electrode as an amperometric flow detector for nitrate determination in mineral water and soft drink samples*. Talanta **80**(2), 581 (2009).

[42] A. Hulanicki, W. Matuszewski, and M. Trojanowicz. *Flow-injection determination of nitrite and nitrate with biamperometric detection at two platinum wire electrodes*. Analytica chimica acta **194**, 119 (1987).

[43] G. A. Sherwood and D. C. Johnson. *A chromatographic determination of nitrate with amperometric detection at a copperized cadmium electrode*. Analytica Chimica Acta **129**, 101 (1981).

[44] S. A. Glazier, E. R. Campbell, and W. H. Campbell. *Construction and characterization of nitrate reductase-based amperometric electrode and nitrate assay of fertilizers and drinking water*. Analytical chemistry **70**(8), 1511 (1998).

[45] A. Y. Chamsi and A. G. Fogg. *Oxidative flow injection amperometric determination of nitrite at an electrochemically pre-treated glassy carbon electrode*. Analyst **113**(11), 1723 (1988).

[46] M. Bertotti and D. Pletcher. *Amperometric determination of nitrite via reaction with iodide using microelectrodes*. Analytica chimica acta **337**(1), 49 (1997).

[47] M. A. Alawi. *Determination of nitrate and nitrite in water with hplc and amperometric detection*. Fresenius' Journal of Analytical Chemistry **313**(3), 239 (1982).

[48] M. E. Bodini and D. T. Sawyer. *Voltammetric determination of nitrate ion at parts-per-billion levels*. Analytical chemistry **49**(3), 485 (1977).

[49] R. J. Davenport and D. C. Johnson. *Voltammetric determination of nitrate and nitrite ions using a rotating cadmium disk electrode*. Analytical Chemistry **45**(11), 1979 (1973).

[50] J. Krista, M. Kopanica, and L. Novotnỳ. *Voltammetric determination of nitrates using silver electrodes*. Electroanalysis: An International Journal Devoted to Fundamental and Practical Aspects of Electroanalysis **12**(3), 199 (2000).

[51] S. M. Shariar and T. Hinoue. *Simultaneous voltammetric determination of nitrate and nitrite ions using a copper electrode pretreated by dissolution/redeposition*. Analytical Sciences **26**(11), 1173 (2010).

[52] V. Mareček, H. Jänchenová, Z. Samec, and M. Březina. *Voltammetric determination of nitrate, perchlorate and iodide at a hanging electrolyte drop electrode*. Analytica Chimica Acta **185**, 359 (1986).

[53] C. Neuhold, K. Kalcher, W. Diewald, X. Cai, and G. Raber. *Voltammetric determination of nitrate with a modified carbon paste electrode*. Electroanalysis **6**(3), 227 (1994).

[54] A. O. Solak, P. Gülser, E. Gökm, and F. Gökmeşe. *A new differential pulse voltammetric method for the determination of nitrate at a copper plated glassy carbon electrode*. Microchimica Acta **134**(1-2), 77 (2000).

[55] A. Osman Solak and P. Çekirdek. *Square wave voltammetric determination of nitrate at a freshly copper plated glassy carbon electrode*. Analytical letters **38**(2), 271 (2005).

[56] A. Jang, Z. Zou, K. K. Lee, C. H. Ahn, and P. L. Bishop. *Potentiometric and voltammetric polymer lab chip sensors for determination of nitrate, ph and cd (ii) in water*. Talanta **83**(1), 1 (2010).

[57] C. Lopez-Moreno, I. V. Perez, and A. M. Urbano. *Development and validation of an ionic chromatography method for the determination of nitrate, nitrite and chloride in meat*. Food chemistry **194**, 687 (2016).

[58] H. Kodamatani, S. Yamazaki, K. Saito, T. Tomiyasu, and Y. Komatsu. *Selective determination method for measurement of nitrite and nitrate in water samples using high-performance liquid chromatography with post-column photochemical reaction and chemiluminescence detection*. Journal of Chromatography A **1216**(15), 3163 (2009).

[59] M. R. Siddiqui, S. M. Wabaidur, Z. A. ALOthman, and M. Rafiquee. *Rapid and sensitive method for analysis of nitrate in meat samples using ultra performance liquid chromatography–mass spectrometry*. Spectrochimica Acta Part A: Molecular and Biomolecular Spectroscopy **151**, 861 (2015).

[60] P. Niedzielski, I. Kurzyca, and J. Siepak. *A new tool for inorganic nitrogen speciation study: Simultaneous determination of ammonium ion, nitrite and nitrate by ion chromatography with post-column ammonium derivatization by nessler reagent*

and diode-array detection in rain water samples. Analytica chimica acta **577**(2), 220 (2006).

[61] K. Tirumalesh. *Simultaneous determination of bromide and nitrate in contaminated waters by ion chromatography using amperometry and absorbance detectors*. Talanta **74**(5), 1428 (2008).

[62] M. Tabatabai and W. Dick. *Simultaneous determination of nitrate, chloride, sulfate, and phosphate in natural waters by ion chromatography 1*. Journal of Environmental Quality **12**(2), 209 (1983).

[63] J. A. Morales, L. S. de Graterol, and J. Mesa. *Determination of chloride, sulfate and nitrate in groundwater samples by ion chromatography*. Journal of Chromatography A **884**(1-2), 185 (2000).

[64] I. Dahllöf, O. Svensson, and C. Torstensson. *Optimising the determination of nitrate and phosphate in sea water with ion chromatography using experimental design*. Journal of Chromatography A **771**(1-2), 163 (1997).

[65] E. Kapinus, I. Revelsky, V. Ulogov, and Y. A. Lyalikov. *Simultaneous determination of fluoride, chloride, nitrite, bromide, nitrate, phosphate and sulfate in aqueous solutions at 10- 9 to 10- 8% level by ion chromatography*. Journal of chromatography B **800**(1-2), 321 (2004).

[66] M. Neal, C. Neal, H. Wickham, and S. Harman. *Determination of bromide, chloride, fluoride, nitrate and sulphate by ion chromatography: comparisons of methodologies for rainfall, cloud water and river waters at the plynlimon catchments of mid-wales*. Hydrology and Earth System Sciences Discussions **11**(1), 294 (2007).

[67] M. Akyüz and Ş. Ata. *Determination of low level nitrite and nitrate in biological, food and environmental samples by gas chromatography–mass spectrometry and liquid chromatography with fluorescence detection*. Talanta **79**(3), 900 (2009).

[68] Y. Li, J. S. Whitaker, and C. L. McCarty. *Reversed-phase liquid chromatography/electrospray ionization/mass spectrometry with isotope dilution for the analysis of nitrate and nitrite in water*. Journal of Chromatography A **1218**(3), 476 (2011).

[69] Y. Zuo, C. Wang, and T. Van. *Simultaneous determination of nitrite and nitrate in dew, rain, snow and lake water samples by ion-pair high-performance liquid chromatography*. Talanta **70**(2), 281 (2006).

[70] S. Rodriguez-Mozaz, M. J. L. de Alda, and D. Barceló. *Biosensors as useful tools for environmental analysis and monitoring*. Analytical and bioanalytical chemistry **386**(4), 1025 (2006).

[71] S. Rodriguez-Mozaz, M. J. L. de Alda, and D. Barceló. *Fast and simultaneous monitoring of organic pollutants in a drinking water treatment plant by a multi-analyte biosensor followed by lc–ms validation*. Talanta **69**(2), 377 (2006).

[72] B. Roig, I. Bazin, S. Bayle, D. Habauzit, and J. Chopineau. *Biomolecular recognition systems for water monitoring*. Rapid Chemical and Biological Techniques for Water Monitoring **23**, 175 (2009).

[73] M. Farré, L. Kantiani, S. Pérez, and D. Barceló. *Sensors and biosensors in support of eu directives*. TrAC Trends in Analytical Chemistry **28**(2), 170 (2009).

[74] H.-H. Zeng, R. B. Thompson, B. P. Maliwal, G. R. Fones, J. W. Moffett, and C. A. Fierke. *Real-time determination of picomolar free cu (ii) in seawater using a fluorescence-based fiber optic biosensor*. Analytical chemistry **75**(24), 6807 (2003).

[75] W. Xuejiang, S. V. Dzyadevych, J.-M. Chovelon, N. J. Renault, C. Ling, X. Siqing, and Z. Jianfu. *Conductometric nitrate biosensor based on methyl viologen/nafion®/nitrate reductase interdigitated electrodes*. Talanta **69**(2), 450 (2006).

[76] S. Cosnier, S. Da Silva, D. Shan, and K. Gorgy. *Electrochemical nitrate biosensor based on poly (pyrrole–viologen) film–nitrate reductase–clay composite*. Bioelectrochemistry **74**(1), 47 (2008).

[77] Z. Zhang, S. Xia, D. Leonard, N. Jaffrezic-Renault, J. Zhang, F. Bessueille, Y. Goepfert, X. Wang, L. Chen, Z. Zhu, *et al. A novel nitrite biosensor based on conductometric electrode modified with cytochrome c nitrite reductase composite membrane*. Biosensors and Bioelectronics **24**(6), 1574 (2009).

[78] T. Madasamy, M. Pandiaraj, M. Balamurugan, K. Bhargava, N. K. Sethy, and C. Karunakaran. *Copper, zinc superoxide dismutase and nitrate reductase coimmobilized bienzymatic biosensor for the simultaneous determination of nitrite and nitrate*. Biosensors and Bioelectronics **52**, 209 (2014).

[79] D. Albanese, M. Di Matteo, and C. Alessio. *Screen printed biosensors for detection of nitrates in drinking water*. In *Computer Aided Chemical Engineering*, vol. 28, pp. 283–288 (Elsevier, 2010).

[80] A. Ayala, L. Leal, L. Ferrer, and V. Cerdà. *Multiparametric automated system for sulfate, nitrite and nitrate monitoring in drinking water and wastewater based on sequential injection analysis*. Microchemical Journal **100**, 55 (2012).

[81] M. Yaqoob, A. Nabi, and P. J. Worsfold. *Determination of nitrite and nitrate in natural waters using flow injection with spectrophotometric detection*. Journal of the Chemical Society of Pakistan **34**(3) (2013).

[82] M. Yaqoob, B. Folgado Biot, A. Nabi, and P. J. Worsfold. *Determination of nitrate and nitrite in freshwaters using flow-injection with luminol chemiluminescence detection*. Luminescence **27**(5), 419 (2012).

[83] S. Wang, K. Lin, N. Chen, D. Yuan, and J. Ma. *Automated determination of nitrate plus nitrite in aqueous samples with flow injection analysis using vanadium (iii) chloride as reductant*. Talanta **146**, 744 (2016).

[84] C. L. Pasquali, A. Gallego-Picó, P. F. Hernando, M. Velasco, and J. D. Alegría. *Two rapid and sensitive automated methods for the determination of nitrite and nitrate in soil samples*. Microchemical Journal **94**(1), 79 (2010).

[85] C. L. Pasquali, P. F. Hernando, and J. D. Alegria. *Spectrophotometric simultaneous determination of nitrite, nitrate and ammonium in soils by flow injection analysis*. analytica chimica acta **600**(1-2), 177 (2007).

[86] S. Feng, M. Zhang, Y. Huang, D. Yuan, and Y. Zhu. *Simultaneous determination of nanomolar nitrite and nitrate in seawater using reverse flow injection analysis coupled with a long path length liquid waveguide capillary cell*. Talanta **117**, 456 (2013).

[87] P. S. Ellis, A. M. H. Shabani, B. S. Gentle, and I. D. McKelvie. *Field measurement of nitrate in marine and estuarine waters with a flow analysis system utilizing on-line zinc reduction*. Talanta **84**(1), 98 (2011).

[88] A. D. Beaton, C. L. Cardwell, R. S. Thomas, V. J. Sieben, F.-E. Legiret, E. M. Waugh, P. J. Statham, M. C. Mowlem, and H. Morgan. *Lab-on-chip measurement of nitrate and nitrite for in situ analysis of natural waters*. Environmental science & technology **46**(17), 9548 (2012).

[89] N. Amini and I. McKelvie. *An enzymatic flow analysis method for the determination of phosphatidylcholine in sediment pore waters and extracts*. Talanta **66**(2), 445 (2005).

[90] M. A. M. Yunus and S. C. Mukhopadhyay. *Novel planar electromagnetic sensors for detection of nitrates and contamination in natural water sources*. IEEE Sensors Journal **11**(6), 1440 (2011).

[91] A. S. M. Nor, M. A. M. Yunus, S. W. Nawawi, and S. Ibrahim. *Low-cost sensor array design optimization based on planar electromagnetic sensor design for detecting nitrate and sulphate*. In *Sensing Technology (ICST), 2013 Seventh International Conference on*, pp. 693–698 (IEEE, 2013).

[92] M. A. M. Yunus, S. Mukhopadhyay, and A. Punchihewa. *Application of independent component analysis for estimating nitrate contamination in natural water sources using planar electromagnetic sensor*. In *Sensing Technology (ICST), 2011 Fifth International Conference on*, pp. 538–543 (IEEE, 2011).

[93] M. A. M. Yunus, S. C. Mukhopadhyay, and S. Ibrahim. *Planar electromagnetic sensor based estimation of nitrate contamination in water sources using independent component analysis*. IEEE Sensors Journal **12**(6), 2024 (2012).

[94] A. S. M. Nor, M. Faramarzi, M. A. M. Yunus, and S. Ibrahim. *Nitrate and sulfate estimations in water sources using a planar electromagnetic sensor array and artificial neural network method*. IEEE Sensors Journal **15**(1), 497 (2015).

[95] M. M. Yunus, S. Mukhopadhyay, M. Rahman, N. Zahidin, and S. Ibrahim. *The selection of novel planar electromagnetic sensors for the application of nitrate contamination*

detection. In *Smart Sensors for Real-Time Water Quality Monitoring*, pp. 171–195 (Springer, 2013).

[96] M. M. Yunus, S. C. Mukhopadhyay, A. Punchihewa, and S. Ibrahim. *The effect of temperature factor on the detection of nitrate based on planar electromagnetic sensor and independent component analysis*. In *Smart Sensing Technology for Agriculture and Environmental Monitoring*, pp. 103–118 (Springer, 2012).

[97] X. Wang, Y. Wang, H. Leung, S. C. Mukhopadhyay, M. Tian, and J. Zhou. *Mechanism and experiment of planar electrode sensors in water pollutant measurement*. IEEE Transactions on Instrumentation and Measurement **64**(2), 516 (2015).

[98] N. Amini, M. Shamsipur, M. B. Gholivand, and K. Naderi. *Electrocatalytic and new electrochemical properties of chloropromazine in to silicanps/chloropromazine/nafion nanocomposite: Application to nitrite detection at low potential*. Microchemical Journal **131**, 43 (2017).

[99] B. Mahieuxe, M. Carré, M. Viriot, J. André, and M. Donner. *Fiber-optic fluorescing sensors for nitrate and nitrite detection*. Journal of fluorescence **4**(1), 7 (1994).

[100] J. Camas-Anzueto, A. Aguilar-Castillejos, J. Castañón-González, M. Lujpan-Hidalgo, H. H. de León, and R. M. Grajales. *Fiber sensor based on lophine sensitive layer for nitrate detection in drinking water*. Optics and Lasers in Engineering **60**, 38 (2014).

[101] M. Y. Chong, M. Z. M. Jafri, L. H. San, and T. C. Ho. *Detection of nitrate ions in water by optical fiber*. In *Computer and Communication Engineering (ICCCE), 2012 International Conference on*, pp. 271–273 (IEEE, 2012).

[102] Y. Moo, M. Matjafri, H. Lim, and C. Tan. *New development of optical fibre sensor for determination of nitrate and nitrite in water*. Optik-International Journal for Light and Electron Optics **127**(3), 1312 (2016).

[103] K. S. Johnson, L. J. Coletti, H. W. Jannasch, C. M. Sakamoto, D. D. Swift, and S. C. Riser. *Long-term nitrate measurements in the ocean using the in situ ultraviolet spectrophotometer: sensor integration into the apex profiling float*. Journal of Atmospheric and Oceanic Technology **30**(8), 1854 (2013).

[104] A. Lalasangi, J. Akki, K. Manohar, T. Srinivas, P. Radhakrishnan, S. Kher, N. Mehla, and U. Raikar. *Fiber bragg grating sensor for detection of nitrate concentration in water*. Sensors & Transducers **125**(2), 187 (2011).

[105] C. Munkholm, D. R. Walt, and F. P. Milanovich. *A fiber-optic sensor for co2 measurement*. Talanta **35**(2), 109 (1988).

[106] Y. Zhu and A. Wang. *Miniature fiber-optic pressure sensor*. IEEE Photonics Technology Letters **17**(2), 447 (2005).

[107] S. Zhang, H. Chen, and H. Fu. *Fiber-optic temperature sensor using an optoelectronic oscillator*. In *Optical Communications and Networks (ICOCN), 2015 14th International Conference on*, pp. 1–3 (IEEE, 2015).

[108] F. Delport, J. Pollet, K. Janssen, B. Verbruggen, K. Knez, D. Spasic, and J. Lammertyn. *Real-time monitoring of dna hybridization and melting processes using a fiber optic sensor*. Nanotechnology **23**(6), 065503 (2012).

[109] P. Bhatia and B. D. Gupta. *Fabrication and characterization of a surface plasmon resonance based fiber optic urea sensor for biomedical applications*. Sensors and Actuators B: Chemical **161**(1), 434 (2012).

[110] V. P. Kafle, Y. Fukushima, and H. Harai. *Design and implementation of dynamic mobile sensor network platform*. IEEE Communications Magazine **53**(3), 48 (2015).

[111] M. S. Khan, M. S. Islam, and H. Deng. *Design of a reconfigurable rfid sensing tag as a generic sensing platform toward the future internet of things*. IEEE Internet of things journal **1**(4), 300 (2014).

[112] A. Gluhak, S. Krco, M. Nati, D. Pfisterer, N. Mitton, and T. Razafindralambo. *A survey on facilities for experimental internet of things research*. IEEE Communications Magazine **49**(11), 58 (2011).

[113] P. Mell, T. Grance, *et al. The nist definition of cloud computing* (2011).

[114] A. Flammini and E. Sisinni. *Wireless sensor networking in the internet of things and cloud computing era*. Procedia Engineering **87**, 672 (2014).

[115] H.-C. Lee, A. Banerjee, Y.-M. Fang, B.-J. Lee, and C.-T. King. *Design of a multi-functional wireless sensor for in-situ monitoring of debris flows*. IEEE Transactions on Instrumentation and Measurement **59**(11), 2958 (2010).

[116] P. Jiang, H. Xia, Z. He, and Z. Wang. *Design of a water environment monitoring system based on wireless sensor networks*. Sensors **9**(8), 6411 (2009).

[117] T. P. Lambrou, C. C. Anastasiou, C. G. Panayiotou, and M. M. Polycarpou. *A low-cost sensor network for real-time monitoring and contamination detection in drinking water distribution systems*. IEEE sensors journal **14**(8), 2765 (2014).

[118] A. Bayo, D. Antolín, N. Medrano, B. Calvo, and S. Celma. *Early detection and monitoring of forest fire with a wireless sensor network system*. Procedia Engineering **5**, 248 (2010).

[119] I. Silva, L. A. Guedes, P. Portugal, and F. Vasques. *Reliability and availability evaluation of wireless sensor networks for industrial applications*. Sensors **12**(1), 806 (2012).

[120] G. Zhao. *Wireless sensor networks for industrial process monitoring and control: A survey*. Network Protocols and Algorithms **3**(1), 46 (2011).

[121] R. Morais, S. G. Matos, M. A. Fernandes, A. L. Valente, S. F. Soares, P. Ferreira, and M. Reis. *Sun, wind and water flow as energy supply for small stationary data acquisition platforms*. Computers and electronics in agriculture **64**(2), 120 (2008).

[122] X. Li, Y. Deng, and L. Ding. *Study on precision agriculture monitoring framework based on wsn*. In *Anti-counterfeiting, Security and Identification, 2008. ASID 2008. 2nd International Conference on*, pp. 182–185 (IEEE, 2008).

[123] J. V. Capella, A. Bonastre, R. Ors, and M. Peris. *In line river monitoring of nitrate concentration by means of a wireless sensor network with energy harvesting*. Sensors and Actuators B: Chemical **177**, 419 (2013).

[124] G. Xu, W. Shen, and X. Wang. *Applications of wireless sensor networks in marine environment monitoring: A survey*. Sensors **14**(9), 16932 (2014).

[125] M. R. Gartia, B. Braunschweig, T.-W. Chang, P. Moinzadeh, B. S. Minsker, G. Agha, A. Wieckowski, L. L. Keefer, and G. L. Liu. *The microelectronic wireless nitrate sensor network for environmental water monitoring*. Journal of Environmental Monitoring **14**(12), 3068 (2012).

[126] J. de Carvalho Silva, J. J. Rodrigues, A. M. Alberti, P. Solic, and A. L. Aquino. *Lorawan—a low power wan protocol for internet of things: A review and opportunities*. In *Computer and Energy Science (SpliTech), 2017 2nd International Multidisciplinary Conference on*, pp. 1–6 (IEEE, 2017).

[127] M. T. Penella-López and M. Gasulla-Forner. *Powering autonomous sensors: an integral approach with focus on solar and RF energy harvesting* (Springer Science & Business Media, 2011).

[128] I. F. Akyildiz, W. Su, Y. Sankarasubramaniam, and E. Cayirci. *Wireless sensor networks: a survey*. Computer networks **38**(4), 393 (2002).

[129] E. Gaura, L. Girod, J. Brusey, M. Allen, and G. Challen. *Wireless sensor networks: Deployments and design frameworks* (Springer Science & Business Media, 2010).

[130] J. Chen, M. Díaz, L. Llopis, B. Rubio, and J. M. Troya. *A survey on quality of service support in wireless sensor and actor networks: Requirements and challenges in the context of critical infrastructure protection*. Journal of Network and Computer Applications **34**(4), 1225 (2011).

[131] W. Dargie. *Dynamic power management in wireless sensor networks: State-of-the-art*. IEEE Sensors Journal **12**(5), 1518 (2012).

[132] J. Li, Y. Zhang, Y.-F. Chen, K. Nagaraja, S. Li, and D. Raychaudhuri. *A mobile phone based wsn infrastructure for iot over future internet architecture*. In *Green Computing and Communications (GreenCom), 2013 IEEE and Internet of Things (iThings/CPSCom), IEEE International Conference on and IEEE Cyber, Physical and Social Computing*, pp. 426–433 (IEEE, 2013).

[133] G. Werner-Allen, P. Swieskowski, and M. Welsh. *Motelab: A wireless sensor network testbed*. In *Proceedings of the 4th international symposium on Information processing in sensor networks*, p. 68 (IEEE Press, 2005).

[134] M. Doddavenkatappa, M. C. Chan, and A. L. Ananda. *Indriya: A low-cost, 3d wireless sensor network testbed*. In *International conference on testbeds and research infrastructures*, pp. 302–316 (Springer, 2011).

[135] A. Burns, B. R. Greene, M. J. McGrath, T. J. O'Shea, B. Kuris, S. M. Ayer, F. Stroiescu, and V. Cionca. *Shimmer™–a wireless sensor platform for noninvasive biomedical research*. IEEE Sensors Journal **10**(9), 1527 (2010).

[136] Z. Riaz, M. Arslan, A. K. Kiani, and S. Azhar. *Cosmos: A bim and wireless sensor based integrated solution for worker safety in confined spaces*. Automation in construction **45**, 96 (2014).

[137] E. Cañete, J. Chen, M. Díaz, L. Llopis, and B. Rubio. *Sensor4pri: A sensor platform for the protection of railway infrastructures*. Sensors **15**(3), 4996 (2015).

[138] A. S. Abu-Abed and R. G. Lindquist. *Capacitive interdigital sensor with inhomogeneous nematic liquid crystal film*. Progress In Electromagnetics Research **7**, 75 (2008).

[139] A. V. Mamishev, K. Sundara-Rajan, F. Yang, Y. Du, and M. Zahn. *Interdigital sensors and transducers*. Proceedings of the IEEE **92**(5), 808 (2004).

[140] Y. Chen, C. Zhu, M. Cao, and T. Wang. *Photoresponse of sno2 nanobelts grown in situ on interdigital electrodes*. Nanotechnology **18**(28), 285502 (2007).

[141] A. M. Syaifudin, M. Yunus, S. Mukhopadhyay, and K. Jayasundera. *A novel planar interdigital sensor for environmental monitoring*. In *Sensors, 2009 IEEE*, pp. 105–110 (IEEE, 2009).

[142] H. Arwin. *Application of ellipsometry techniques to biological materials*. Thin Solid Films **519**(9), 2589 (2011).

[143] A. M. Syaifudin, K. Jayasundera, and S. Mukhopadhyay. *A low cost novel sensing system for detection of dangerous marine biotoxins in seafood*. Sensors and Actuators B: Chemical **137**(1), 67 (2009).

[144] A. M. Syaifudin, S. Mukhopadhyay, and P. Yu. *Electromagnetic field computation using comsol multiphysics to evaluate the performance of novel interdigital sensors*. In *Applied Electromagnetics Conference (AEMC), 2009*, pp. 1–4 (IEEE, 2009).

[145] Y. Yang, G. Chiesura, G. Luyckx, T. Vervust, F. Bossuyt, J. Vanfleteren, J. Degrieck, *et al. In situ on-line cure monitoring of composites by embedded interdigital sensor*. In *16th European Conference on Composite Materials (ECCM-16)* (2014).

[146] A. I. Zia, A. M. Syaifudin, S. Mukhopadhyay, P. Yu, I. Al-Bahadly, C. P. Gooneratne, J. Kosel, and T.-S. Liao. *Electrochemical impedance spectroscopy based mems sensors for phthalates detection in water and juices*. In *Journal of Physics: Conference Series*, vol. 439, p. 012026 (IOP Publishing, 2013).

[147] A. I. Zia, S. C. Mukhopadhyay, P.-L. Yu, I. H. Al-Bahadly, C. P. Gooneratne, and J. Kosel. *Rapid and molecular selective electrochemical sensing of phthalates in aqueous solution*. Biosensors and Bioelectronics **67**, 342 (2015).

[148] A. I. Zia, S. C. Mukhopadhyay, I. H. Al-Bahadly, P. Yu, C. P. Gooneratne, and J. Kosel. *Introducing molecular selectivity in rapid impedimetric sensing of phthalates*. In *Instrumentation and Measurement Technology Conference (I2MTC) Proceedings, 2014 IEEE International*, pp. 838–843 (IEEE, 2014).

[149] J. Fischer, H. Dejmkova, and J. Barek. *Electrochemistry of pesticides and its analytical applications*. Current Organic Chemistry **15**(17), 2923 (2011).

[150] M. Khafaji, S. Shahrokhian, and M. Ghalkhani. *Electrochemistry of levo-thyroxin on edge-plane pyrolytic graphite electrode: Application to sensitive analytical determinations*. Electroanalysis **23**(8), 1875 (2011).

[151] L. Li, F. Yang, J. Yu, X. Wang, L. Zhang, Y. Chen, and H. Yang. *In situ growth of zno nanowires on zn comb-shaped interdigitating electrodes and their photosensitive and gas-sensing characteristics*. Materials Research Bulletin **47**(12), 3971 (2012).

[152] M. Dhull and A. G. Arora. *Design of MEMS Based Microheater for Efficient Gas Sensor*. Ph.D. thesis (2015).

[153] S. C. Mukhopadhyay and C. P. Gooneratne. *A novel planar-type biosensor for noninvasive meat inspection*. IEEE Sensors Journal **7**(9), 1340 (2007).

[154] M. S. A. Rahman, S. C. Mukhopadhyay, P.-L. Yu, J. Goicoechea, I. R. Matias, C. P. Gooneratne, and J. Kosel. *Detection of bacterial endotoxin in food: New planar interdigital sensors based approach*. Journal of Food Engineering **114**(3), 346 (2013).

[155] C. Xhoffer, K. Van den Bergh, and H. Dillen. *Electrochemistry: a powerful analytical tool in steel research*. Electrochimica acta **49**(17-18), 2825 (2004).

[156] C. V. Vidal and A. I. Muñoz. *Effect of physico-chemical properties of simulated body fluids on the electrochemical behaviour of cocrmo alloy*. Electrochimica Acta **56**(24), 8239 (2011).

[157] X. Li, K. Toyoda, and I. Ihara. *Coagulation process of soymilk characterized by electrical impedance spectroscopy*. Journal of Food Engineering **105**(3), 563 (2011).

[158] C. Liu, Q. Bi, A. Leyland, and A. Matthews. *An electrochemical impedance spectroscopy study of the corrosion behaviour of pvd coated steels in 0.5 n nacl aqueous solution: Part ii.: Eis interpretation of corrosion behaviour*. Corrosion Science **45**(6), 1257 (2003).

[159] A. Ghasemi, V. Raja, C. Blawert, W. Dietzel, and K. Kainer. *Study of the structure and corrosion behavior of peo coatings on am50 magnesium alloy by electrochemical impedance spectroscopy*. Surface and Coatings Technology **202**(15), 3513 (2008).

[160] R. M. Souto, M. M. Laz, and R. L. Reis. *Degradation characteristics of hydroxyapatite coatings on orthopaedic tialv in simulated physiological media investigated by electrochemical impedance spectroscopy*. Biomaterials **24**(23), 4213 (2003).

[161] F. Lisdat and D. Schäfer. *The use of electrochemical impedance spectroscopy for biosensing*. Analytical and bioanalytical chemistry **391**(5), 1555 (2008).

[162] D. Andre, M. Meiler, K. Steiner, C. Wimmer, T. Soczka-Guth, and D. Sauer. *Characterization of high-power lithium-ion batteries by electrochemical impedance spectroscopy. i. experimental investigation*. Journal of Power Sources **196**(12), 5334 (2011).

[163] B.-Y. Chang and S.-M. Park. *Electrochemical impedance spectroscopy*. Annual Review of Analytical Chemistry **3**, 207 (2010).

[164] P. Electrochemistry, C. Elements, C. Equivalent, and C. Models. *Basics of electrochemical impedance spectroscopy*. Appl Note AC **286**, R491 (2010).

[165] I. I. Suni. *Impedance methods for electrochemical sensors using nanomaterials*. TrAC Trends in Analytical Chemistry **27**(7), 604 (2008).

[166] J. R. Macdonald and E. Barsoukov. *Impedance spectroscopy: theory, experiment, and applications*. History **1**(8) (2005).

[167] J. E. B. Randles. *Kinetics of rapid electrode reactions*. Discussions of the faraday society **1**, 11 (1947).

[168] Z. Karpas, Z. Berant, and O. Shahal. *Effect of temperature on the mobility of ions*. Journal of the American Chemical Society **111**(16), 6015 (1989).

[169] A. Prodic, D. Maksimovic, and R. W. Erickson. *Design and implementation of a digital pwm controller for a high-frequency switching dc-dc power converter*. In *Industrial Electronics Society, 2001. IECON'01. The 27th Annual Conference of the IEEE*, vol. 2, pp. 893–898 (IEEE, 2001).

[170] C. E. Murphy. *All about direct digital synthesis*. http://www.analog.com/library/analogdialogue/archives/38-08/dds.pdf (2004). [Online; accessed 28-July-2018].

[171] Unknown. *PWM Sine Wave Generation*. http://web.csulb.edu/~hill/ee470/Lab%202d%20-%20Sine_Wave_Generator.pdf (2014). [Online; accessed 28-July-2018].

[172] L. Liao, W. Jin, and R. Pavel. *Enhanced restricted boltzmann machine with prognosability regularization for prognostics and health assessment*. IEEE Transactions on Industrial Electronics **63**(11), 7076 (2016).

[173] L. Da Xu, W. He, and S. Li. *Internet of things in industries: A survey*. IEEE Transactions on industrial informatics **10**(4), 2233 (2014).

[174] H. Yanti. *The applications of wifi-based wireless sensor network in internet of things and smart grid*. Buletin Inovasi ICT & Ilmu Komputer **2**(1) (2015).

[175] Thingspeak. *Thingspeak-Open IoT based CLoud Server*. https://thingspeak.com/ (2018). [Online; accessed 28-July-2018].

[176] T. Berners-Lee, R. Fielding, and H. Frystyk. *Hypertext transfer protocol–http/1.0*. Tech. rep. (1996).

[177] J. Singh, H. Chu, J. Abell, R. A. Tripp, and Y. Zhao. *Flexible and mechanical strain resistant large area sers active substrates*. Nanoscale **4**(11), 3410 (2012).

[178] C. Lee, J. Ahn, K. B. Lee, D. Kim, and J. Kim. *Graphene-based flexible no2 chemical sensors*. Thin Solid Films **520**(16), 5459 (2012).

[179] M. Akiyama, Y. Morofuji, T. Kamohara, K. Nishikubo, M. Tsubai, O. Fukuda, and N. Ueno. *Flexible piezoelectric pressure sensors using oriented aluminum nitride thin films prepared on polyethylene terephthalate films*. Journal of applied physics **100**(11), 114318 (2006).

[180] X. Wang, H. Zhang, R. Yu, L. Dong, D. Peng, A. Zhang, Y. Zhang, H. Liu, C. Pan, and Z. L. Wang. *Dynamic pressure mapping of personalized handwriting by a flexible sensor matrix based on the mechanoluminescence process*. Advanced Materials **27**(14), 2324 (2015).

[181] Eurolaser. *Laser cutting and engraving of PET.* https://www.eurolaser.com/materials/pet-petg/ (2018). [Online; accessed 28-July-2018].

[182] GCCWorld. *Cutting pet with co2 laser*. http://www.gccworld.com/showcase.php?act=view&no=138 (2018). [Online; accessed 28-July-2018].

[183] A. De La Escosura-Muñiz, M. Espinoza-Castañeda, M. Hasegawa, L. Philippe, and A. Merkoçi. *Nanoparticles-based nanochannels assembled on a plastic flexible substrate for label-free immunosensing*. Nano Research **8**(4), 1180 (2015).

[184] GCCWorld. *Advantages and Properties of Aluminium*. http://www.azom.com/article.aspx?ArticleID=1446 (2018). [Online; accessed 28-July-2018].

[185] J. Lin, Z. Peng, Y. Liu, F. Ruiz-Zepeda, R. Ye, E. L. Samuel, M. J. Yacaman, B. I. Yakobson, and J. M. Tour. *Laser-induced porous graphene films from commercial polymers*. Nature communications **5**, 5714 (2014).

[186] T.-T. Ngo, A. Bourjilat, J. Claudel, D. Kourtiche, and M. Nadi. *Design and realization of a planar interdigital microsensor for biological medium characterization*. In *Next Generation Sensors and Systems*, pp. 23–54 (Springer, 2016).

[187] A. Devices. *Datasheet of AD5933*. http://www.analog.com/media/en/technical-documentation/data-sheets/AD5933.pdf (2018). [Online; accessed 28-July-2018].

[188] A. Devices. *Description of Arduino Uno WiFi*. https://store.arduino.cc/usa/arduino-uno-wifi (2018). [Online; accessed 28-July-2018].

[189] *Ciao Library for Arduino*. https://www.arduino.cc/en/Reference/Ciao/ (2018). [Online; accessed 28-July-2018].

[190] *Circuit Maker*. https://circuitmaker.com/ (2018). [Online; accessed 28-July-2018].

[191] D. Cochlin. *Graphene paints a corrosion-free future*. http://www.manchester.ac.uk/discover/news/graphene-paints-a-corrosion-free-future/ (2014). [Online; accessed 28-July-2018].

[192] A. K. Geim and K. S. Novoselov. *The rise of graphene*. In *Nanoscience and Technology: A Collection of Reviews from Nature Journals*, pp. 11–19 (World Scientific, 2010).

[193] L. D. Mafu, T. A. Msagati, and B. B. Mamba. *Ion-imprinted polymers for environmental monitoring of inorganic pollutants: synthesis, characterization, and applications*. Environmental Science and Pollution Research **20**(2), 790 (2013).

[194] G. Wulff. *The covalent and other stoichiometric approaches*. Molecularly Imprinted Materials: Science and Technology, Yan, M., Ramström, O.(Eds), Marcel Dekker: New York pp. 59–92 (2005).

[195] V. Vishnuvardhan, K. Prathish, G. Naidu, and T. P. Rao. *Fabrication and topographical analysis of non-covalently imprinted polymer inclusion membranes for the selective sensing of pinacolyl methylphosphonate—a simulant of soman*. Electrochimica acta **52**(24), 6922 (2007).

[196] K. Mosbach, Y. Yu, J. Andersch, and L. Ye. *Generation of new enzyme inhibitors using imprinted binding sites: the anti-idiotypic approach, a step toward the next generation*

of molecular imprinting. Journal of the American Chemical Society **123**(49), 12420 (2001).

[197] O. Ramstroem, L. I. Andersson, and K. Mosbach. *Recognition sites incorporating both pyridinyl and carboxy functionalities prepared by molecular imprinting*. The Journal of Organic Chemistry **58**(26), 7562 (1993).

[198] N. Candan, N. Tüzmen, M. Andac, C. A. Andac, R. Say, and A. Denizli. *Cadmium removal out of human plasma using ion-imprinted beads in a magnetic column*. Materials Science and Engineering: C **29**(1), 144 (2009).

[199] G. Wulff. *Enzyme-like catalysis by molecularly imprinted polymers*. Chemical reviews **102**(1), 1 (2002).

[200] L. Chen, S. Xu, and J. Li. *Recent advances in molecular imprinting technology: current status, challenges and highlighted applications*. Chemical Society Reviews **40**(5), 2922 (2011).

[201] E. Caro, R. Marcé, F. Borrull, P. Cormack, and D. Sherrington. *Application of molecularly imprinted polymers to solid-phase extraction of compounds from environmental and biological samples*. TrAC Trends in Analytical Chemistry **25**(2), 143 (2006).

[202] J. Matsui, I. A. Nicholls, T. Takeuchi, K. Mosbach, and I. Karube. *Metal ion mediated recognition in molecularly imprinted polymers*. Analytica Chimica Acta **335**(1-2), 71 (1996).

[203] H. Su, J. Li, and T. Tan. *Adsorption mechanism for imprinted ion (ni2+) of the surface molecular imprinting adsorbent (smia)*. Biochemical Engineering Journal **39**(3), 503 (2008).

[204] T. Li, S. Chen, H. Li, Q. Li, and L. Wu. *Preparation of an ion-imprinted fiber for the selective removal of cu2+*. Langmuir **27**(11), 6753 (2011).

[205] A. C. Mesquita, M. N. Mori, and L. G. A. e Silva. *Polymerization of vinyl acetate in bulk and emulsion by gamma irradiation*. Radiation Physics and Chemistry **71**(1-2), 253 (2004).

[206] K.-C. Ho, W.-M. Yeh, T.-S. Tung, and J.-Y. Liao. *Amperometric detection of morphine based on poly (3, 4-ethylenedioxythiophene) immobilized molecularly imprinted polymer particles prepared by precipitation polymerization*. Analytica Chimica Acta **542**(1), 90 (2005).

[207] P. J. Dowding and B. Vincent. *Suspension polymerisation to form polymer beads*. Colloids and Surfaces A: Physicochemical and Engineering Aspects **161**(2), 259 (2000).

[208] Hach. *NITRATE: Chromotropic Acid Method.* https://www.hach.com/asset-get.download.jsa?id=7639984361. [Online; accessed 28-July-2018].

[209] Hioki. *HIOKI IM3536 LCR Meter.* . https://www.hioki.com/hdfile.jsp?id=11853. [Online; accessed 28-July-2018].

[210] A. S. Bondarenko and G. A. Ragoisha. *EIS Spectrum Analyser*. http://www.abc.chemistry.bsu.by/vi/analyser/ (2018). [Online; accessed 28-July-2018].

[211] U. S. E. P. Agency. *Environmental Protection Agency*. https://www.epa.gov/ (2018). [Online; accessed 28-July-2018].